FEDERAL UNIVERSITY OF MINAS GERAIS
Graduate Program in Metallurgical, Materials and Mining Engineering

Doctoral Thesis

# Evaluation of the gravity induced stirred mills screw liner wearing in laboratory-scale and using Discrete Element Method

# Avaliação do desgaste do revestimento do agitador de moinhos verticais através da execução de testes de laboratório e simulações com o Método dos Elementos Discretos

Author:
Priscila Maria Esteves Brandão

Academic Supervisors:
Dr. Douglas B. Mazzinghy
Dr. Roberto Galéry

August/2020

FEDERAL UNIVERSITY OF MINAS GERAIS
Graduate Program in Metallurgical, Materials and Mining Engineering

Priscila Maria Esteves Brandão

# Evaluation of the vertical stirred mills screw liner wearing in laboratory-scale and using Discrete Element Method

# Avaliação do desgaste do revestimento do agitador de moinhos verticais através da execução de testes de laboratório e simulações com o Método dos Elementos Discretos

**Final Version**

Doctorate thesis submitted to the Graduate Program in Metallurgical, Materials and Mining Engineering from the School of Engineering at the Federal University of Minas Gerais, as partial fulfillment requirement for the degree of Doctor in Metallurgical, Materials and Mining Engineering

Area of concentration: Mineral Technology

Academic Supervisors:
Dr. Douglas Batista Mazzinghy
Dr. Roberto Galéry

Belo Horizonte
Federal University of Minas Gerais
School of Engineering
2020

Brandão, Priscila Maria Esteves.
B817e Evaluation of the vertical stirred mills screw liner wearing in laboratory-scale and using Discrete Element Method [recurso eletrônico] / Priscila Maria Esteves Brandão. - 2020.
1 recurso online (101 f. : il., color.) : pdf.

Orientador: Douglas Batista Mazzinghy.
Coorientador: Roberto Galéry..

Tese (doutorado) - Universidade Federal de Minas Gerais, Escola de Engenharia.

Anexos: f. 94-101.

Inclui bibliografia.
Exigências do sistema: Adobe Acrobat Reader.

1. Engenharia de minas - Teses. 2. Tecnologia mineral - Teses. 3. Moagem (Beneficiamento de minério) - Teses. 4. Simulação (Computadores digitais) - Teses. I. Mazzinghy, Douglas Batista. II. Galéry, Roberto. III. Universidade Federal de Minas Gerais. Escola de Engenharia. IV. Título.

CDU: 622(043)

Ficha catalográfica elaborada pelo bibliotecário Reginaldo Cesar Vital dos Santos CRB/6 2165
Biblioteca Prof. Mário Werneck, Escola de Engenharia da UFMG

**UNIVERSIDADE FEDERAL DE MINAS GERAIS**
**ESCOLA DE ENGENHARIA**
**Programa de Pós-Graduação em Engenharia Metalúrgica, Materiais e de Minas**

PPGEM

Tese intitulada **"Evaluation of the Gravity Induced Stirred Mills Screw Liner Wearing in Laboratory-scale and Using Discrete Element Method"**, área de concentração: Tecnologia Mineral, apresentada pela candidata **Priscila Maria Esteves Brandão**, para obtenção do grau de Doutora em Engenharia Metalúrgica, Materiais e de Minas, aprovada pela comissão examinadora constituída pelos seguintes membros:

Prof. Douglas Batista Mazzinghy
Orientador - Dr. (UFMG)

Prof. Roberto Galéry
Coorientador - Dr. (UFMG)

Prof. Maurício Guimarães Bergerman
Dr. (USP)

Engº. Luís Cláuzio de Rennó Machado
Dr. (Anglo American)

Prof. Rodrigo Magalhães de Carvalho
Dr. (UFRJ)

Prof. Vladmir Kronemberger Alves
Dr. (UFOP)

Prof. Rodrigo Lambert Oréfice
Coordenador do Programa de Pós-Graduação em Engenharia Metalúrgica, Materiais e de Minas/UFMG

Belo Horizonte, 31 de agosto de 2020

To Rafael and Mateus, for the unconditional love and support.

## ACKNOWLEDGMENTS

To Mateus, for giving me all love and purpose, teaching me so much kindness and simplicity.

To Rafael, for sharing my dreams and plans and specially for encouraging me to take this challenge, including following me to the other side of the world.

To my mother Lilian, for your unconditional support, infinite love and specially for having such a big heart.

To my father Eduardo, for giving me so much strength and love.

To Daniel and Natalia for all the conversations, advices and friendship in our Australian adventure.

To Erica Avelar for all the PhD conversations, advices, company, kindness and friendship.

To my grandfathers and grandmothers, for all love and kindness.

To Douglas, for all dedication, patience, valuable guidance, and interest discussions.

To Galéry, for all support, trust and specially for introducing me to the mining and minerals processing engineering.

To Malcolm Powell, for all meetings, explanations, and key insights.

To Marko, for all patience, guidance, and brilliant perspective of all details.

To Mohsen, for all discussions, patience and encouraging counselling.

To Alberto, for all talks and unconditional support in the laboratory.

Thanks to Anglo American for all the support and for providing data available for this research.

Thanks for CAPES for funding my candidature and my international scholarship under the grant number 88881.187997/2018-01.

Thanks for the Brazilian agencies PROEX-CAPES, CNPq, and FAPEMIG.

Thanks to PPGEM program and students.

Thanks to JKMRC researchers and students, who received me so well in Brisbane.

To Steinert Latinoamericana colleagues, who shared my last candidature year.

A persistência é o caminho do

êxito.

“Charles Chaplin”

## RESUMO

A crescente escassez de recursos minerais faz com que a exploração de depósitos de reduzidos teores e complexas mineralogias se apresente como uma nova realidade no setor mineral. Esse fato eleva a dependência da indústria às tecnologias de moagem que apresentam maior eficiência energética, como é o caso dos moinhos verticais de carga agitada. Embora sua eficiência energética e modelagem sejam discutidas na literatura, o desgaste do revestimento da espiral se apresenta como um tópico pouco abordado. Esse desgaste afeta os principais componentes do custo operacional do equipamento, que são o consumo energético, consumo de carga moedora e o custo de substituição do próprio revestimento. Nesse sentido, a estratégia atual de compensação do desgaste consiste na manutenção da energia elétrica em um nível constante, através do aumento do enchimento de carga moedora do moinho durante um ciclo de vida útil do revestimento. Neste estudo, diferentes abordagens foram usadas no intuito de promover uma melhor compreensão sobre o desgaste e seus efeitos na performance da moagem. Experimentos foram realizados usando um moinho vertical de laboratório e os conceitos de energia específica, distribuição granulométrica e energia específica de tamanho (*Size Specific Energy* - SSE). Os resultados apontam para uma tendência de elevada redução na energia específica de tamanho (SSE) ao operar com enchimento constante. Adicionalmente, foram realizadas simulações de desgaste usando o Método dos Elementos Discretos (DEM). Os resultados obtidos foram comparados com medições de desgaste realizadas em um VTM-1500, a partir do escaneamento tridimensional dos revestimentos, em distintas condições de desgaste. De forma similar, simulações DEM foram realizadas para avaliação das condições experimentais testadas em escala de laboratório. Os resultados foram usados na obtenção de um melhor entendimento dos resultados experimentais. Por fim, um método não invasivo e de baixo custo foi aplicado para monitoramento do desgaste do revestimento da espiral, utilizando variáveis elétricas e vibracionais. Os resultados indicam um relativo potencial para uso das informações na obtenção de um indicador das condições do desgaste do revestimento.



**PALAVRAS-CHAVE:** Vertimill, Tower Mill, Desgaste do revestimento, Moagem fina, Energia específica de tamanho.

## ABSTRACT

The increasing pressure to unlock value from fine grained and low-grade ore deposits increases the industry's reliance on energy efficient fine grinding technologies. In fine grinding applications, gravity induced stirred mills presents a better energy performance in comparison to conventional tumbling ball mills. While energy efficiency, scale up and modelling are widely discussed in the literature, the liner wear of the screw agitators is a less-researched topic. The screw liner wear affects all the important equipment operational costs, namely energy consumption, grinding media consumption and the cost of the liner itself. In this sense, the current strategy for wear compensating is to maintain constant electrical power by increasing mill media filling during the liner lifecycle. In this study, different approaches were used to provide a better understanding about the effects of the screw liner wear and recharging media strategy on the performance of gravity induced stirred mills. Test work was performed using a laboratory scale wet grinding with an itabirite iron ore. Specific energy, particle size distribution and the size specific energy approach (SSE) were compared in the results. The test data qualitatively demonstrate a tendency for greater reduction in the SSE when operating with constant filling. Additionally, Discrete Element Method (DEM) simulations were performed. Three dimensional measurements of wear, in a full-scale equipment, were used to correlate the simulation results. Wear design, wear measurements, particle collision spectra, simulation power and particle trajectory were evaluated at different wear stages. The DEM simulations model setup was applied for the experimental conditions tested in laboratory scale. The simulation outputs were used to gather a better understanding about experimental results. Lastly, a non-intrusive and low-cost method was applied for monitoring the agitator screw liner wear. The method is based on electrical measurements, vibration signature and spectral analysis. Experimental data was obtained at Minas-Rio Project, an Anglo-American iron ore processing plant , located in Brazil. The results indicate a reasonable potential to provide a good correlation with liner wear conditions.



**KEYWORDS:** Vertimill, Tower Mill, Liner wear, Fine grinding, Size Specific Energy.

## LIST OF FIGURES

# LISTA DE FIGURAS

# LIST OF TABLES

## SYMBOLS

| | |
|---|---|
| $A$ | Surface area of a boundary element ($m^2$) |
| $d$ | Screw diameter (m) |
| $h$ | Loss in depth (m) |
| $K$ | Wear rate ($m^3/J$) |
| $Kurt$ | Kurtosis |
| $n$ | Number of samples |
| $S$ | Skewness |
| $v$ | Tip speed (m/s) |
| $w$ | Shear work (J) |
| $\sigma$ | Standard deviation |
| $\omega$ | Rotational speed (rpm) |
| $\bar{x}$ | Average value |

## ABBREVIATIONS

| | |
|---|---|
| *CF* | Constant filling |
| *CP* | Constant power |
| *DEM* | Discrete Element Method |
| *DOE* | US Department of Energy |
| *PSD* | Particle Size Distribution |
| *SE* | Specific energy |
| *SSE* | Size Specific Energy |
| *VTM* | Vertimill |

# TABLE OF CONTENTS

## PUBLICATIONS DURING CANDIDATURE

Esteves, P., Stopa, M. M., Galery, R., Mazzinghy, D. B., & Russo, J. F. (2016). Relation between electrical power and filling in gravity induced stirred mills. *Metallurgy, Materials and Mineral Technologies (TMM)*, *13*(3), pp. 288-294. Source: http://dx.doi.org/10.4322/2176-1523.1013 *(in Portuguese).*

Esteves, P., Mazzinghy, D., Galéry, R., Montenegro, L., & Russo, J. (2017). Indirect method for liner wear monitoring in gravity induced stirred mills. Belém: XXVII Brazilian National Meeting of Mineral Treatment and Extractive Metallurgy (ENTMME) *(in Portuguese).*

Esteves, P., Mazzinghy, D., Galéry, D., Stopa, M., & Filho, B. (2018). Load Torque Estimation For Monitoring Ball Mill Filling. *IMPC - International Mineral Processing Congress* , (pp. 1-10). Moscow.

Esteves, P., Mazzinghy, D. B., Hilden, M., Yahyaei, M., Powell, M., & Galery, R. (2019). Qualitative evaluation of the grinding efficiency of a gravity induced stirred mill using the size specific energy approach. *16th European Symposium on Comminution & Classification* (pp. 101-102). Leeds: Edited by Mojtaba Ghadiri, Sadegh Nadimi, Mehrdad Pasha.

Esteves, P., Mazzinghy, D., Galéry, R., Filho, B., Silva, J., & Russo, J. (2019). Predictive Modelling of Vertical Stirred Mills Liner Wear Using Vibration Signature Analysis. *11 th International Comminution Symposium* (p. 18p). Cape Town: MEI Conferences.

Esteves, P., Mazzinghy, D., Hilden, M., Yahyaei, M., Powell, M., & Galéry, R. (2021). An alternative strategy to compensate for screw wear in gravity induced stirred mills. *Powder Technology*, Volume 379, p. 384-392. ISSN 0032-5910, https://doi.org/10.1016/j.powtec.2020.10.075.

Esteves, P., Mazzinghy, D., Galéry, R., & Rennó, L. (2021). Industrial vertical stirred mills screw liner wear profile compared to discrete element method simulations. *Minerals*, 11*(4), 397*; https://doi.org/10.3390/min11040397.

# CAPÍTULO 1 - INTRODUÇÃO

## 1.1. Considerações Iniciais

O cenário atual da indústria mineral contempla desafios contínuos relativos à menor disponibilidade de recursos minerais, aos teores decrescentes e à elevação da complexidade dos minérios disponíveis para beneficiamento. À medida que novos projetos começam a explorar minérios mais complexos e de granulação fina e ultrafina, faz-se necessária a incorporação de estágios de moagem fina e ultrafina, no intuito de maximização da recuperação metalúrgica nas plantas de beneficiamento. Neste contexto, verifica-se uma crescente importância na utilização de moinhos verticais de carga agitada, dada a sua elevada eficiência energética.

Em relação ao consumo energético dos processos de moagem, verifica-se uma reduzida eficiência, razão pela qual os processos de moagem são apontados como responsáveis por cerca de 34% a 44% da energia necessária em uma planta de processamento mineral (Marsden, 2008; DOE, 1981). Num contexto global, ao fim da década de 80, a moagem foi apontada pelo Departamento de Energia dos Estados Unidos (DOE) como responsável por cerca de 3% a 4% do consumo total de energia elétrica mundial (DOE, 1981). Mais recentemente, Napier-Munn (2015) apontou esse número como 1,8%, considerando-se apenas o consumo energético dos moinhos. De fato, os números tornam-se ainda mais expressivos levando-se em conta os gastos energéticos indiretos, como aqueles envolvidos na produção de cargas moedoras e revestimentos de desgaste desses moinhos. Independentemente de qual seja o número correto, é conclusivo que o processo de moagem representa uma parcela significativa do consumo de energia mundial.

Ainda em relação ao consumo energético dos processos de moagem, verifica-se uma significativa elevação da energia específica (kWh/t) à medida que ocorre a redução do tamanhos das partículas. Nesse sentido, faz-se necessária uma elevação substancial na parcela de energia requerida para atingir tamanhos reduzidos de partículas, conforme mostrado na Figura 1.1.

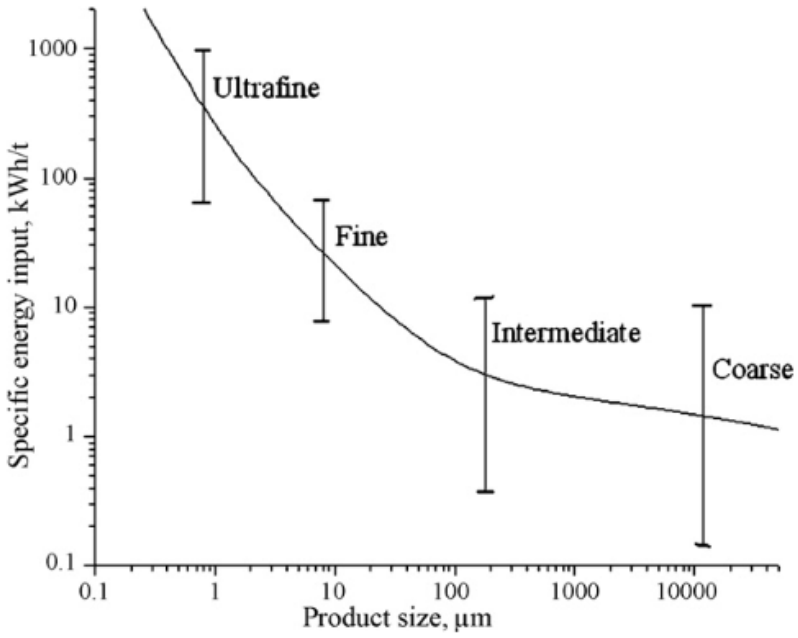


Figura 1.1 - Relação entre a energia específica de moagem e o tamanho de partícula do produto, para equipamentos de cominuição (Wang & Forssberg, 2007).

Nas aplicações de moagem fina os moinhos verticais de carga agitada apresentam uma eficiência energética superior aos moinhos tubulares convencionais (Jankovic, et al., 2003). Esse comportamento consiste no principal motivo pelo qual os moinhos verticais de carga agitada vêm apresentando-se como uma tendência para aplicações de moagem fina.

No contexto das últimas três décadas, os moinhos verticais Metso Vertimills vem sendo empregados em aplicações de remoagem, moagem secundária e terciária, com mais de 450 unidades instaladas ao redor do mundo (Metso Minerals Industries, 2018). Da mesma forma, os moinhos verticais Nippon Eirich Tower Mills foram instalados em mais de 200 plantas ao redor do mundo, contemplando a moagem de mais de 40 tipos de materiais distintos (Eirich, 2018). Os principais motivos que justificam o amplo uso desses equipamentos consistem no reduzido custo operacional e elevada eficiência energética. Nesse sentido, diversos estudos apontam para a elevada eficiência energética desses equipamentos em aplicações de moagem fina e remoagem, na comparação com moinhos tubulares (Stief De, 1987; Cleary, Sinnott and Morrison, 2006; Sinnott, Cleary and

Morrison, 2006; Mazzinghy, 2012; Bergerman, *et al.*, 2012; Rosa, Oliveira and Donda, 2014; Mazzinghy, *et al.*, 2015; Mazzinghy, *et al.*, 2017). De forma semelhante, essa redução no consume energético também é observada para moagens de partículas mais grosseiras, com tamanho máximo de partículas na alimentação de até 6 mm (Shi, 2009; Mazzinghy, *et al.*, 2014; Mazzinghy, *et al.*, 2015).

Em relação aos estudos mais recentes no assunto, Rocha (2018) aplicou o Modelo de Balanço Populacional (PBM – *Population Balance Model*) para a avaliação do efeito de diversas variáveis operacionais no consumo energético e distribuição granulométrica do produto. Adicionalmente, o Método dos Elementos Discretos (DEM – *Discrete Element Method*) foi utilizado para realizar a previsão do consumo energético de um moinho em escala reduzida. Huang (2018) focou na caracterização e avaliação de variáveis operacionais, concluindo que o enchimento e a velocidade de rotação do agitador apresentam a maior influência no desempenho do equipamento. Nesse sentido, é apresentada uma recomendação interessante, sugerindo que a compensação do desgaste do revestimento poderia ser realizada em função da variação da velocidade de rotação do agitador, em detrimento da alteração de enchimento. Finalmente, uma avaliação do efeito das variáveis operacionais no consumo energético foi realizada por Silva (2019), com base em testes de laboratório, PBM e medições industriais realizadas no Projeto Minas Rio, que consiste na maior planta de remoagem com moinhos verticais de carga agitada no mundo.

Embora a eficiência energética superior dos moinhos verticais de carga agitada seja amplamente discutida na literatura, é importante ressaltar que essa melhor performance está atrelada à uma janela operacional estreita. Nesse sentido, variáveis operacionais como as propriedades da alimentação ou o desempenho do circuito de classificação, podem afetar essa melhor performance energética (Palaniandy, et al., 2017). Nesse sentido, torna-se imprescindível o conhecimento e o teste das condições operacionais ideais, de forma a maximizar o uso da energia na quebra de partículas. Caso a intensidade energética aplicada seja muito baixa, as colisões de partículas podem não resultar em quebra e, portanto, o tamanho especificado para o produto poderá não será alcançado. De forma semelhante, caso a intensidade energética aplicada seja maior do que a necessária,

pode ocorrer desperdício de energia e, consequentemente, o melhor desempenho energético não será alcançado (Jankovic, et al., 2003). Com relação a essa otimização, a interação entre as variáveis operacionais parece ter um efeito significativo na eficiência da moagem em moinhos verticais (Jankovic, 2003).

Embora a eficiência energética de moinhos verticais seja amplamente discutida na literatura, a abordagem do desgaste do revestimento do agitador apresenta-se como um tema mais recente. Nesse sentido, Radziszewski e Moore (2017) propuseram a aplicação de métodos mecanicistas, buscando um entendimento qualitativo do problema e realizando uma validação gráfica por meio de imagens obtidas em um moinho em escala industrial.

Em relação às estratégias operacionais de compensação de desgaste, a prática atual é promover a elevação gradual do enchimento de carga moedora, ao longo da vida útil do revestimento. Isso é realizado com o intuito de manter o consumo energético constante durante todo o ciclo de vida do revestimento. A lógica por trás dessa estratégia consiste no fato de que, com o desgaste, ocorre a redução do consumo energético do moinho. Elevando-se o enchimento, as partes superiores do moinho são ativadas, fazendo com que essa redução do consumo energético seja compensada pela adição de carga moedora.

## 1.2. Objetivos

O objetivo principal desta pesquisa é o de propiciar um melhor entendimento sobre os efeitos do desgaste dos revestimentos do agitador dos moinhos verticais de carga agitada, assim como sobre o impacto das estratégias de compensação desse desgaste.

Para atingir este objetivo, foram utilizadas três abordagens distintas: testes de laboratório, simulações computacionais utilizando o Método dos Elementos Discretos (DEM) e medições industriais. Dessa forma, os seguintes os objetivos secundários são listados abaixo:

i. Desenvolvimento de uma metodologia de teste para equipamento em escala

laboratorial;

ii. Comparar diferentes estratégias operacionais para compensação do desgaste, com base nos resultados dos testes em laboratório;

iii. Aplicar um indicador de desempenho adequado para a comparação;

iv. Realizar simulação de desgaste usando DEM e posterior correlação com medições industriais;

v. Utilizar simulações DEM para comparação das diferentes estratégias operacionais;

vi. Obtenção de correlação entre a condição de desgaste do revestimento, medições vibracionais e elétricas.

## 1.3. Estrutura do Texto

A tese está dividida em nove capítulos.

O Capítulo 1 consiste em uma introdução ao assunto e define os objetivos da tese.

O Capítulo 2 detalha o moinho vertical e propõe uma breve revisão da literatura relacionada. Além disso, aborda-se o desgaste do revestimento do agitador, assim como as estratégias operacionais para compensação do desgaste.

O Capítulo 3 apresenta os resultados obtidos em testes de laboratório. Consiste na descrição do equipamento utilizado, metodologia e resultados.

O Capítulo 4 descreve as simulações de desgaste realizadas com DEM e apresenta uma correlação com medições de desgaste realizadas em um VTM-1500.

O Capítulo 5 aplica as simulações DEM apresentadas no Capítulo 4, no contexto das condições experimentais apresentadas no Capítulo 3.

O Capítulo 6 descreve a aplicação de um método não intrusivo para avaliação das condições de desgaste de um moinho vertical, com base em medições de grandezas elétricas e análise espectral vibracional.

O Capítulo 7, por fim, resume as conclusões e resultados da tese, assim como apresenta recomendações para investigações futuras.

# CHAPTER 1 - INTRODUCTION

## 1.1. Background

The mining industry faces continuing challenges related to the lower availability of mineral resources, decreasing grades, and increasing complexity of ores. As many mining projects start to exploit more complex and fine-grained ore, there is a need to incorporate fine grinding stages to maximize recovery in mineral processing plants. In this context, there is a growing importance of gravity induced stirred mills, due to their high energy efficiency when compared to tumbling mills in fine grinding applications.

At the same time, grinding is very low energy efficient and this is the main reason why it is pointed as responsible for around 34% to 44% of energy required in a mineral processing plant (Marsden, 2008; DOE, 1981). The numbers are even alarming if we consider the situation in a global context. In the 80's grinding was pointed by the US Department of Energy (DOE) as responsible for around 3% to 4% of total world electrical energy consumption (DOE, 1981) and, more recently, this number was indicated as 1.8% (Napier-Munn, 2015). In fact, Napier-Munn (2015) went beyond and argued that overall grinding energy consumption is even greater than these numbers, once consumption of liners and grinding media represents a representative extra amount of energy (DOE, 1981). Regardless which is the correct number, it is conclusive that grinding process are responsible for a significant portion of world's power consumption.

In relation to energy consumption, there is a significant increase in the specific energy (kWh/t) when decreasing particle size. In this sense, representative additional power is required to achieve finer grain size, as shown in Figure 1.1.

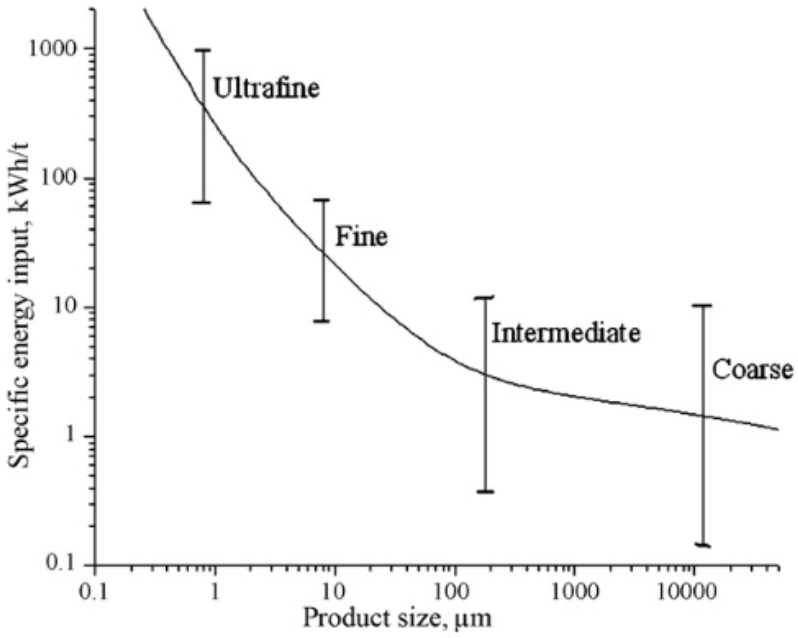


Figure 1.1 – Relation between specific energy and product size in comminution equipment. (Wang & Forssberg, 2007)

In fine grinding applications, gravity induced stirred mills have a higher energy efficiency compared to conventional tumbling ball mills (Jankovic, et al., 2003). This behaviour is the main reason why vertical mills are pointing as trend equipment for fine-grinding and ultra-fine-grinding applications.

Gravity induced stirred mills are widely applied in fine grinding applications. During the last three decades, Metso Vertimills have been used in regrinding, secondary and tertiary grinding applications with more than 450 units installed around the world (Metso Minerals Industries, 2018). Additionally, Nippon Eirich Tower Mills are installed in more than 200 plants worldwide, grinding more than 40 types of different materials (Eirich, 2018). The main reason for such a wide use of this type of equipment is its energy and cost efficiency. According to several studies, the vertical stirred mills presents high energy efficiency for fine-grinding and ultra-fine grinding applications (Stief De, 1987; Cleary, Sinnott and Morrison, 2006; Sinnott, Cleary and Morrison, 2006; Mazzinghy, 2012; Bergerman, *et al.*, 2012; Rosa, Oliveira and Donda, 2014; Mazzinghy, *et al.*, 2015; Mazzinghy, *et al.*, 2017). Similarly, energy savings are also reported for coarser grinding

with feed top sizes up to 6 mm (Shi, 2009; Mazzinghy, *et al.*, 2014; Mazzinghy, *et al.*, 2015).

More recently, Rocha (2018) applied a population balance model (PBM) to evaluate the effect of operational conditions on power and product size and Discrete Element Method (DEM) to evaluate the effect of operational variables on power draw. In a different study, Huang (2018) focused on characterization and the evaluation of operational variables, thus concluding that mill speed and filling have the greatest influence on equipment performance. An interesting recommendation of control strategy to compensate for screw wear was proposed, suggesting that mill speed should be adjusted rather than using grinding media addition. Finally, an evaluation of the effect of process variables on power consumption was performed based on laboratory test work, PBM simulation and industrial measurements obtained at Minas Rio, the largest regrind mill installation in the world using gravity induced stirred mills (Silva, 2019).

Although it is widely reported that gravity induced stirred mills are energy efficient, the operational window where this is true is narrow and can be affected by several operational conditions, such as feed properties and classification circuit performance (Palaniandy, et al., 2017). In relation to this, it is important to perform the tests at the best operational conditions, to achieve and maximize energy use for particle breakage. If the energy intensity is too low, collisions that do not result in breakage can occur, and hence the required product size will not be achieved. Similarly, if energy is greater than necessary, it can be wasted and consequently the best energy performance will not be achieved (Jankovic, et al., 2003). Regarding this optimization, the interaction between variables appears to have a significant effect on grinding efficiency (Jankovic, 2003).

While energy efficiency of gravity induced stirred mills is well-researched in technical literature, the understanding of the screw liner wear is less very well documented. Radziszewski and Moore (2017) proposed the application of mechanistic methods for a qualitative understanding of the problem, with graphical validation using industrial pictures.

In relation to operational strategies regarding wear compensation, the current practice is to continuously increase mill filling during the liner lifecycle. This is performed within the aim of keeping power draw stable during the complete liner lifecycle. At the start of the liner lifecycle, a fraction of the screw height is above the charge level. By increasing filling, the upper parts of the mill are activated and so grinding can be compensated as the lower portion of the screw wears.

## 1.2. Thesis Objectives

The main object of this research is to provide a better understanding about the effects of the screw liner wear and recharging media strategy on the performance of gravity induced stirred mills.

To achieve this objective, two different approaches were used: laboratory test work and Discrete Element Method (DEM) simulations and industrial measurements. Based on this, the secondary objectives are listed as:

i. Development of test work methodology using laboratory scale equipment;
ii. Compare results with different operational strategies to compensate for liner wear, based on test work results;
iii. Obtaining an adequate performance indicator for the comparison;
iv. Evaluation by DEM simulation and validation with industrial data;
v. Compare results with different operational strategies, based on DEM simulations;
vi. Obtain a correlation between liner wear condition, vibration, and electrical data.

## 1.3. Thesis Structure

The thesis is divided in seven chapters.

Chapter 1 consists in an introduction to the subject and defines the objectives for the

thesis.

Chapter 2 details the gravity induced stirred mill and reviews the related literature. Furthermore, the agitator screw liner wear is approached, such as the operational strategies for wear compensation.

Chapter 3 presents the laboratory test work used to assess the effect of the screw liner wear. It consists in a description about the equipment, methodology and outcomes.

Chapters 4 describes the wear simulations performed with Discrete Element Method to evaluate the wear design and effects. Three-dimensional laser measurement performed in a VTM-1500 are used for the comparison.

Chapter 5 describes the application of the Discrete Element Method setup presented in Chapter 4 for the experimental conditions presented in Chapter 3.

Chapter 6 describes the application of a non-intrusive method to evaluate wear conditions of a gravity induced stirred mill, based on electrical measurements, vibration signature and spectral analysis.

Chapter 7, finally, summarizes conclusions and outcomes for the thesis, such as recommendation for further investigations.

## 1.4. References

Bergerman, M. G., Machado, L. C. D. R., Alves, V. K. & Delboni, H., 2012. *Copper concentrate regrind at Sossego plant using Vertimill: an evaluation on the first years of operation.* s.l., XXVI IMPC Proceedings.

Cleary, P. W., Sinnott, M. & Morrison, R., 2006. Analysis of stirred mill performance using DEM simulation: Part 2 – Coherent flow structures, liner stress and wear, mixing and transport. *Minerals Engineering*, Volume 19, pp. 1551-1572.

DOE, 1981. Comminution and Energy Consumption: Report of the committee on comminution and energy consumption. Em: Washington, D.C.: National Materials Advisory Board, Commission on Sociotechnical Systems, p. 283.

Eirich, 2018. *Brochure: EIRICH Tower Mill - Vertical agitated media mill.* [Online] Available at: https://www.eirichusa.com/products/towermills/tower-mill-vertical-ag-med-mill. [Access in 27th July 2020].

Huang, M., 2018. *Development of a tower mill model using hardgrove mill tests*, Vancouver: Master Thesis; University of British Columbia.

Jankovic, A., 2003. Variables affecting the fine grinding of minerals using stirred mills. *Minerals Engineering*, pp. 337-345.

Jankovic, A., Valery, W. & Rosa, D. L., 2003. *Fine Grinding in the Australian Mining Industry*. Malaysia, s.n.

Marsden, J. 2., 2008. Energy efficiency and copper hydrometallurgy.. *Proc Hydrometall (SME)*, pp. 29-42.

Mazzinghy, D. (2012). Methodology for scale up and simulation of vertical mills. Doctoral thesis submitted at Universidade Federal de Minas Gerais (*in Portuguese*).

Mazzinghy, D., Galery, R., Schneider, C. & Alves, V. K., 2014. Scale up and simulation of Vertimill™ pilot test operated with copper ore. *Journal of Materials Research and Technology*, March, Issue 3(1), pp. 86-89.

Mazzinghy, D. et al., 2017. Vertical stirred mill scale-up and simulation: Model validation by industrial samplings results. *Minerals Engineering*, Volume 103-104, pp. 127-133.

Mazzinghy, D., Schneider, L. C., Alves, K. V. & Roberto, G., 2015. Vertical mill simulation applied to iron ores. *Journal of Materials Research and technology*, pp. 186-90.

Metso Minerals Industries, 2018. Metso Vertimills® - Brochure no. 3758-07.

Palaniandy, S., Yahyaei, M. & Powell, M., 2017. Assessment of hydrocyclone operation in gravity induced stirred mill circuits. *Minerals Engineering*, pp. 83-92.

Radziszewski, P. & Moore, A., 2017. Understanding the effect of pressure profile on stirred mill impeller wear. *Minerals Engineering*, pp. 54-59.

Rocha, D. C., 2018. *Predicting the product particle size distribution from a vertical stirred mill.* Golden, Colorado: Doctoral thesis submitted to the Colorado School of Mines.

Rosa, A., Oliveira, P. & Donda, J., 2014. *Comparing ball and vertical mills performance: An industrial case study.* Chile, XXVII IMPC.

Shi, F. et al., 2009. Comparison of energy efficiency between ball mills and stirred mills in coarse grinding. *Minerals Engineering*, pp. 673-680.

Silva, J., 2019. *Effect of process parameters on vertical mill power.* Belo Horizonte: Master thesis submitted at Universidade Federal de Minas Gerais *(in Portuguese).*

Sinnott, M., Cleary, P. W. & Morrison, R., 2006. Analysis of stirred mill performance using DEM simulation: Part 1 - Media motion, energy consumption and collisional enviroment. *Minerals Engineering*, Volume 19, pp. 1537-1550.

Stief D., L. W. W. L., 1987. Tower mill and its application to fine grinding. *Transactions of the American Institute of Mining and Metallurgical Engineers*, Volume 4.

Napier-Munn, T., 2015. Is progress in energy-efficient comminution doomed?. *Minerals Engineering*, Volume 73, pp. 1-6.

Wang, Y. & Forssberg, E., 2007. Enhancement of energy efficiency for mechanical production of fine and ultra-fine particles in comminution. *China Particuology*, pp. 193-201.

# CHAPTER 2 - GRAVITY INDUCED STIRRED MILL

## 2.1 Introduction

The gravity induced stirred mill consists of a grinding chamber and a vertical agitator screw, as shown in Figure 2.1. The agitator screw is driven by an electrical motor of fixed speed and coupled by a gearbox.

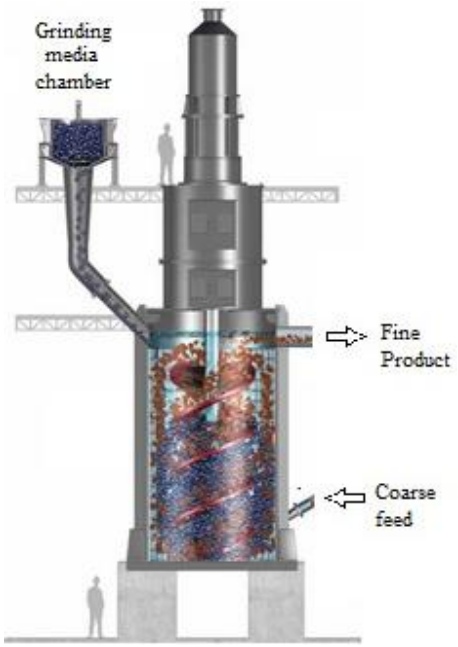


Figure 2.1 – Gravity induced stirred mill main schematic and main components. Adapted from Eirich (2018).

The equipment operates with slurry that can be either top or bottom fed, depending on the application. A comparison between top and bottom feed configuration was performed for a magnetite operation, where the change from top to bottom feed resulted in a finer product size. For this case, the change was due to the occurrence of low-density coarser gangue material that was bypassing the hydrocyclone overflow (Palaniandy, et al., 2018).

To replace grinding media consumed during operation, additional media can be fed to the mill by using a grinding media chamber on the top of the equipment. Extra media addition can be added with the aim to keep power constant, compensating for screw liner wear.

The screw agitator is responsible for media motion while the contact between grinding media and ore particles is responsible for breakage. According to DEM simulations, breakage in gravity induced mills is mostly caused by abrasion rather than impact (Mazzinghy, et al., 2018; Sinnott, Cleary and Morrison, 2006; Morrison, Cleary and Sinnott, 2009).

The mill consists of two operational zones: classification and grinding. Figure 2.1 shows grinding media in blue and ore particles in brown. The bottom part of the mill contains both grinding media and ore particles that are located at the grinding zone. In the grinding zone, a constant flow between media and particles promotes grinding creating finer particles. The classification part of the mill is located at the top part of the grinding chamber, where there is only the presence of slurry. In the classification zone, the coarser particles can return to the grinding zone and finer particles can finally overflow out. Separate models for grinding and classification in the gravity induced stirred mills was developed based on laboratory test work by Hasan (2016).

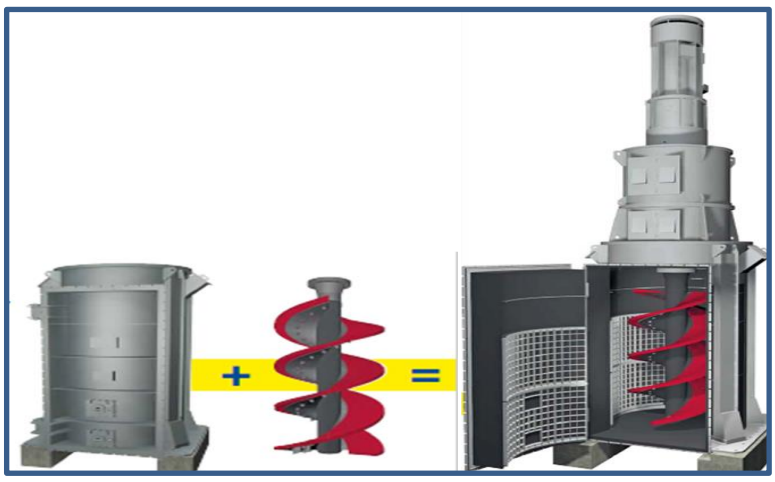

Figure 2.2- Gravity induced stirred mill components (Eirich, 2018).

In order to avoid chamber wear, the grinding chamber is covered by magnetic or grid liners that enable grinding media to attach and form a protective layer, as shown in Figure 2.3.

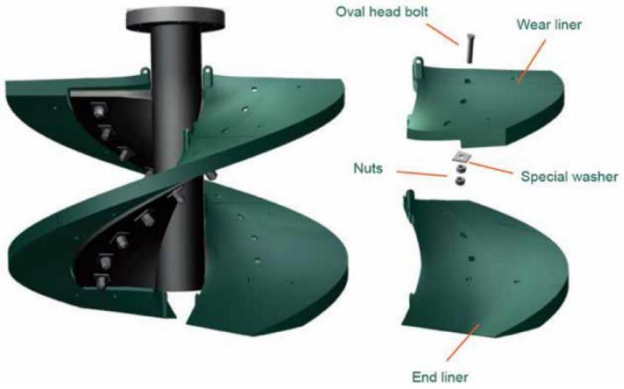


Figure 2.3 – Agitator screw liner parts (Metso Minerals Industries, 2015).

The impeller consists of a double helical screw, formed around a shaft. The screw flights are capped with a replaceable liner. The screw liner is divided in several parts that are directly attached to the screw by bolts, as shown in Figure 2.3. The number of liner parts are dependent on mill size and according to Allen and Noriega (2011), larger mills have fewer flights as for larger mills the screw diameter increases proportionally more than the height.

## 2.2. Liner Wear

As described by Allen and Noriega (2011), Radzizewski (2017) and Mazzinghy (2018), the wear is greater at the bottom of the mill and at the edge of the screw. For this reason, different liner parts have different life cycles and therefore are replaced at different stages. The liners at the bottom, also known as end liners, are usually the first ones that require replacement.

Figure 2.4 shows the screw liner after completely emptying the mill. It can be seen the difference between a new and an old liner of the VTM-1500. The figure on the left side shows a liner with intensive wear and the right side shows the replaced liner. The comparison confirms the indication that wear predominates at the bottom and edges of the screw, causing a great decrease in screw area.

Figure 2.4 - Left: screw liner with intensive wear at the bottom. Right: new screw liner (Esteves et al., 2018).

Figure 2.5 shows the expected wear shape of the base liner part, located at the bottom part of the mill. From that, it is possible to note that the liner does not suffers homogeneous wear. In this sense, it is expected that the bottom part of the liner suffers more intensive wear at the edges.

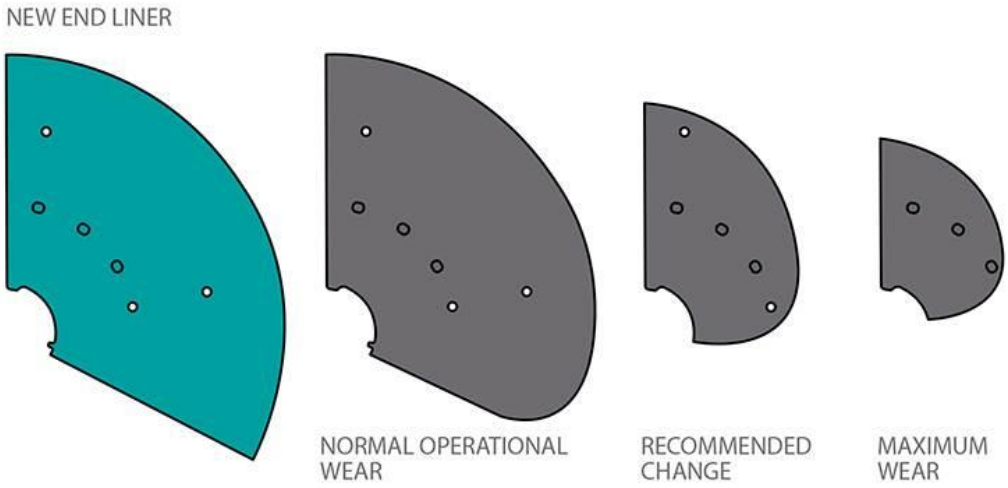


Figure 2.5 – Wear pattern for the bottom liner (Metso, 2017).

As the liner wears, the total surface area decreases and consequently both media motion and power draw decreases. Once media motion is directly related with frequency and intensity of breakage mechanisms, grinding is also affected.

In the operational context, the liner wear compensation is performed by adding additional grinding media to keep constant power draw. In this sense, the liner wear measurement can be estimated and accomplished by measuring mill filling. Although this provides an idea about wear conditions, visual inspections of the liner are necessary. For this inspection, it is necessary to completely empty the mill, in a very effort and time-consuming inspection.

As the liners wear, there is a reduction of the screw surface area in contact with grinding media, decreasing both media motion and required torque. Consequently, power consumption decreases. Because media motion is directly related with frequency and intensity of breakage mechanisms, grinding is also affected. Based on that, the current operational procedure is to continuously increase filling during liner lifecycle, to keep constant power. While for new screws the initial filling is set up as 80% of the screw length, a higher filling is observed at the end of a liner lifecycle, as shown in Figure 2.6.

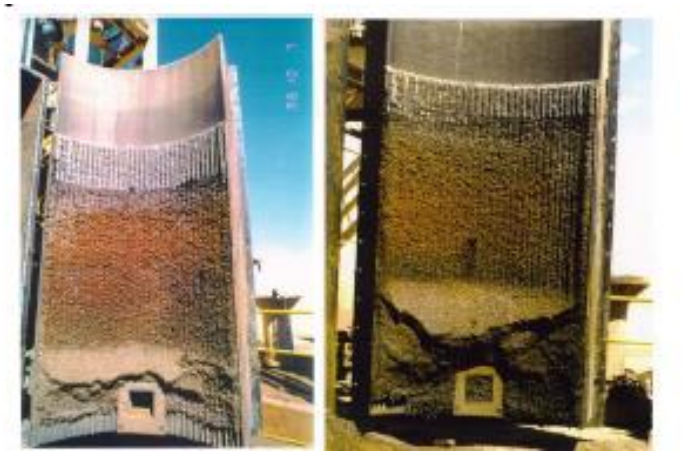

Figure 2.6 – Mill filling at different screw liner wear stages. Left: new liner – Right: worn liner (Allen and Noriega, 2011).

The basic idea behind this control strategy is that by adding additional grinding media to the mill, the upper parts of the screw are activated to compensate for the lost grinding capacity. This filling increase keeps torque and power consumption fixed. Although this is quite effective, the effect on grinding efficiency requires more investigation.

Related to grinding efficiency, it is possible to list three key operational parameters: energy consumption, throughput, and product size. Regarding the operational cost of gravity induced stirred mills, it can be divided into energy consumption, media replacement and liner replacement. In this context, the liner costs itself represents about 10% of operational costs of the mill. Secondly, in the current wear compensation procedure, liner conditions intensify grinding media consumption that represents about 40% of total operational costs. As mentioned above, the screw surface area reduces due to wear, affecting energy consumption and grinding mechanisms that directly affects product size. In addition, and due to the current compensation method, liner wear increases mill filling and consequently affects electrical power consumption, which is the largest operational cost. Finally, liner wear affects maintenance practices and equipment availability.

To conclude, the screw liner wear is directly or indirectly related to all operational cost, such as key production parameters. However, the understanding of the screw liner wear is not very well known yet (Radizizewski, 2017).

## 2.3.References

Allen, J. & Noriega, R., 2011. *Screw liner replacement in a VERTIMILL® grinding mil—determining best practice.* Antofagasta, Chile: 8th Internacional Mining Plant Maintenance Meeting.

Eirich, 2018. *Brochure: EIRICH Tower Mill - Vertical agitated media mill.* [Online] Available at: https://www.eirichusa.com/products/towermills/tower-mill-vertical-ag-med-mill. [Access in 27th July 2020].

Esteves, P. M. et al., 2018. *Predictive modelling of vertical stirred mills liner wear using vibration signature analysis.* Cape Town, 11th International Comminution Symposium.

Hasan, M., 2016. Process Modelling of Gravity Induced Stirred Mills. Volume Doctoral thesis at The University of Queensland.

Mazzinghy, D. et al., 2018. *Qualitative analysis of the screw liner wear prediction in vertical stirred mills by the discrete element method.* Cape Town, 11th International Comminution Symposium.

Metso, 2017. *Blog: When to change Vertimill™ liners and how to do it safely!*. [Online] Available at: https://www.metso.com/blog/mining/blog-when-to-change-vertimill-liners-and-how-to-do-it-safely/. [Access in 17th September 2019].

Morrison, R. D., Cleary, P. W. & Sinnott, M. D., 2009. Using DEM to compare energy efficiency of pilot scale ball mill and tower mills. *Minerals Engineering*, Volume 22, pp. 665-672.

Palaniandy, S., Halomoan, R. & Ishikawa, H., 2018. *Shifting the comminution workload from the primary ball mill to towermill circuit.* Brisbane, AusiMM, pp. 29-31.

Radziszewski, P. & Moore, A., 2017. Understanding the effect of pressure profile on stirred mill impeller wear. *Minerals Engineering*, pp. 54-59.

Sinnott, M., Cleary, P. W. & Morrison, R., 2006. Analysis of stirred mill performance using DEM simulation: Part 1 - Media motion, energy consumption and collisional enviroment. *Minerals Engineering*, Volume 19, pp. 1537-1550.

# CHAPTER 3 - AN ALTERNATIVE STRATEGY TO COMPENSATE FOR SCREW WEAR IN GRAVITY INDUCED STIRRED MILLS

## 3.1. Introduction

Concerning operational strategies regarding wear compensation, the current practice is to continuously increase mill filling during the liner wear lifecycle. This is performed with the aim of keeping power draw stable during the complete liner lifecycle. The mills mostly have fixed speed motors, hence control using speed adjustment is usually not possible. At the start of the liner lifecycle, a fraction of the screw height is above the charge level. By increasing filling, the upper parts of the mill are activated and so loss of grinding energy can be compensated for as the lower portion of the screw wears. Based on this, the aim of this paper is to evaluate how grinding is affected by screw liner wear, using test work conducted with a batch gravity induced stirred mill at a laboratory scale, with three different screws that simulate sequential stages of wear. The performance evaluation is based on the Size Specific Energy (SSE) approach, as described in the work of Ballantyne, Peukert & Powell (2015).

The results include a preliminary evaluation of two strategies for compensating for liner wear effects. A better understanding of this can affect operational procedures, maintenance plan, equipment reliability and energy efficiency.

## 3.2. Methodology

A batch gravity induced stirred mill of approximately 25 L chamber capacity, with a diameter of 380 mm and height of 200 mm, loaded with 17 mm diameter chrome steel balls as grinding media, as used by Hasan et al (2017), was used to conduct test work. An itabirite iron ore sample with a top size of 212 microns was tested. The size distribution of the feed sample was obtained using standard test sieving, as shown in Figure 3.1 - PSD of feed material used for test work (Adapted from Esteves et al., 2019).

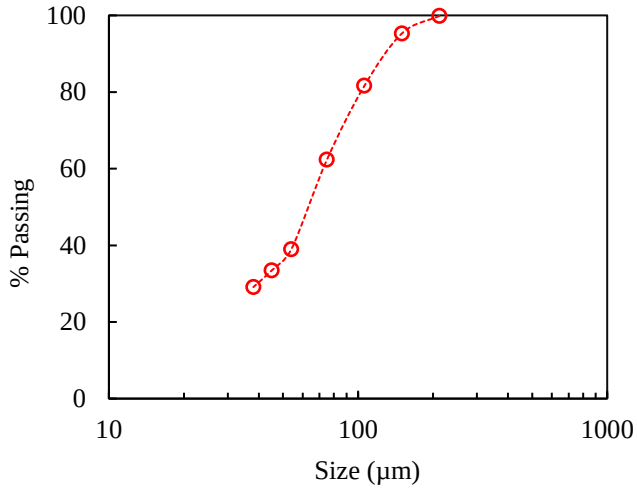


Figure 3.1 - PSD of feed material used for test work (Adapted from Esteves et al., 2019).

The solids concentration was fixed at 65%, ball filling at 80% and torque and speed were measured at a 10 Hz sampling frequency. Torque and speed were calibrated before test work to ensure the reliability of the measurements. Speed selection was based on an equipment database presented by Mazzinghy et al. (2017), for the relation between screw speed and screw diameter, and adapted by Esteves (2019), as shown in Figure 3.2.

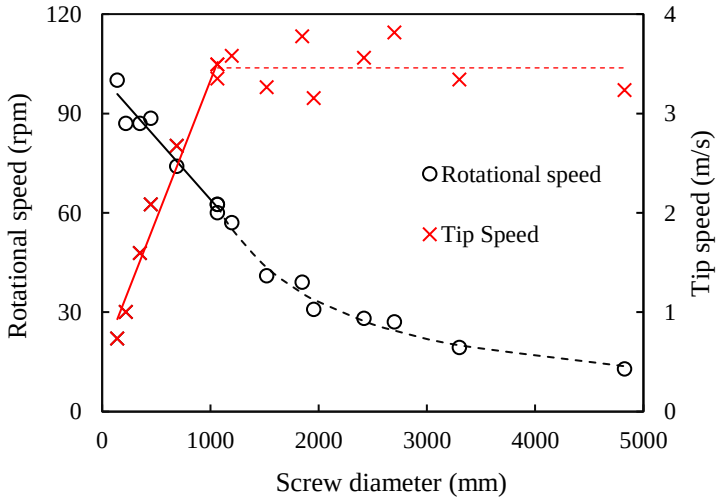


Figure 3.2 - Relation between screw diameter and rotational speed for gravity induced stirred mills (Esteves, et al., 2019).

For screw diameters greater than one meter, the trend seems to follow a fixed tip speed relationship. However, for smaller diameters tip speed is approximately proportional to diameter. Based on the equipment dataset, the following model given by Equations 3.1 and 3.2 was used:

$$\omega = \begin{cases} -37d + 101;\ d < 1 \\ \dfrac{66}{d};\ d \geq 1 \end{cases} \tag{3.1}$$

$$v = \begin{cases} 2.8d + 0.54;\ d < 1 \\ 3.46;\ d \geq 1 \end{cases} \tag{3.2}$$

Where $d$ = screw diameter (m), $\omega$ = rotational speed (rpm) and $v$ = tip speed (m/s). For the laboratory mill, the resultant screw speed was 88.4 rpm.

Different screw wear stages and fillings were tested to simulate the industrial operational procedure that is used to compensate for wear. In this context, three different screws were used to simulate different stages of wear: new screw, half worn and fully worn. The designs were based on the wear profile obtained by Mazzinghy et al. (2018) based on DEM simulations and qualitatively compared to industrial observations. Designs and pictures are shown together in Figure 3.3. Note the progressive reduction in screw diameter at the base.

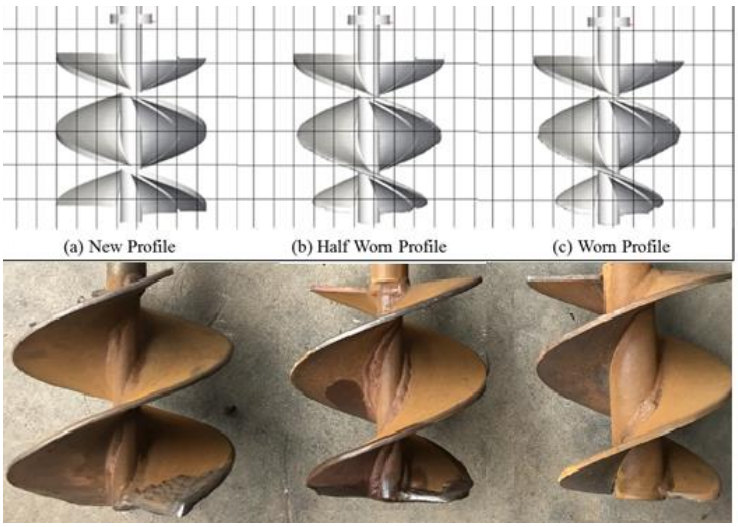


Figure 3.3 - Wear profile obtained by DEM (above) and the respective screws manufactured for laboratory scale tests (below).

The tests were performed with a fixed grinding time at 60 min. The whole mill content was extracted, the slurry was filtered, dried and a rotary splitter was used for obtaining a representative sample. The representative sample was firstly wet screened using a 38 µm sieve. The material above 38 µm was then dried and sizing was performed using a √2 series standard sieve, with a 212 µm top size and using a Rotap shaker for 15 min.

The basis for comparison was taken as the new screw with an 80% filling. For the case of half and fully worn screws, two filling conditions were tested: constant filling (CF) at 80% and an over filling value corresponding to constant power (CP), as shown in Table 3.1 and Figure 3.4.

Table 3.1 – Summary of Test Parameters

| **Test ID** | **New Screw** | **Constant Power (CP)** | | **Constant Filling (CF)** | |
|---|---|---|---|---|---|
| | **0%** | **CP-50%** | **CP-100%** | **CF-50%** | **CF-100%** |
| Wear stage | 0% | 50% | 100% | 50% | 100% |
| Filling | 80% | 92% | 95% | 80% | 80% |

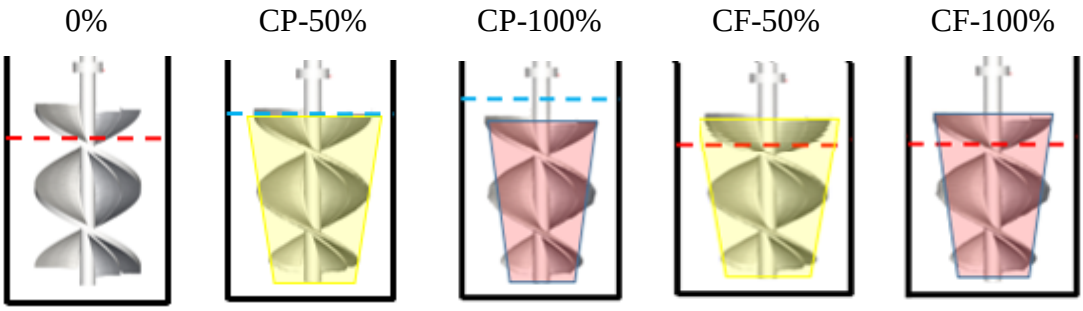


Figure 3.4 - Schematic of test conditions with different wear stages and filling conditions.

The first test corresponds to a new screw with 80% filling, which is defined as the base case (0% screw wear). Two tests considered the constant power (CP) condition, with 50% and 100% of wear stage. In this sense, tests CP-50% and CP-100% corresponds to the current methodology of keeping power constant during the liner lifecycle by increasing mill filling. This means they are conducted with constant power and fillings over 80%,

for both half worn and fully worn screws. The last two tests were performed with constant filling (CF), at 50% and 100% of screw wear stage, and are indicated as CF-50% and CF-100%. They were performed to verify grinding efficiency under constant filling during different stages in the liner lifecycle. This means they use half worn and fully worn screws with 80% filling fixed.

The importance of maintaining a constant interstitial filling must be emphasised in comparative work of this nature. As established by Powell and Mainza (2006), allowing the solids interstitial filling to vary in comparative test work invalidates the results. A consequence is that the amount of ore in the tests varies with the volumetric ball filling.
The performance evaluation was based on specific energy (SE) and particle size distribution (PSD), which were used to calculate the SSE. The SSE represents the energy required to generate a unit quantity of new fine material, based on a defined marker size. It enables proper benchmark and comparison of grinding performance between equipment (Ballantyne, Peukert & Powell, 2015). The SSE can be calculated using different marker sizes that should be chosen accordingly. By using different marker sizes, the comminution performance can be assessed independent of particle size fineness and PSD shape (Ballantyne, 2019). As proposed by Palaniandy (2018), the marker size of 25 μm and 38 μm can both be used to assess the efficiency of gravity induced stirred mills. Based on that, a 38 μm marker size was selected for evaluation of SSE. The SSE is calculated, as shown in Equation 3.3:

$$SSE_{38}\left(\frac{kWh}{t}\right) = \frac{SE}{\%\ \text{New} - 38\mu m\ generated} \tag{3.3}$$

## 3.3. Results and discussion

The experimental conditions were conducted at defined levels of filling and power draw. A plot between power and filling was used to establish the correlation between filling and power for both half and fully worn screws. This relationship was obtained based on preliminary test work, which consisted of measuring torque at different fillings for each screw using only grinding media and water, as presented in Figure 3.5.

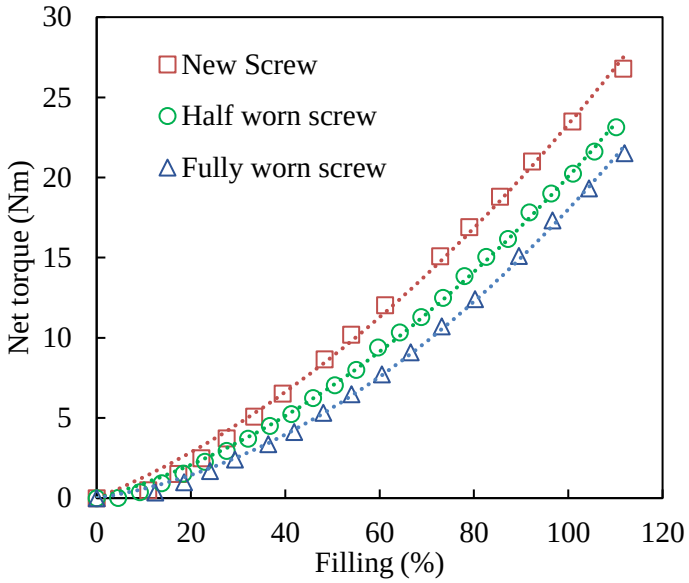


Figure 3.5 - Relation between net torque and filling at different wear conditions for the agitator screw with the fixed speed at 88.4 rpm.

Table 3.2 – Summary of Test Parameters and Results

| **Test ID** | | **New Screw** | **Constant Power** | | **Constant Filling** | |
|---|---|---|---|---|---|---|
| | | **0%** | **CP-50%** | **CP-100%** | **CF-50%** | **CF-100%** |
| Operational Parameters | Wear stage | 0% | 50% | 100% | 50% | 100% |
| | Filling | 80% | 92% | 95% | 80% | 80% |
| Test Results | Power (kW) | 0.15 | 0.15 | 0.15 | 0.13 | 0.11 |
| | SE (kWh/t) | 17.8 | 15.2 | 14.8 | 14.1 | 13.4 |
| | New -38µm (%) | 55.4 | 47.5 | 41.4 | 46.3 | 43.1 |
| | SSE 38 (kWh/t) | 32.1 | 32.1 | 35.9 | 30.4 | 31.2 |

Based on the torque curves, the test conditions were selected as summarized at the top part of Table 3.2. The speed was fixed at 88.4 rpm, interstitial filling was fixed at 100% and solids concentration were kept constant at 65%.

Based on speed and torque measurement, the SE was calculated for each test. Particle size distributions were obtained from screening and are shown in Figure 3.6. It is noticeable that mill product gets coarser with wear. The SE and PSD were used to calculate the SSE and the obtained results are presented in the bottom part of Table 3.2.

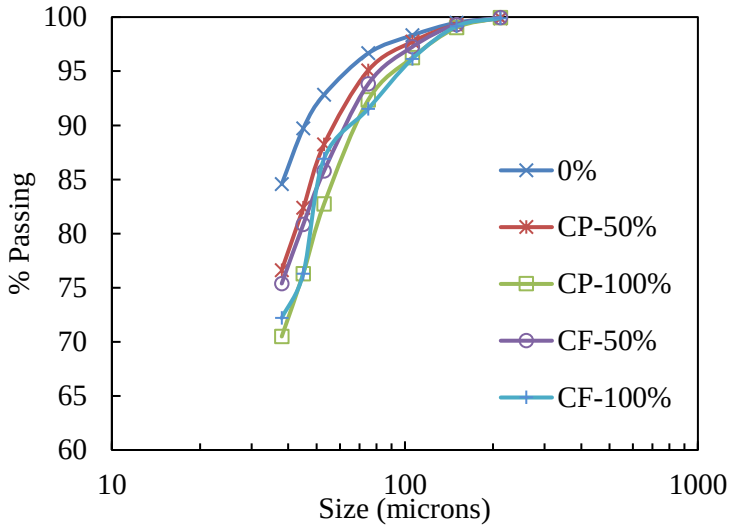


Figure 3.6 – PSD of mill products.

Figure 3.7 shows the relation between specific energy and new -38 µm material for the tests. The linear trend presents an average relation between specific energy and fines generation, providing an indication of how energy is being used to generate material below the selected marker size. Considering the SSE = 100/gradient, then, SSE = 100/3.098, the average SSE = 32.2 kWh/t-38 µm for all the tests. Points above the trend indicate a better energy performance, thus creating greater fines generation. Conversely, a point below the trend indicates that comminution becomes inefficient and a greater amount of energy would be necessary to maintain fines generation. The constant filling tests are both above the trend, with CF-50% being the most efficient with SSE of 30.4 kWh/t-38 µm. For the constant power test, the efficiency falls off to a far higher 35.9 kWh/t-38 µm for the fully worn liner (CP-100%). This indicates that operating at constant filling can slightly improve energy performance at half of liner lifecycle, while operating with constant power can decrease fines generation for the fully worn screw, in a less efficient comminution behaviour.

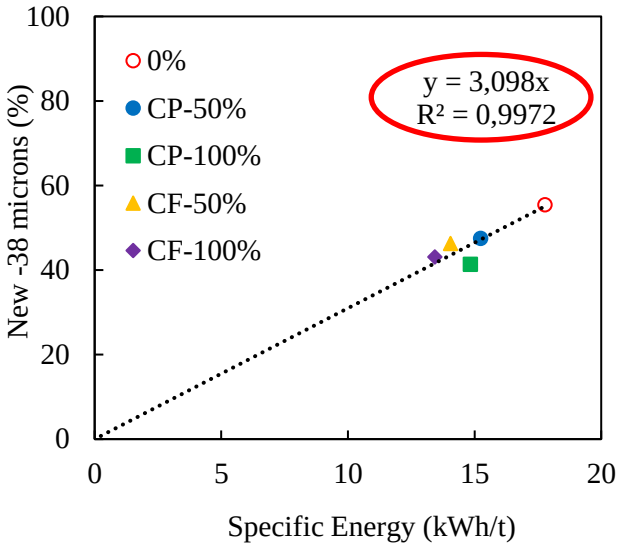


Figure 3.7 - Generation of new -38µm in relation as a function of specific energy.

Figure 3.8 shows the specific energy, new - 38 microns and SSE for the tests.

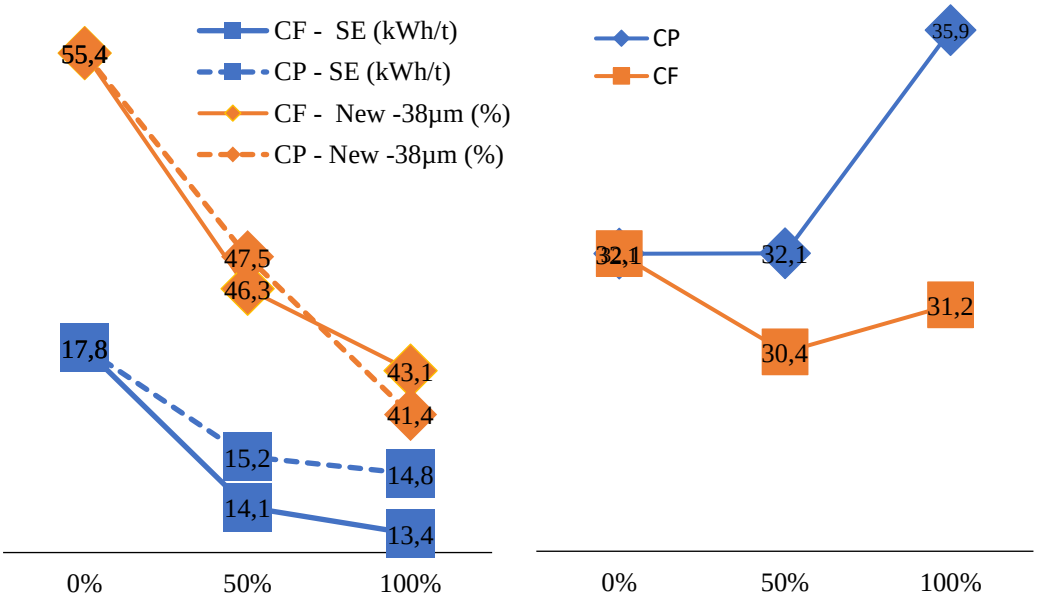


Figure 3.8 – Energy consumption, production and efficiency as a function of screw wear. Left: Specific Energy (SE) and New -38 microns

Right: Size Specific Energy (SSE).

Considering the new screw as a base case for comparison, it can be noted that SE decreases for all performed tests. Regarding tests with constant power (CP-50% and CP-100%), this happens due to the increase in the quantity of ore, to maintain a constant

interstitial filling. As for batch test work, the SE is the ratio between power consumption and ore amount, the SE decreased due to the filling increase. For tests with constant filling (CF-50% and CF-100%), power consumption reduces with screw wear assuming that filling, interstitial filling, and ore amount are fixed. As the screw wears, the surface area decreases and the contact with grinding media reduces, thus affecting media motion, and consequently, required torque. Therefore, the SE reduction is greater for the fully worn screw case operating with fixed filling.

The fines generation, based on the 38 µm marker size, indicates the amount of new material generated below the selected size. The fines generation decreases as the screw wears, independent of operational procedure, which means the product gets coarser. For constant power, this is due to both the reduced SE and increased SSE. For the constant filling, this coarsening of the product despite the higher milling efficiency is due to the lower SE.

In relation to the SSE, the results indicate that wear presents contrary effects for the two different operational procedures. While the SSE increases with wear, for the fixed power condition, there is an indication of SSE reduction when operating with fixed filling conditions over the complete liner lifecycle.

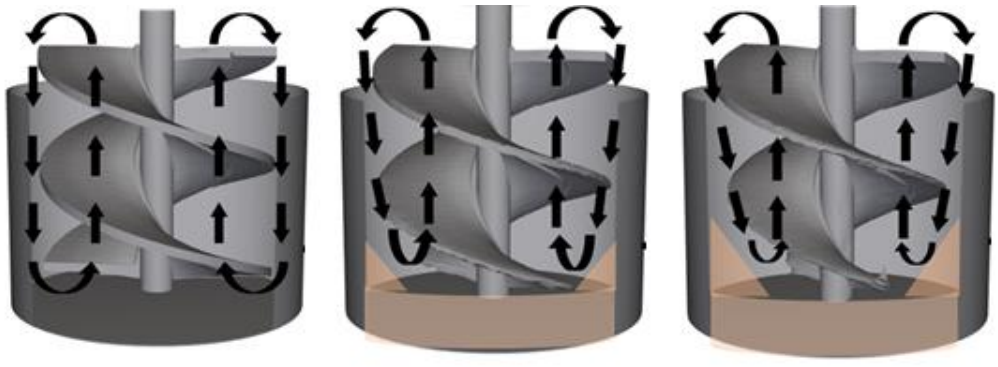

Figure 3.9 - Particle flow and the dead zone in the gravity induced stirred mill at different wear stages. Left: New screw – Middle: Half worn screw – Right: Fully worn screw.

In relation to product PSD, there is a clear indication for obtaining a coarser product at worn conditions. Figure 3.9 shows conceptual images of the particle flow and the dead zone in the gravity induced stirred mill, at different wear stages.

The material flow, indicated by the black arrows, is clearly affected by wear, especially at the bottom part of the mill, where wear is more intensive. Due to the reduction in the bottom screw surface area, segregation occurs at the bottom part of the mill, and particle flow reduces, such as media motion. This is defined as the dead zone effect and the segregated, static bed of particles are known as hold up material. The dead zone affects breakage and creates a coarser product size within the hold-up fraction. In this batch mill test work, the entire contents are removed and sized, so the coarser material retained in the dead zone has a significant influence on the overall product size distribution. For continuous operation over an extended period, this hold-up would be an insignificant fraction of the total product, so this effect would be negligible.

The filling apparently also affects the dead zone. During the test work, it was noticeable that hold-up material was strongly compacted for worn screws cases. This effect was intensified when operating at high filling conditions, for obtaining constant power. In these cases, a greater handling effort was necessary to clean the mill content after batch grinding. This might be explained by a pressure increase above the particles, thus intensifying particle segregation at the dead zone.

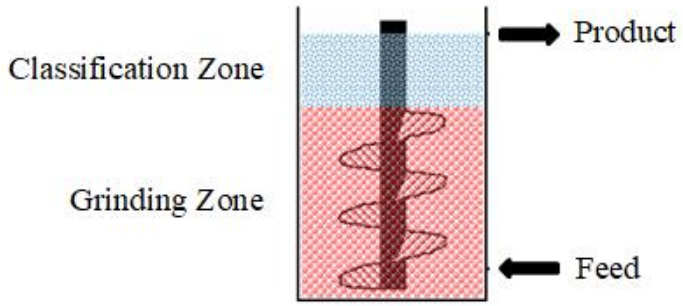


Figure 3.10 - Grinding (red) and classification (blue) zones in the gravity induced stirred mill (Adapted from Mazzinghy, 2012).

The filling increase can also have an impact in the classification zone, at the top part of the mill. Figure 3.10 shows the classification zone in blue, at the top part of the mill and the grinding zone in red, at the bottom (Adapted from Mazzinghy, 2012).

In the classification zone, coarse particles return to the grinding zone while fine particles can overflow to discharge. As defined by Hasan (2016), the operational factors affect the particle classification cut size in the classification zone, at the top part of the mill. The filling increase under the constant power strategy can impact the interaction between the grinding and classification zones and thus it is necessary to evaluate this effect when operating in continuous mode. The bottom or top feed configurations can also present an influence on both dead zone effect and the classification zone. This topic requires further investigation in continuous laboratory or industrial test work.

To summarize, the results indicate a better energy utilization when operating with fixed filling. In addition, segregation in the bottom part of the mill, or the dead zone effect, was apparently intensified when operating with constant power and greater media fillings. However, a better understanding of the effects of wear on grinding efficiency is necessary. This understanding can be used for an economic evaluation of the best time to change liners, such as the best operational procedure, taking into account media consumption, liner lifecycle and energy consumption.

## 3.4. Conclusions

The current procedure to compensate the screw liner wear is to keep electrical power draw constant by increasing mill filling during the liner lifecycle. The basic idea is to activate upper parts of the mill to maintain grinding, once the screw liner wear decreases media motion in the bottom parts of the mill which wears the most. This paper aimed to provide an initial evaluation of the effects of the wear of the screw liner on grinding efficiency by using laboratory scale test work. A comparison between two different operational procedures was performed: operating with fixed power and with fixed filling.

The comparison was based on specific energy and particle size distribution. In preliminary test work, a relation between torque and filling was established for different wear stages of the screw, with tests with only water and grinding media. It was conclusively shown that net torque decreases with wear. Based on this curve, the operational filling for constant power tests were defined and wet grinding test work was performed with an itabirite iron ore sample.

The batch milling results demonstrate that specific energy decreases with wear evolution, and the product gets coarser. It is acknowledged that this is a specific result of batch testing. The segregation of material in the bottom part of the mill exacerbates the coarsening of the product in batch milling tests. This is known as the dead zone effect, which minimizes grinding in this area thus creating a hold-up of material. The dead zone effect apparently is influenced by both wear stage and filling condition. The interaction between grinding and classification zone can also be affected, thus impacting equipment performance. These relations require further investigation which might be better understood by conducting continuous test work.

SSE was used to evaluate and compare the grinding performance between the two operational procedures. The results indicate a tendency for the SSE to decrease when operating under fixed filling conditions. Although the results indicate a better energy utilization when operating with constant filling, it is important to bear in mind that the test work was performed at laboratory scale and batch mode, and no scale up was performed to correlate with industrial and continuous performance.

To summarize, the paper raises discussion about the current procedure to compensate for wear of the screw in gravity induced stirred mills, by increasing operational filling. A controlled methodology was developed for the quantitative comparison of operating strategies as the screw wears. It was established that the grinding efficiency improves when maintaining a constant filling whereas it decreases when running at a fixed mill power. The results indicate that an improved understanding of how to compensate for screw wear can present an opportunity for energy saving. Although clear relationships of energy efficiency are obtained, further evaluation of operating conditions is

recommended. Test work at a fixed specific energy is recommended by conducting continuous operating tests at laboratory scale. Additionally, industrial tests with continuous sampling is required, for a conclusive comparison between operating with fixed power versus operating with fixed filling. Based on the promising results of maintaining a constant mill filling, changing mill speed presents an interesting possibility for future evaluation. This can be initially assessed at laboratory scale as an extension of the current work.

## 3.5. References


Ballantyne, G. (2019). Assessing comminution energy efficiency with the Size Specific Energy (SSE) approach. In Proc. 16th European Symposium on Comminution & Classification (ESCC 2019), September 2019, Leeds, UK.

Ballantyne, G., Peukert, W., & Powell, M. (2015). Size specific energy (SSE) - energy required to generate minus 75 micron material. International Journal of Mineral Processing, 136, pp. 2-6.

Esteves, P., Mazzinghy, D. B., Hilden, M., Yahyaei, M., Powell, M., & Galery, R. (2019). Qualitative evaluation of the grinding efficiency of a gravity induced stirred mill using the size specific energy approach. In Proc. 16th European Symposium on Comminution & Classification pp. 101-102. Leeds, UK. Edited by Mojtaba Ghadiri, Sadegh Nadimi, Mehrdad Pasha.

Hasan, M. (2016). Process Modelling of Gravity Induced Stirred Mills. Doctoral thesis submitted at The University of Queensland.

Hasan, M., Palaniandy, S., Hilden, M.H. and Powell, M.S., 2017. Calculating breakage parameters of a batch vertical stirred mill. Minerals Engineering, Vol. 111, pp. 229–237

Mazzinghy, D. (2012). Methodology for scale up and simulation of vertical mills. Doctoral thesis submitted at Universidade Federal de Minas Gerais (*in Portuguese*).

Mazzinghy, D., Esteves, P., Faioli, D., Andrade, K., & Ribeiro, F. (2018). Qualitative analysis of the screw liner wear prediction in vertical stirred mills by the discrete element method. 11th International Comminution Symposium, Cape Town.

Mazzinghy, D., Lichter, J., Schneider, L., Galery, R., & Russo, J. (2017). Vertical stirred mill scale-up and simulation: Model validation by industrial samplings results, Minerals Engineering, Vols. 103-104 pp. 127-133. Elsevier.

Palaniandy, S., Halomoan, R., & Ishikawa, H. (2018). Shifting the comminution workload from the primary ball mill to towermill circuit. 14th AusIMM Mill Operators' Conference pp. 29-31. Brisbane, AusIMM.

Powell, M.S., and Mainza, A.N. 2006. Extended grinding curves are essential to the comparison of milling performance. Minerals Engineering, Vol. 19, no. 15, pp 1487-1494. DOI: 10.1016/j.mineng.2006.08.004

# CHAPTER 4 - USING DEM FOR THE UNDERSTANDING OF GRAVITY INDUCED STIRRED MILLS SCREW LINER WEAR

## 4.1. Introduction

In this chapter, DEM simulations are used to predict wear behaviour of a gravity induced stirred mill, in reduced scale. The results are then compared with industrial measurements performed in the Minas Rio Project, an iron ore beneficiation plant of Anglo American which is in the southeast region of Brazil.

## 4.2. Discrete Element Method (DEM)

Computational simulations based on DEM made many contributions to the mineral processing industry since its first application by Cundall (1979). Lately, the method was applied in the comminution area by Mishra and Rajamani (1992) for the simulation and modelling of tumbling ball mills. According to Weerasekara (2013) since the last two decades, the DEM became an essential tool to help design, optimisation, and modelling of comminution devices. More recently, there is also an increasing interesting in applying the method for the prediction of liners and lifters wear, such as its effects on load behaviour (Cleary et al., 2010).

As there is no available information about how to determine and quantify wear for vertical stirred mills, the approach is based in what is presented for other grinding equipment. The understanding of liner and lifters wear, especially in tumbling mills, is not a new subject in the area and several papers are found addressing this issue.

In the specific case of wear evaluation, Cleary (1998) proposed a method that used DEM to predict liner wear rates and distribution in a 5 m diameter ball mill. With a similar approach, Cleary (2001) evaluated wear in a 3D slice of a SAG mill and, finally, Cleary (2006) performed an evaluation and comparison between wear in tower and pin mills. Kalala (2004) used DEM to estimate adhesion, abrasion, and impact wear in dry ball mills with further validation with industrial wear measurement. Later, Kalala (2005) validated

the use of DEM for wear prediction in mill liners by comparing normal and tangential forces between experimental data and DEM simulations. More recently, Cleary (2010) simulated liner wear evolution in a Hicom Mill and was able to convert DEM abrasion measurements in a wear rate measurement that was calibrated with experimental data. Boemer (2017) established a generic wear prediction procedure applying DEM to a 3D ball mill and validated the results with experimental data obtained in a 5.8m diameter industrial cement ball. Finally, Xu (2018) obtained a numerical prediction of wear in SAG mills using DEM simulations that were quantitatively validated by experiment data available in other researches. In fact, the use of DEM for wear prediction in SAG mills reached such a high level that is has recently been used to evaluate operational strategies to account for liner wear (Cleary, 2018).

For the specific case of gravity induced stirred mills, DEM was first applied by Sinnott (2006) and Clearly (2006) to investigate the relative performance of stirred mills with two different agitator designs. The paper analysis media flow, energy absorption, flow structures, wear, mixing and transport efficiency and allows a good and wide understanding of the performance of stirred mills. For the case of the screw agitator media motion is a simultaneously lifting and circulating movements inside the equipment. The simulations indicate that the collisional energy associated with media motion is mostly dominated by shear. In relation to media-media and media-liner interactions, shear energy represents more than three times impacts energy. Based on shear energy absorptions, the author infers that the equipment wear is dominated by abrasion and is more intensive on the outer radial edge of the screw. In a slightly different approach, Morrison (2009) used DEM to compare the energy efficiency between ball and vertical stirred mills in pilot scale and proposed that the higher efficiency associated with the stirred mill can be explained by analysing energy spectra associated with collisions frequencies inside the mill. Therefore, the higher energy efficiency of the vertical mill can be explained by the presence of a great number of contacts of low energy, mostly associated with shear. Sinnott (2011) applied DEM to understand how flow and energy are affected by media shape in stirred mills, concluding that grinding performance tends to deteriorate strongly when using non-spherical media. By analysing rates of shear power absorption, the author

also proposes that the increase in non-sphericity of the media can significantly intensifies the screws wear.

In a different approach, Sinnott (2011) evaluated slurry transport inside the mill using the SPH (Smoothed Particle Hydrodynamics) method and based on DEM simulations. Allen and Noriega (2011) applied DEM (Discrete Element Method) with SPH to understand the screw liner wear. The results demonstrate that shear power is more intensive at the screw outside edges and at the bottom of the mill. This explains why the screw wears from the outside to inside and from the bottom to the top, such as have been seen in industry. In addition, results indicate that shear power is exponentially related to screw diameter and consequently, worn screws tends to wear slower as they present smaller diameters. Based on this description, it is possible to note that although DEM is being widely applied in the understanding and evaluation of vertical stirred mills performance, the liner wear topic is still superficially approached.

To summarize, the use of DEM to evaluate liner wear in tumbling mills came from a quantitative evaluation and evolved to a different level. Nowadays, DEM can predict and quantify wear in tumbling mills, being used in the optimization of materials and operational parameters. Unfortunately, for the case of the vertical stirred mills, the studies are still preliminary and qualitative. To solve this issue requires more in-depth studies and validation with experimental data.

## 4.3. Wear Measurement

Empirical evaluation of wear is an important tool for validation and calibration of modelling techniques, such as performed by Kalala (2004), Radizizewski (2010), Cleary (2010), Powell (2011), Boemer (2017) and Xu (2018) for several types of grinding equipment. However, there are few available information about how to determine and quantify wear for vertical stirred mills. Based on that, the approach is based on what is presented for other mills.

The understanding of liner and lifters wear in tumbling mills is not a new subject in the area and several papers are found addressing this topic. In the case of tumbling mills, the wear profile is commonly estimated in two dimensional methods, taking the assumption that wear has a uniform profile. More recently, with the advent of new technologies, it is easier to perform three dimensional measurements and there are also highly sophisticated devices available (Boemer, 2017). Three dimensional measurements are being widely used to calculate wear on the surface of liners in grinding equipment, and the technique was successfully used for SAG mills (Yahyaei, 2009; Xu, 2018) and for a Hicom Mill (Cleary, 2010).

## 4.4. Objective

The constant contact between both grinding media and slurry, with the screw liners, causes continuous liners wear. The aim of the study presented in this chapter is to provide a better understanding about wear patterns and its effects on grinding, during a liner lifecycle. The study takes in account the current operational procedure to compensate wear by increasing grinding media filling in the mill.

## 4.5. Methodology

### 4.5.1. DEM Model Setup

DEM simulations were performed using the Rocky 4.2.2 software. A 1/10th scale version of the VTM-1500 was simulated. Table 4.1 and Figure 4.1 shows geometry dimensions and screw design.

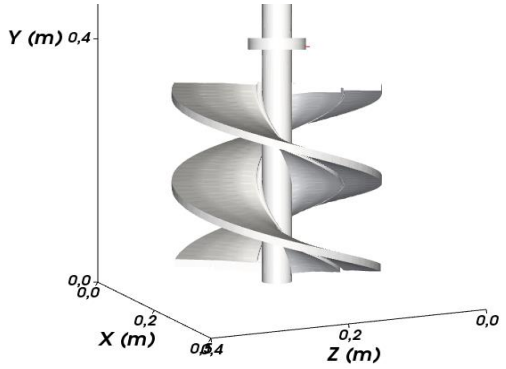


Figure 4.1 - Vertimill 1/10 scale of the VTM-1500.

Table 4.1 - Dimensions and operation parameters of VTM-1500 and its scaled-down version considered in the DEM simulations

| Mill | VTM-1500 | Scaled down (Simulated) |
|---|---|---|
| Scale | 1/1 | 1/10 |
| Screw Diameter (mm) | 3300 | 330 |
| Ball load (kg) | 80000 | 80 |

The contact model used in the simulations were Linear Hysteresis for normal forces and Elastic Coulomb for tangential forces (Rocky, 2018). Table 4.2 summarizes contact model parameters and materials properties setup used for the simulation.

Table 4.2 - Material and contact parameters used in the DEM simulations

| Variable | Value |
|---|---|
| Young's Modulus (Pa) | $1x10^{11}$ |
| Density (kg/m3) | 7850 |
| Poisson's Ratio | 0.3 |
| Coefficient of Static Friction (particle-particle) | 0.7 |
| Coefficient of Dynamic Friction (particle-particle) | 0.7 |
| Coefficient of Static Friction (particle-geometry) | 0.3 |
| Coefficient of Dynamic Friction (particle-geometry) | 0.3 |
| Restitution coefficient | 0.3 |

The simulation was performed considering only grinding media in the grinding environments, in the absence of slurry and ore particles. This can be acceptable for process where the ore contributions for breakage are negligible, such as in the gravity induced stirred mills, where breakage mechanisms are mainly created by the energy involved in grinding media collisions. However, it is also known that grinding media

interaction is affected by ore and slurry properties. Consequently, both solids concentration and particle size distribution can affect power consumption and grinding performance. More recently, Oliveira (2020) applied a mechanistical model to predict product size distribution by using DEM simulations. The simulation considered grinding media as the mill charge, in the absence of ore and slurry. By taking into consideration different proportions of shear power involved in inter particle collision, the model successfully predicted product size distribution of laboratory scale experiment, for different solids concentration ratios.

To approximate the slurry effect in the grinding environment, the shear modulus was reduced, thus making the contact between balls much softer, in comparison to steel-steel contact (Steel: 200GPa). This approximates to the ore and slurry interactions behaviour.

In relation to the mill rotational speed, three different velocities were simulated: 87 rpm, 130 rpm and 190 rpm. The 87 rpm was obtained based on a model for velocity scale-up, as proposed by Mazzinghy (2017) and adapted by Esteves (2019). The model is based on an equipment dataset and consists in a more recent approach for velocity scale up. The 190 rpm is obtained considering a fixed tip speed of 3.5 m/s for the mill agitator. This is the usual method for velocity scale up and was widely applied for reduced scale equipment test work and simulation. The 130 rpm was obtained as an intermediary velocity in between the two scale up approaches.

### 4.5.2. DEM Outputs

During the simulation, the interaction between particles and geometry is individually described by first physical principles, according to the contact model defined. This information is saved during each simulation step and is further used to generate the simulation outputs, such as: particle energy spectra, particle trajectory, particle absolute translational velocity, power consumption and wear design

## 4.5.3. Wear Model

The Archard's wear law, together with the DEM outputs, were used to quantify liner boundary wear. The wear quantification is realized step by step and this information is used to currently update the liner shape during the simulation. The Archard's equation is presented by Rocky (2019) and adapted below, in Equation 4.1:

$$A.dh = K.dw \tag{4.1}$$

Where $A$ = surface area of a boundary element ($m^2$), $h$ = loss in depth (m), $w$ = shear work (J) and $K$ = wear rate ($m^3/J$).

The incremental loss in depth consists in the amount of wear generated in the liner surface. This information is used to currently update the liner shape and volume. The shear work consists in the DEM shear outputs. In this sense, the DEM shear stress results for the interaction between liner and grinding media are used to continuously quantify the boundary wear. The wear factor is defined as the relation between the contact energy and the amount of lost surface. A wear factor of 1 e-6 $m^3/J$ was established for the simulation. This indicated the amount of volume that is lost according to energy amount involved at each contact between grinding media and liner. The increase of this parameters can extremely accelerate wear ratio. Although the use of greater values can accelerate the obtaining of a wear surface, it can also generate unwanted damages in the surface, that are not in accordance with reality. In the opposite, the use of very small factors can bring the need for a very long simulation to obtain representative wear information. In the present case, several values were tested, until the obtaining of a feasible shape for the wear. As a result, it is necessary to adapt simulation and real time.

## 4.5.4. Boundary definition

The boundary definition of the geometrical mesh directly affects the computational cost to run the wear simulation, such as the wear results Figure 4.2 shows the effect of triangle size in mesh refinement. The defining of greater triangle sizes decreases the total number

of triangles and creates a bad refinement for the mesh, decreasing the simulation computational cost. In the opposite, the existence of smaller triangle sizes highly increases the number of triangles, refining the geometrical mesh and causing a representative increase in the simulation computational cost. Figure 4.3 shows the effect of mesh refinement in the wear simulation results.

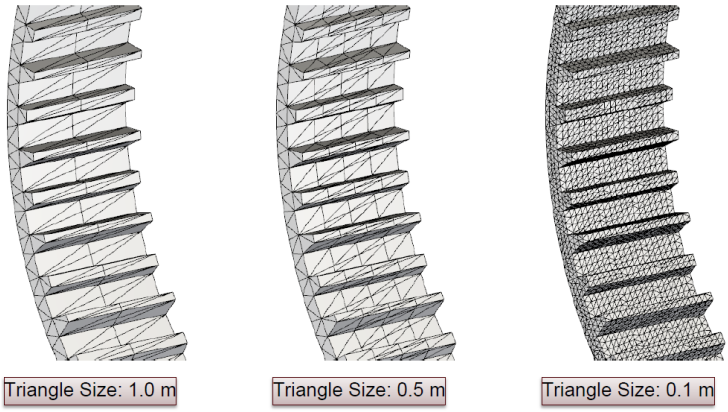


Figure 4.2 - Boundary definition for the geometrical mesh of the wear parts (Rocky, 2017).

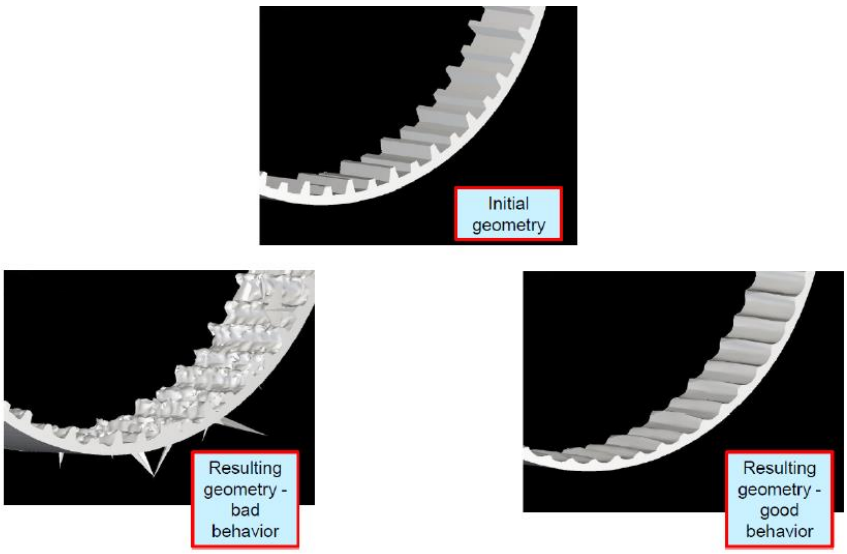


Figure 4.3 - Effect of boundary definition and mesh refinement in the obtained wear pattern (Rocky, 2017).

From the figure, it is possible to note the final wear shape is affected by refinement degree. In this sense, the existence of a more refined mesh brings a better wear resolution

in the final geometry of the object. However, as finer meshes representatively increases computational cost, it is very important to investigate sensitivity of mesh refinement degree, to obtain a reasonable balance between wear resolution and feasibility of computational cost (Rocky, 2018).

## 4.5.5. Industrial wear Measurement

The industrial measurements presented were obtained by Silva (2019) from the regrinding circuit of the Minas-Rio project, that is an iron ore plant from Anglo American located in the southeast region of Brazil. The regrinding circuit is composed of two parallel lines, each one with eight VTM-1500. Regrinding product is specified with a P80 of 36µm, mill capacity as 190t/h per mill and finally, specific energy is established as 5.9kWh/t.

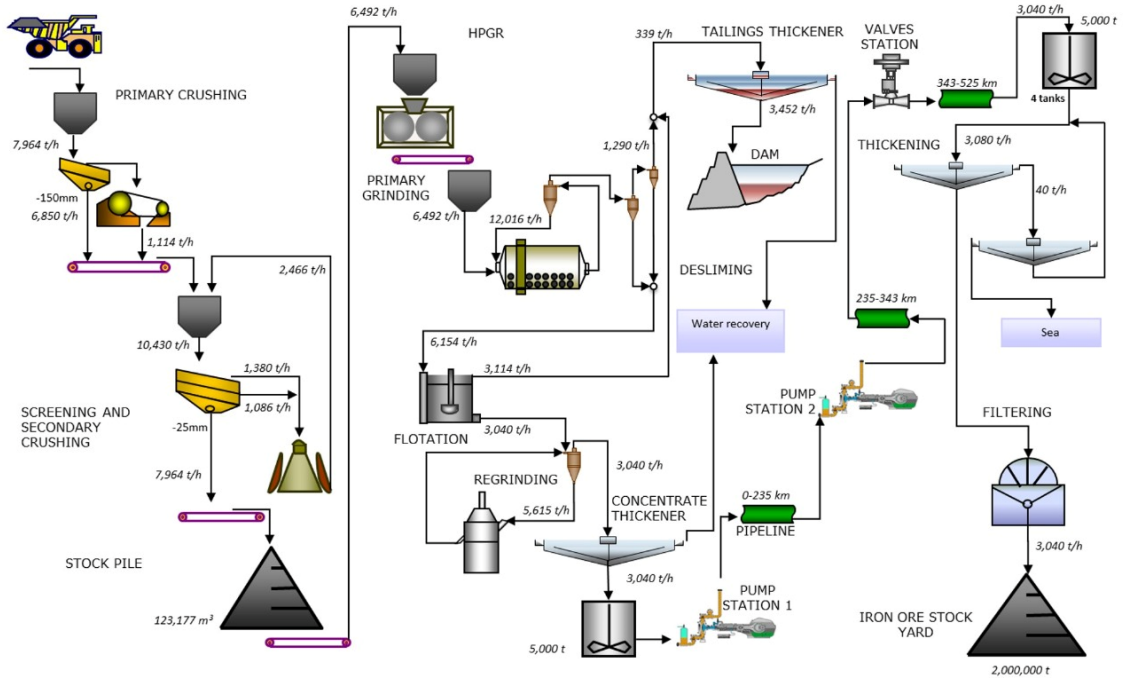


Figure 4.4 - Minas-Rio process flowsheet (Mazzinghy, et al. 2015).

The process flowsheet is indicated in Figure 4.4 and shows that regrinding circuit is located downstream of the flotation plan. Thus, the regrinding plant is fed with concentrate material which tends to present greater stability in relation to density and

solids concentrate. This creates the perfect space to use this data as input for simulation validation.

The wear measurements were performed for the base and intermediate liner parts at three different liner lifetimes: 0h, 1000h, 2000h and 3000h. The measurement was performed using three-dimensional laser scanning technique. Performing the measurement require to complete stop and unload the mill, as shown in Figure 4.5.

Figure 4.5 - Scanning procedure to obtain three dimensional measurement of liner parts. (Silva, 2019).

After unloading the mill, a laser device and a reception sensor are used to capture data that is used to generate a three-dimensional geometry of the worn parts. The generated geometry is then compared with the new liner model, in a coordinate system. The gaps associated with geometrical positions are used to generate a dimensional report and a deviation map, which are later converted into wear quantification.

The wear measurements obtained on the VTM-1500 will be presented and used for the comparison with DEM wear simulations.

## 4.5.6. Wear Model

The wear industrial measurements were compared with the DEM simulation results. For that, three dimensional geometries of the agitator screw were exported at different simulation times. Each geometry was sliced in different liner parts, such as the industrial VTM-1500 design. The Meshlab software was used to calculate volume of base and intermediate worn liners, thus generating a relation between liner volume and simulation time.

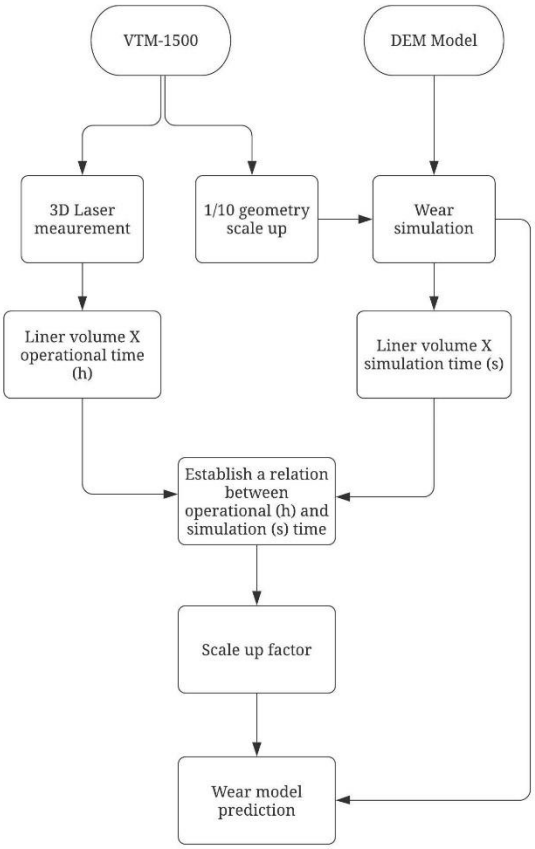


Figure 4.6 – Flowsheet explaining the wear model development based on the DEM model and VTM-1500 equipment.

This result was then compared with industrial wear measurement of the full scale VTM-1500. A liner fitting was established to correlate DEM simulation time (in seconds) and operational time (in hours). This scale up factor was obtained for each simulation, at different agitator velocities. Finally, the scale up factor and wear simulation are

combined, to predict base and intermediate liners wear. The prediction can then me compared with industrial measurement. The explained process is shown in Figure 4.6.

## 4.6. Results and Discussion

Results are divided in four sections: steady state simulation results, wear simulation results, VTM-1500 wear measurements and, finally, the DEM wear model prediction. The steady state simulation results are shown in the initial section and presents results obtained at the beginning of simulation, after a minimum of three mill revolutions and before the beginning of the wear simulation. This is defined as steady state simulation and aims to understand the mill behaviour before wear.

The second section presents results obtained during the wear simulation, after wear parameters were settled. It comprises the evaluation of simulation outputs, such as wear quantification.

The VTM-1500 wear measurement consists in the next stage and is focused on presenting and adapting wear industrial measurements presented by Silva (2019).

Finally, last section comprises the correlation between industrial and simulated wear pattern, such as the presentation of the wear model prediction. This is performed for the three different mill agitator velocities.

### 4.6.1. Steady State Simulation

#### 4.6.1.1. Particle Trajectory

Figure 4.7 shows particle trajectory coloured as a function of particle absolute translational velocity, for the three agitator velocities. A red box was constructed in the surrounding area of the particle trajectory, for the 190 rpm condition. By placing the same box over particle trajectory of the mills operating at 130 rpm and 87 rpm, it noticeable that the top part of the box is not filled with trajectory streaming lines. This means that

media motion height range is reduced when reducing mill velocity. In other words, it indicates that by increasing mill velocity, the upper parts of the mill were activated.

A dashed red line is placed at the bottom part of the mill. It is visible that streaming lines are also reduced in this bottom area. Because of the reduced motion, this area is identified as “dead zone”. The velocity reduction and thus dead zone effect is intensified for reduced mill velocities. This is in accordance with the velocity behaviour at the mill top zone. Based on that, it was verified that agitator rotational velocity has a direct effect on the particle trajectory distribution, over the complete height of the mill.

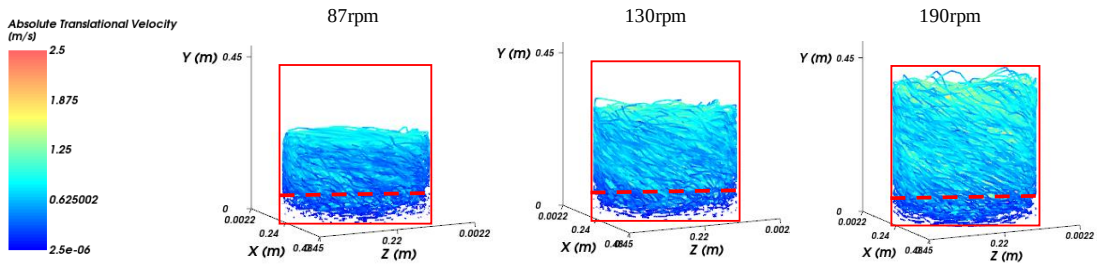


Figure 4.7 – Particle trajectory at different mill rotational velocities.

## 4.6.1.2. Particle Velocity and Power

Figure 4.8 shows particle average translational velocity and simulation power as a function of mill rotational speed.

It is conclusive that both particles velocity and power increases with mill speed. This demonstrate that the agitator rotational velocity influences the mill overall power and grinding media kinetic energy, thus having a direct relation in the energy that can be transferred into breakage mechanisms

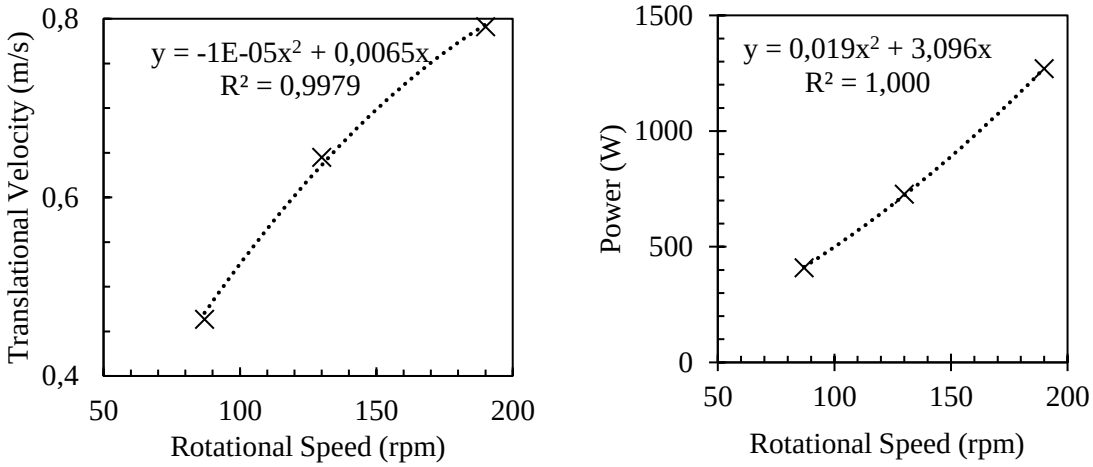


Figure 4.8 – Left: Relation between agitator speed and particle average translational velocity (m/s). Right: Relation between agitator speed and simulation power (W).

## 4.6.1.3. Particle Spectrum

The collision frequency distribution of particle specific energy was plotted for normal and tangential particle contact in Figure 4.9. This represents the collisions statistics for specific energy that are applied to particles per time unit. The x axis indicates the specific energy of contact, which means the amount of energy that is transferred per mass of grinding media. The y axis indicates the number of contacts per unit of time, at each specific energy level.

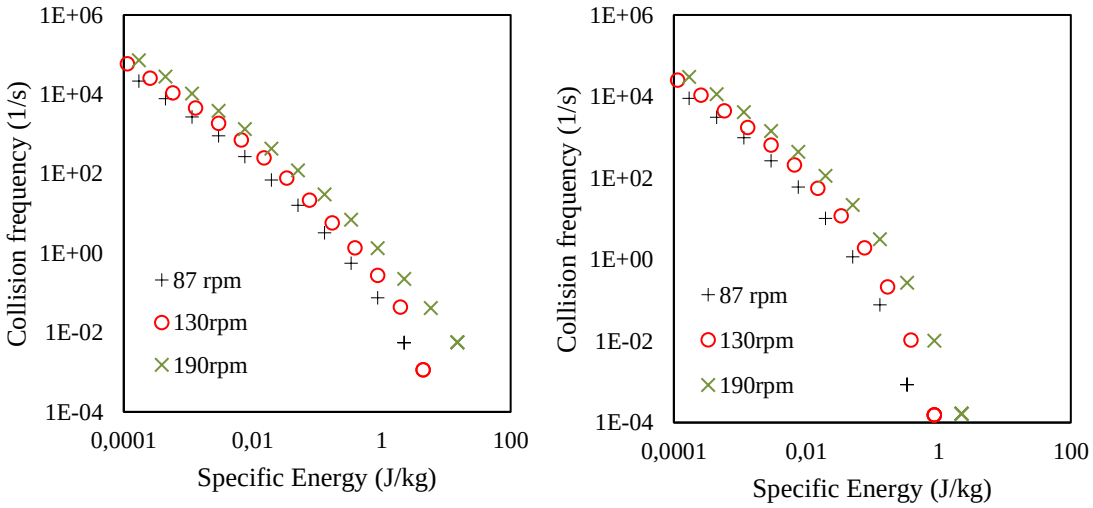


Figure 4.9 – Particle collision spectra for normal (left) and shear (right) contact at different operational velocities.

A wider specific energy distribution is observed for normal contact, in comparison to the shear contact distribution. This means that normal contacts can have a higher specific energy value than shear contacts. In relation to the agitator rotational velocity, higher velocities are associated with a small increase in both collisions frequency and specific energy range. This can be observed for both normal and tangential contacts.

By looking at the relation between energy levels and collision frequency, it is also possible to correlate with breakage behaviour. In this sense, contacts with greater values of specific energy have a higher tendency to overcome the minimum specific energy required for a certain particle to break. This means that contacts of higher specific energy values have a higher probability to cause breakage in a single or fewer number of contacts. However, this can also lead to a non-energy efficient behaviour once this increases the chance to apply more energy than necessary to cause particle breakage. In contrast, smaller values of specific energy might initially lead to particle weakness, instead of direct breakage. Because of that, it can be necessary a larger amount of low specific energy collisions, to cause breakage. At the same time, by applying a greater amount of small specific energy contacts increases the chance to apply the minimum amount of energy that is required for particle breakage.

## 4.6.2. Wear simulation

The wear simulation started after at least three revolutions at steady state condition, thus allowing the wear simulation to be performed under stable conditions.

### 4.6.2.1. Particle Trajectory and Velocity

Figure 4.10 shows the streaming lines associated with particle absolute translational velocity. A red box surrounds media grinding media trajectory for the new liner condition, shown in the left side of the image. Comparing left and right side of the picture it can be noted that red boxes in the right side misses the streaming lines both at top and bottom parts of the mill. This indicate that media motion is negligible in those regions. In the bottom part of the mill, it is noted that the dead zone effect is emphasized by liner wear.

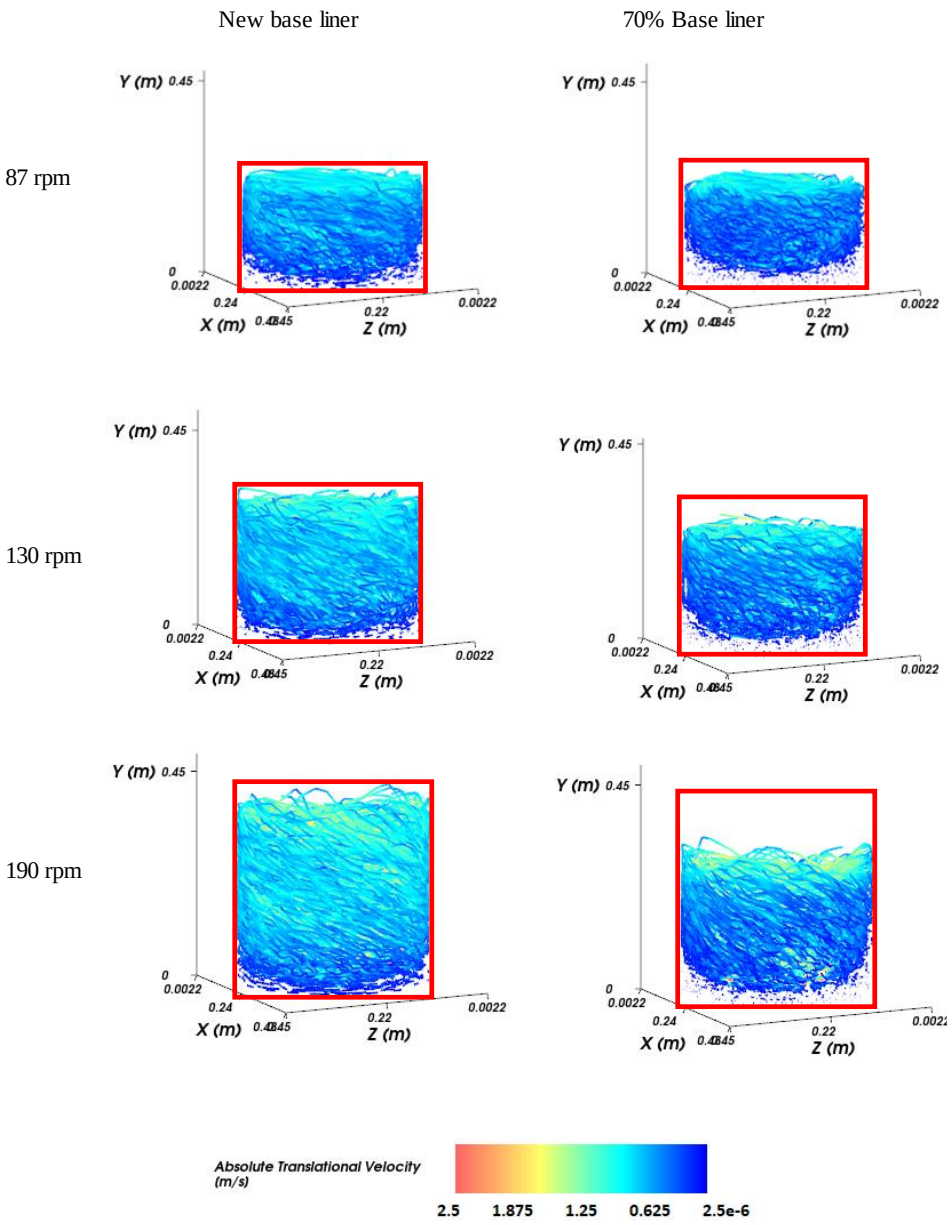


Figure 4.10 – Particle trajectory and absolute translational velocity for new (left) and worn liner (right) conditions, at different mill velocities.

Figure 4.11 shows the relation between particle absolute translational velocity and the base liner wear. It is possible to note that particle velocity reduces with wear, due to the reduction in the liner surface area. This reduction is more aggressive for higher agitator velocities. This means that a more representative decrease in particle velocity is obtained when operating at higher agitator velocity. Based on the extrapolated data, it can be

expected that particle velocity will be independent on agitator velocity when the base liner is approximately 40% to 50% worn.

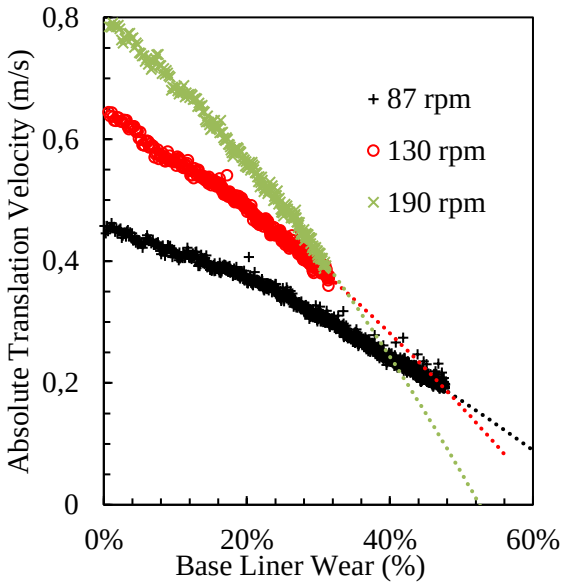


Figure 4.11 – Relation between average particle velocity and the base liner wear intensity.

## 4.6.2.2. Power

Figure 4.12 shows the relation between base liner volume and simulation power reduction. It is possible to note that power reduction is intensified at higher rotational velocities. In the operational context the power is kept constant during liner lifecycle by increasing mill filling.

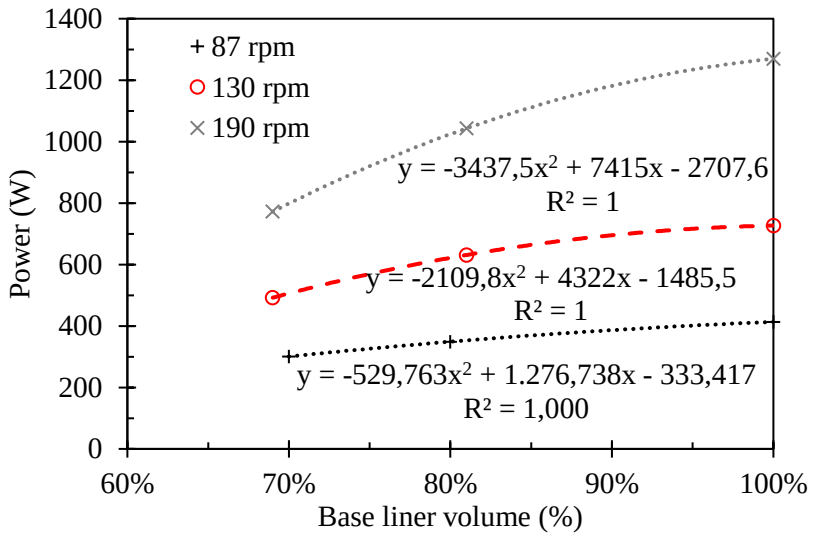


Figure 4.12 - Relation between simulation power and base liner volume.

## 4.6.2.3. Particle Spectrum

Figure 4.13 shows normal and shear energy spectrums for the three operational velocities, at different wear stages. By comparing shear (right) and normal (left) collision spectra, it is possible to note that normal contacts are more affected by wear. In this sense, a greater reduction in the collision frequency was observed for normal contacts, in comparison to shear. This reduction is emphasized at greater specific energies, especially above 1e-1J/kg. Based on the idea that collisions of greater specific energies can lead to an inefficient use of energy, it can be suggested that wear scenarios can be related to a better energy use behaviour. However, it is important to emphasize that the collision frequency and energy reduction will probably generate a coarser product and thus the better energy use behaviour will be mainly caused by the overall power consumption reduction.

Comparing the collision spectra behaviour at different mill rotational velocities it can be noted that higher rotational velocities intensified the overall collision frequency reduction, such as reduced the maximum value of specific energy (J/kg). This explains the greater power reduction observed for this rotational velocity.

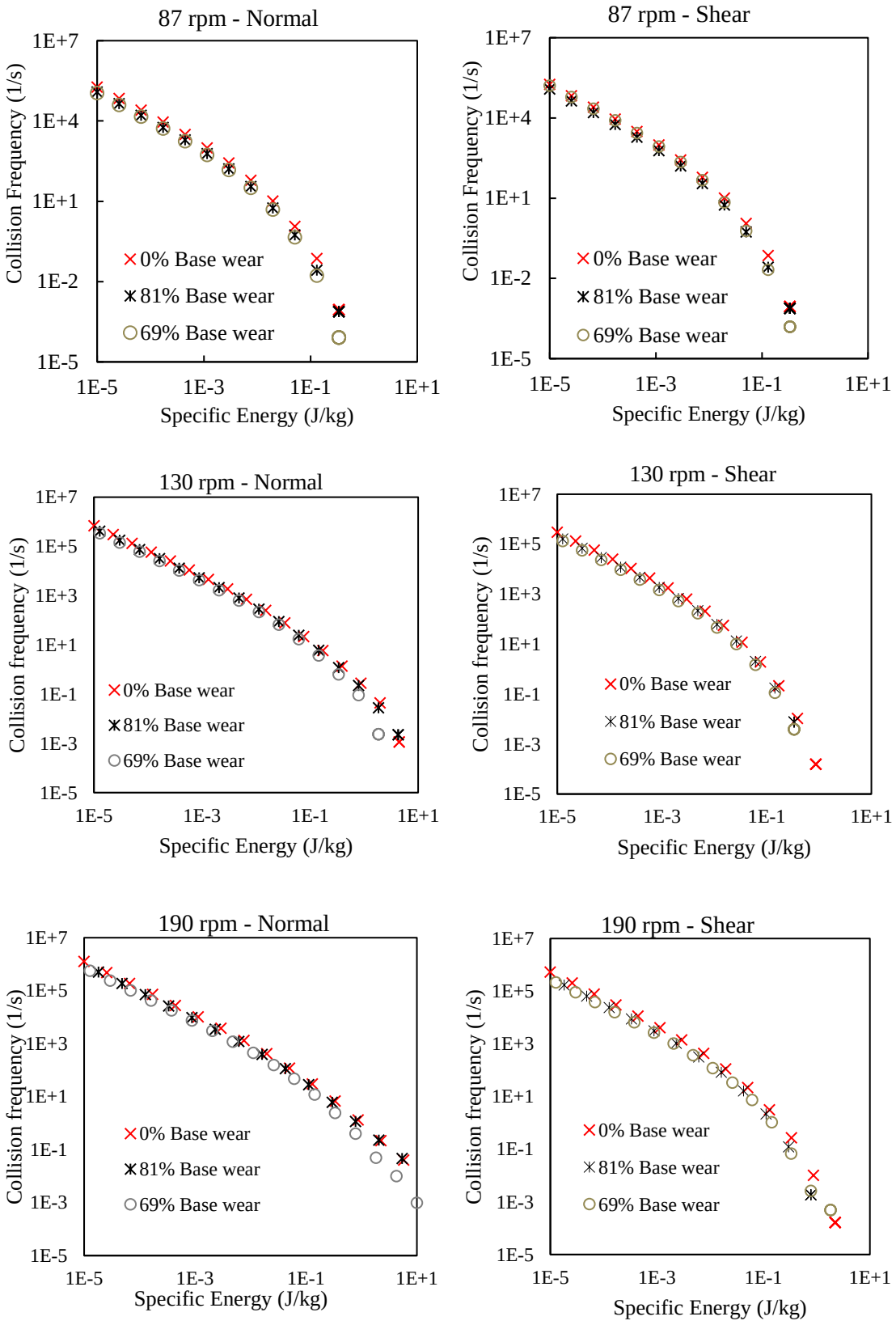


Figure 4.13 – Particle collision spectra at different liner conditions and rotational velocities.

## 4.6.2.4. Wear Volume

The relation between liner volume and simulation time is shown in Figure 4.14 for base and intermediate liner parts. It can be noted that wear is more intensive in the base liner, resulting in a more representative volume reduction. The increase in the agitator velocity also intensifies wear. This effect is more representative for the intermediate liner part. This is a consequence of a wider distribution of particles trajectory when operating at higher rotational velocity, as discussed in Figure 4.10.

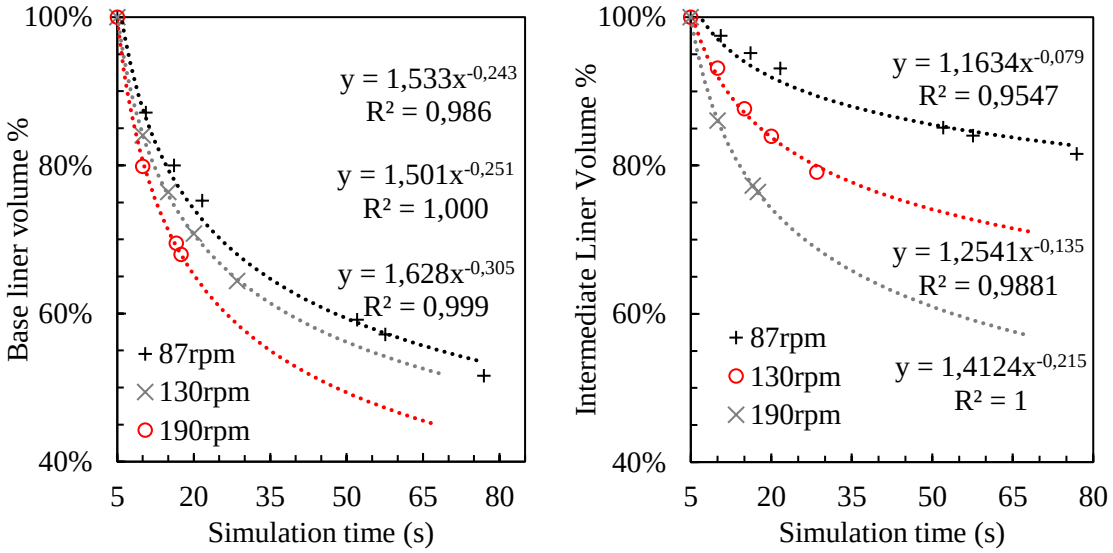


Figure 4.14 – Base and intermediate liner volume during simulation time.

## 4.6.3. VTM-1500 wear measurement

Based on the three-dimensional scanning of a VTM-1500 liner parts, Silva (2019) presented the relation between operational hours and liner mass, separately for base and intermediate liner parts.

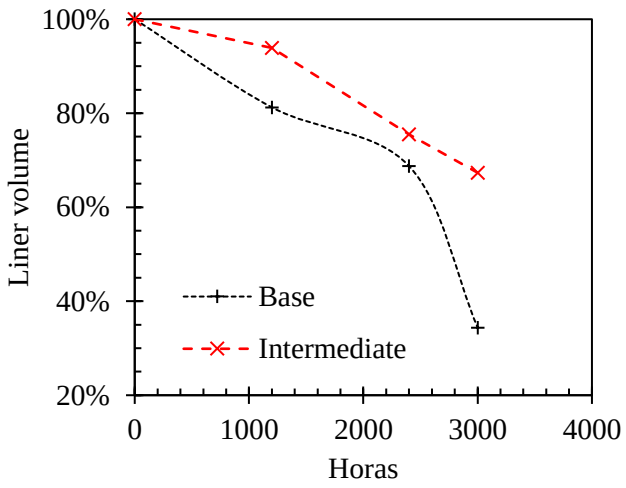


Figure 4.15 – Base and intermediate liner volume reduction during liner operational time (in hours).

The absolute mass value was converted as liner volume percentage, and are presented in Figure 4.15, in relation to the operational time. The wear ratio is defined as the relation between wear percentage and operational time.

The liner volume comparison between the two liner parts reinforces that wear is more aggressive in the base liner. In this sense, at the end of the lifecycle, or 3000h, the intermediate liner reached approximately 67% of the initial volume while the base liner reached 35.5% of its initial volume. Because of that, the base liner requires sooner and more frequent replacement. Also, the base liner wear ratio significantly increases after 2000h.

## 4.6.4. DEM Wear Modelling

Figure 4.16 compares the simulated geometry and industrial liner designs under several wear conditions. The visual comparison between wear patterns shows that DEM provided a remarkably similar wear design. The next stage would be to quantify the wear relation. For that, a time relation was established in order obtain a scale up factor that correlate simulation seconds and operational hours.

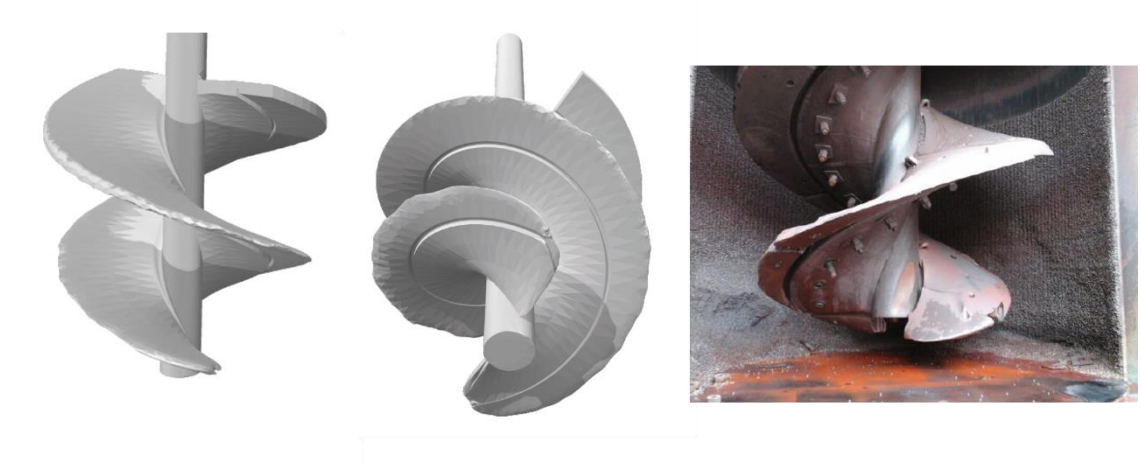

Figure 4.16 - Comparison between 3D worn screw after DEM simulation and industrial worn liner.

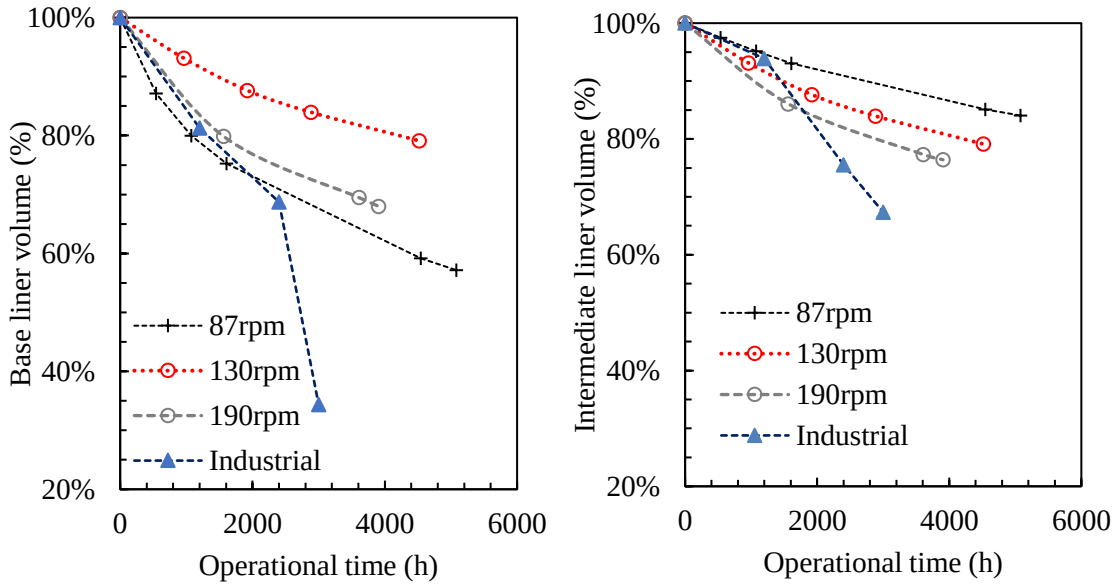


Figure 4.17 – Model predicted and measured values of base and intermediate liner volume during operational time (h).

Figure 4.17 shows the predicted liner volume, based on the obtained DEM model. By comparing the intermediate and base liner predictions, a better agreement was achieved when using the 87 rpm as agitator velocity. In relation to the base liner, the results compared favourably during most of the operational time, except for the last liner measurement, which corresponds to approximately 3000 h. This is probably since the last liner measurement presents a very aggressive behaviour, which representatively differs from the trend.

For the intermediate liner, the behaviour was well predicted up to approximately 1500h. This is probably due to the fact of filling increase during the liner lifetime. The filling increasing is performed during the liner lifetime with the aim to keep constant power by activating upper parts of the mill. Because of that, added grinding media gets in contact with upper parts of the intermediate liner, thus resulting in additional wear.

In contrast, the liner volume predictions for 130 rpm and 190 rpm did not fit very well when evaluating base and intermediate liner parts.

## 4.7. Conclusions

Once the liner is responsible for media movement and consequently grinding, it is very important to perform an accurate monitoring of wear progress. However, it is not possible to directly install sensor for wear measurement. The paper addressed this issue by performing DEM simulations, with the aim to provide a better understanding about screw liner wear behaviour and effects. The simulation was performed for a 1/10th reduced scale equipment geometry, to reduce simulation effort.

The model did not consider particle breakage, as ore particles itself are not included in the simulation. Grinding media wear is also not considered, once the computational effort for that would significantly increase. Finally, the current work did not consider the slurry (fluid), so as a there would be a recommendation to apply CFD (Computational Fluid Dynamics) or SPH (Smoothed Particle Hydrodynamics) to describe the mill charge with more details.

The simulations applied different scale up methodologies for agitator rotational velocity. In this sense, three different mill velocities were simulated. Firstly, a reduced velocity obtained based on a dataset model. This consists in a more recent approach for velocity scale up in laboratory scale equipment. Also, a direct scale up factor based on the geometry reduction was applied, thus resulting in a higher operational velocity of 190

rpm. Finally, an intermediary velocity was tested to provide a better understanding in the effects of operating in between the lower and maximum mill velocities.

The wear simulation results qualitatively showed that wear profile obtained using DEM presents a strong similarity to the wear design observed in the full-scale equipment. The agitator worn geometries were exported, at different simulation times, to provide a volume quantification of wear. By comparing worn geometries obtained from DEM simulations and industrial measurement, a time correlation was proposed. In this sense, a scale up factor was obtained to correlate simulation time, in seconds, and operational time, in hours. This scale up factor was then applied to simulation results to predict wear in the operational context, for base and intermediate liner parts. By comparing the obtained wear prediction and industrial measurement, a better agreement was encountered for the 87 rpm mill velocity. Based on that, the recommendation would be to apply the developed model under different operational conditions, to evaluate different strategies for wear compensation, such as changing mill speed and grinding media filling.

Additionally, DEM outputs were evaluated to provide a better understanding of wear effects. From that, it was noted that wear introduced a significant decrease in simulation power and particle average translational velocity. In relation to particle trajectory, the particle velocity reduction was intensified in the top and bottom part of the mill, thus resulting in null particle motion in those areas. In the bottom part of the mill this is known as dead zone effect. The particle collision spectra indicated that wear affects more intensively normal contacts of greater specific energy. Although this might cause a decrease in fines generation, this can lead to an improvement in energy usage. This is since the predominance of low energy contacts is related to an increase in energy efficiency, once this reduces the occurrence of high intensity contacts which apply greater energy than required for particle breakage.

To summarize, the obtained results point that liner wear affects particle breakage and energy consumption. A better understanding and proper quantification about its effects can play a key role in the development of strategies for optimizing operational procedures to keep grinding efficiency and to reduce wear rates. In this sense, the recommendations

would be to evaluate the relation between operational conditions and liner wear, in the industrial context.

## 4.8. References


Allen, J. & Noriega, R., 2011. *Screw liner replacement in a VERTIMILL® grinding mil—determining best practice.* Antofagasta, Chile: 8th Internacional Mining Plant Maintenance Meeting.

Boemer, D. & Ponthot, J., 2017. A generic wear prediction procedure based on the discrete element method for ball mill liners in the cement industry. *Minerals Engineering*, pp. 55-79.

Cleary, P., 1998. Predicting charge motion, power draw, segregation and wear in ball mills using Discret Element Methods. *Minerals Engineering*, Volume 11, pp. 1061-1080.

Cleary, P. & Owen, P., 2010. Effect of liner design on performance of a HICOM (R) mill over the predicted liner life cycle. *International Journal of Mineral Processing,* Volume 134.

Cleary, P. & Owen, P., 2018. Development of models relating charge shape and power draw to SAG mill operating parameters and their use in devising mill operating strategies to account for liner wear.. *Minerals Engineering,* Volume 117, pp. 42-62.

Cleary, P. W., Sinnott, M. & Morrison, R., 2006. Analysis of stirred mill performance using DEM simulation: Part 2 – Coherent flow structures, liner stress and wear, mixing and transport. *Minerals Engineering*, Volume 19, pp. 1551-1572.

DOE, 1981. Comminution and Energy Consumption: Report of the committee on comminution and energy consumption. Em: Washington, D.C.: National Materials Advisory Board, Commission on Sociotechnical Systems, p. 283.

Eirich, 2018. *Brochure: EIRICH Tower Mill - Vertical agitated media mill.* [Online] Available at: https://www.eirichusa.com/products/towermills/tower-mill-vertical-ag-med-mill. [Access in 27th July 2020].

Esteves, P. et al., 2019. *Qualitative evaluation of the grinding efficiency of a gravity induced stirred mill using the size specific energy approach.* Leeds, Edited by Mojtaba Ghadiri, Sadegh Nadimi, Mehrdad Pasha, pp. 101-102.

Esteves, P. M. et al., 2018. *Predictive modelling of vertical stirred mills liner wear using vibration signature analysis.* Cape Town, 11th International Comminution Symposium.

Hasan, M., 2016. Process Modelling of Gravity Induced Stirred Mills. Volume Doctoral thesis at The University of Queensland.

Kalala, J., Bwalya, M. & Moys, H., 2005. Discrete element method (DEM) modelling of evolving mill liner profiles due to wear. Part I: DEM validation. *Minerals Engineering,* Volume 18, pp. 1386-1391.

Kalala, J. & Moys, M., 2004. Discrete element method modelling of liner wear in dry ball milling. *The Journal of The South African Institute of Mining and Metallurgy*, pp. 597-602.

Marsden, J. 2., 2008. Energy efficiency and copper hydrometallurgy.. *Proc Hydrometall (SME)*, pp. 29-42.

Mazzinghy, D. et al., 2017. Vertical stirred mill scale-up and simulation: Model validation by industrial samplings results. *Minerals Engineering*, Volume 103-104, pp. 127-133.

Mazzinghy, Russo, Lichter, Schneider, Sepúlveda & Videla, 2015. The grinding efficiency of the currently largest Vertimill installation in the world. *SAG Conference 2015*, Vancouver.

Mazzinghy, D., Schneider, L. C., Alves, K. V. & Roberto, G., 2015. Vertical mill simulation applied to iron ores. *Journal of Materials Research and technology*, pp. 186-90.

Metso, 2017. *Blog: When to change Vertimill™ liners and how to do it safely!*. [Online] Available at: https://www.metso.com/blog/mining/blog-when-to-change-vertimill-liners-and-how-to-do-it-safely/. [Access in 17th September 2019].

Mishra, B. K. & Rajamani, R. K., 1992. Analysis of Media Motion in Industrial Ball Mills. Em: *Comminution - Theory and Practice*. Littleton: Society for Mining, Metallurgy and Exploration, Inc., pp. 426-440.

Morrison, R. D., Cleary, P. W. & Sinnott, M. D., 2009. Using DEM to compare energy efficiency of pilot scale ball mill and tower mills. *Minerals Engineering*, Volume 22, pp. 665-672.

Napier-Munn, T., 2015. Is progress in energy-efficient comminution doomed?. *Minerals Engineering*, Volume 73, pp. 1-6.

Oliveira, A., Rodriguez, V., Carvalho, R., Powell, M., & Tavares, L. (2020). Mechanistic modeling and simulation of a batch vertical stirred mill. *Minerals Engineering*.

Radziszewski, P. & Moore, A., 2017. Understanding the effect of pressure profile on stirred mill impeller wear. *Minerals Engineering*, pp. 54-59.

Rocky, 2017. *Workshop 4 - SAG Mill (Wear and Particle Energy Spectra)*, s.l.: s.n.

Rocky, 2018. *Rocky Capabilities Chart*. [Online]. Available at: http://rocky-dem.com/index.php?pg=capability. [Access in 22th January 2018].

Silva, J., 2019. *Effect of process parameters on vertical mill power*. Belo Horizonte: Master thesis submitted at Universidade Federal de Minas Gerais *(in Portuguese)*.

Sinnot, M., Cleary, P. W. & Morrison, R., 2006. Analysis of stirred mill performance using DEM simulation: Part 2 - Coherent flow structures, liner stress and wear, mixing and transport. *Minerals Engineering*, Volume 19, pp. 1551-1572.

Sinnott, M. C. P. M. R., 2011. Is media shape important for grinding performance in stirred mills?. *Minerals Engineering*, Volume 24, pp. 138-151.

Sinnott, M. C. P. M. R., 2011. Slurry flow in a tower mill. *Minerals Engineering*, Volume 24, pp. 152-159.

Toor, P., Perkins, T., Powell, M. & Franke, J., 2011. The influence of liner wear on milling efficiency. *METPLANT 2011 - Metallurgical Plant Design and Operating Strategies*, pp. 193-212.

Weerasekara, N. et al., 2013. The contribution of DEM to the science of comminution. *Powder Technology*, Volume 248, pp. 3-24.

Xu, Lei, Zhao & Yongzhi, 2018. Numerical prediction of wear in SAG mills based on DEM simulations. *Powder Technology*, Volume 39, pp. 353-363.

Yahyaei, M., Banisi, S. & Hadizadeh, M., 2009. Modification of SAG mill liner shape based on 3-D liner wear profile measurements. *International Journal of Mineral Processing*.

# CHAPTER 5 - DEM SIMULATIONS APPLIED TO THE EXPERIMENTAL CONDITIONS

## 5.1. Introduction

This chapter comprises results obtained by applying DEM simulations for different laboratory test work conditions. For that, the DEM model setup presented in Chapter 4 was applied for the evaluation of the five scenarios presented in Chapter 3.

## 5.2. Objective

The current procedure to compensate for agitator liner wear is to keep electrical power constant, by continuously increasing filling during liner lifecycle. The aim of the present chapter is to apply DEM simulations to obtain a better understanding about the effects of operating with fixed filling or fixed power, at different liner wear conditions. The chapter also provides a correlation between DEM simulation and laboratory test work results.

## 5.3. Methodology

The DEM model setup used was presented in Chapter 3 and using the 1/10 scale mill geometry. To simulate the liner at different wear stages, required exporting the worn geometry from the 87 rpm wear simulation, at different simulation times.

The laboratory experimental conditions presented in Chapter 3 were used as basis for the simulation scenarios. In this sense, five case scenarios were chosen, representing the base case (0%), constant power (CP-50% and CP-100%) and constant filling (CF-50% and CF-100%). The base case was set as the new liner condition with 80% filling. The CP and CF conditions were evaluated at different liner wear stages: 50% and 100%. A summary of the operational conditions used for the DEM simulations setup is presented in Table 5.1.

Table 5.1 – Case scenarios used for the DEM simulations

| | Test ID | New Screw | Constant Power | | Constant Filling | |
|---|---|---|---|---|---|---|
| | | 0% | CP-50% | CP-100% | CF-50% | CF-100% |
| **Operational Conditions** | Wear stage | 0% | 50% | 100% | 50% | 100% |
| | Filling | 80 kg | 92 kg | 95 kg | 80 kg | 80 kg |

To summarize, the process consisted in using physical parameters and geometries from previous DEM simulations, to simulate the experimental conditions tested in laboratory scale equipment. The DEM outputs considered were simulation power, particle collision spectra, velocity, and trajectory. The process is shown in Figure 5.1.

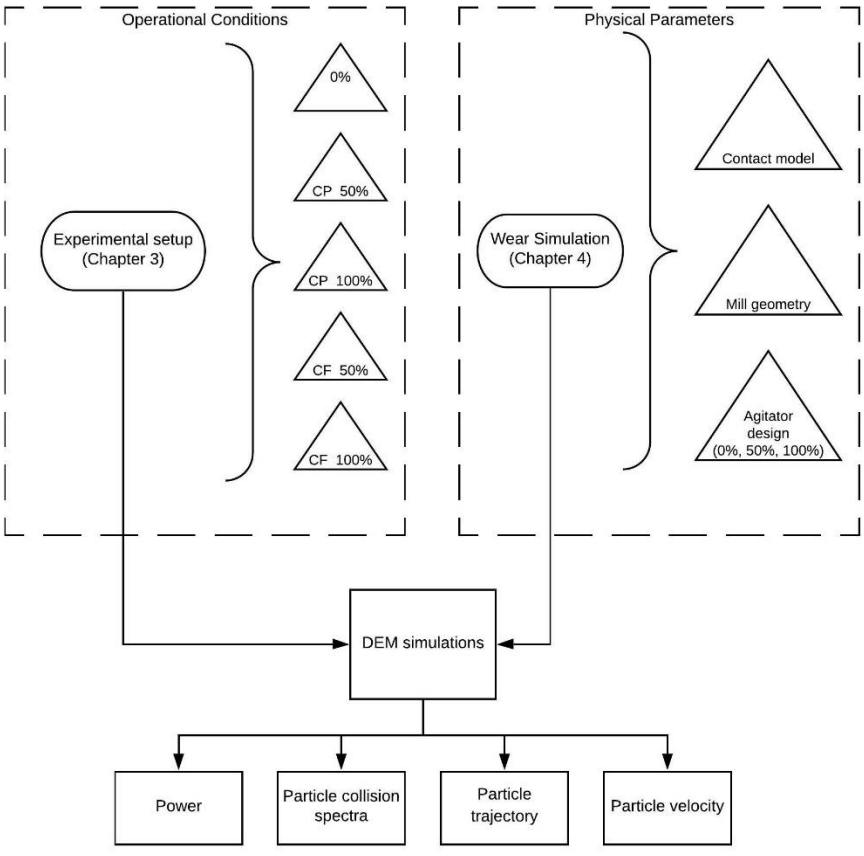


Figure 5.1 – Flowsheet of the DEM mode setup.

## 5.4.Results and Discussion

A summary of the five simulation results is shown in Table 5.2 and Figure 5.2, indicating the average particle translational velocity and simulation power. In relation to the simulation power, a representative reduction was observed for CF conditions, such as observed in the experimental results. This can be explained by the reduced liner surface area, thus reducing the number of particles in contact with liner and representatively decreasing particle velocity. Differently, power remained reasonably constant for the CP simulations. This indicates a proper agreement with experimental conditions once they were used as base for the simulation filling setup. In relation to particle velocity, it was noted a reduction, irrespective of the constant power condition. This indicates that energy was transferred in other forms than particle kinetic energy.

Table 5.2 – Average particle velocity and simulation power for the five case scenarios

| | **Test ID** | **New Screw** | **Constant Power** | | **Constant Filling** | |
|---|---|---|---|---|---|---|
| | | **0%** | **CP-50%** | **CP-100%** | **CF-50%** | **CF-100%** |
| Test Results | Power (W) | 0.41 | 0.42 | 0.40 | 0.35 | 0.30 |
| | Particle Velocity (m/s) | 0.46 | 0.41 | 0.37 | 0.38 | 0.32 |

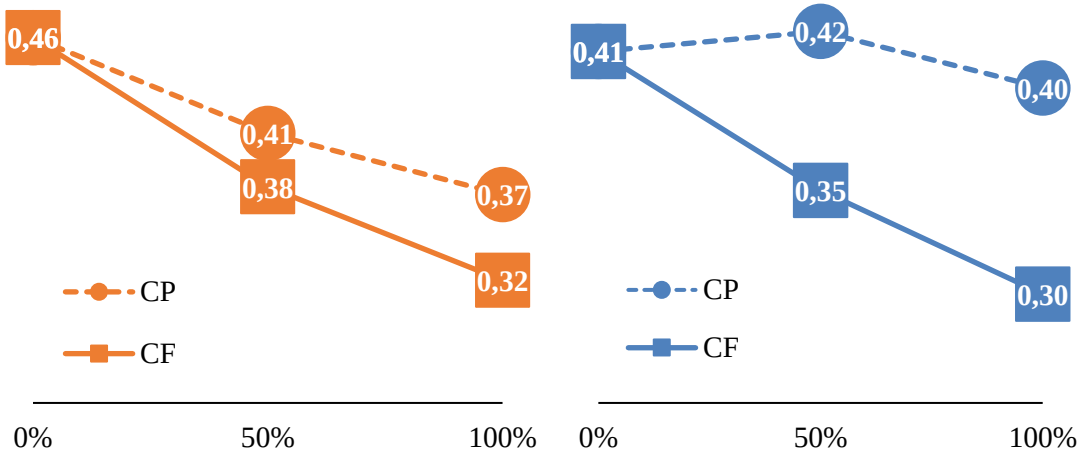


Figure 5.2 – Left: Average particle translational velocity - Right: DEM power.

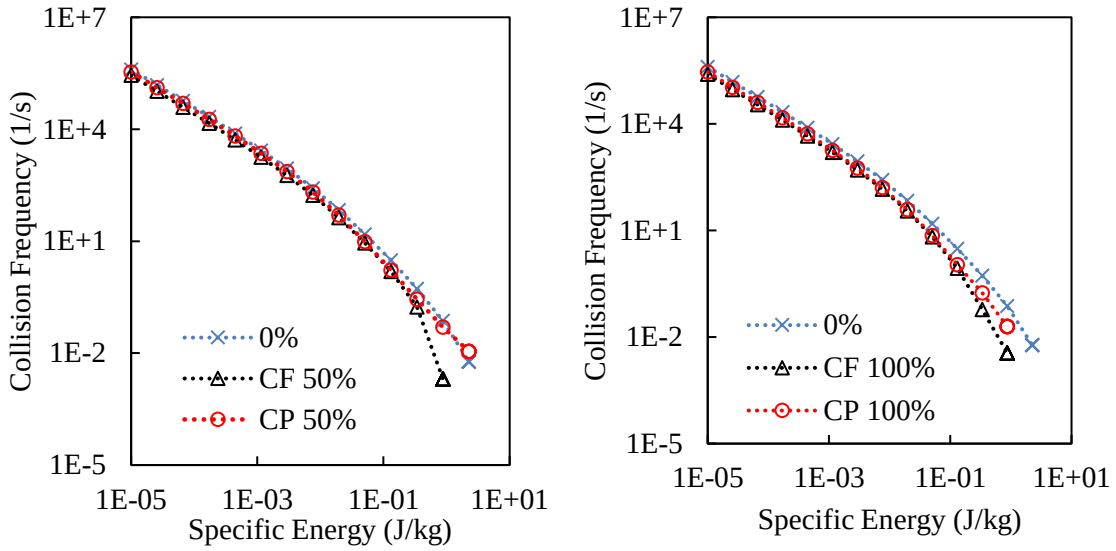


Figure 5.3- Particle collision spectra for normal contacts.

Figure 5.3 shows the collision spectra for normal contacts, for the five case scenarios. The y axis indicates the cumulative collision frequency, which means the amount of normal inter particle collisions per second, in the mill environment. The x axis indicates the specific energy (J/kg) related to normal contacts. This value can be directly correlated with breakage, once this represents the energy level which is applied to ore particles. From the graphics, it can be noted that collision frequency decreases with the increase of specific energy. This indicates the greater number of normal collisions are due to low energy contacts.

The comparison for the 50% wear condition, shown in the left, indicate that particle energy spectra is very similar between 0% and CP-50%, while a slight decrease in the greater specific energy range occurs for the CF-50% condition, especially above 1e-1J/kg. The collision frequency decrease is accompanied by a reduction in the maximum specific energy value. Based on that it is suggested that wear mostly affects contacts of higher specific energy, thus decreasing the maximum energy involved in contacts, such as the number of contacts per second.

In relation to the CF-100% and CP-100%, it also can be noted a decrease in the specific energy range, being this reduction more representative for the CF-100%. This reflects in the greater power reduction for the constant filling condition, especially for the CF-100%

case. Based on that, it can be concluded that an overall normal power decrease takes place due to the reduction in both collision frequency and maximum contact specific energy.

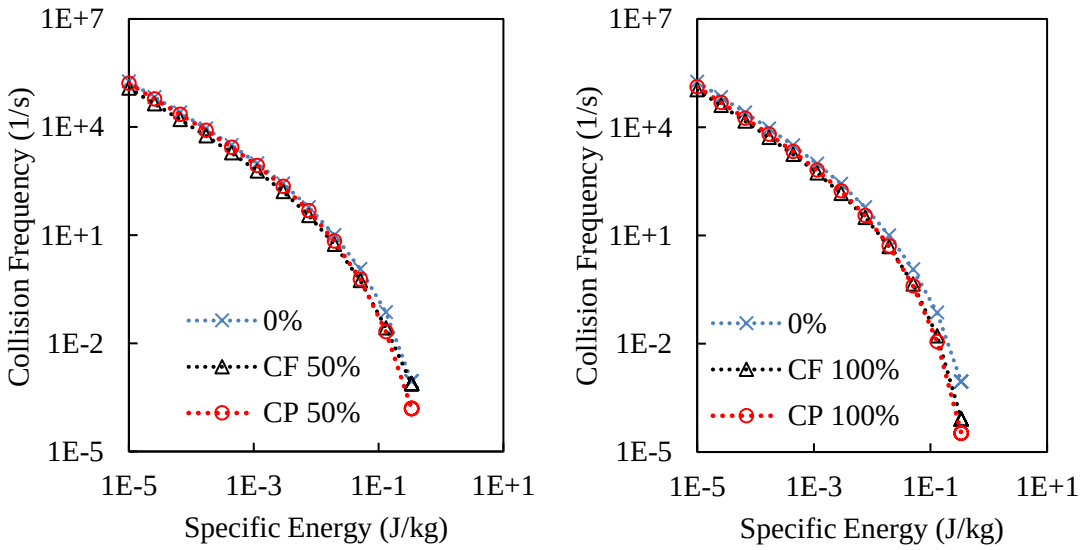


Figure 5.4 - Particle collision spectra for normal contacts.

In a similar graphic, Figure 5.4 shows the collision spectra for shear contacts. It can be noted a similar range of specific energy levels, thus indicating a similarity in the specific energy values involved in shear and normal contacts. In relation to the wear effect in shear contacts, it is observed a simillar pattern with normal contact spectra. In this sense, a slight decrease is observed for the collision frequency, being this effect emphasized at higher specific energy values. However, the maximum contact specific energy value remained almost constant. In this sense, the overall inter particle shear power reduction occurs due to the smaller amount of collisions per second.

Shear and normal collision spectra are related to the product size distribution, once this represents the particle contact involved in breakage mecanisms. Based on the simulation spectra results, it can be expected that operating at worn conditions will generate a coarser product. This occurs due to the reduction in the overall shear and normal contact power. In this sense, the spectra behaviour can than be used to explain the obtained particle size distribution presented in Chapter 3 for the laboratory experimental results. From that, it was noted that agitator wear was associated with the generation of a coarser product when operating at CP and CF conditions. By comparing CF and CP at fixed wear stages, fines

generation was reduced for CF conditions, this is probably due to tne greater decrease observed in inter particle collision spectra.

Finally, grinding efficiency can be explained by the combination between mill energy consumption and product fineness. In CHAPTER 3 -3, those two information were used to provide a grinding efficiency evaluation, in the form of the SSE evaluation. Although the DEM simulations results were not combined with mechanistical models, to quantify particle breakage or product size, the combination between particle collision spectra and simulation power can be used to evaluate energy use of the simulated scenarios. In this sense, the simulation indicated a representative power reduction when operating with worn agitators. This simulation power reduction is emphasized when operating at constant filling condition. Similarly, an overall shear and normal power reduction was observed for inter particle collision, in the form of reduced collision frequency and maximum specific energy. This effect was mainly observed in contacts of greater specific energy. As discussed, energy intensive contacts are associated with an increase of energy use that does not completely convert to breakage. From that, it is suggested that overall power reduction during the liner lifecycle did not convert to a proportional decrease in fines generation.

Based on that, it is suggested that an energy efficiency increase can be obtained as the liner wears. However, this is mainly since overall power consumption decreases and so a coarser product should be expected. This is in accordance with the experimental results encountered in Chapter 3.

## 5.5. Conclusion

DEM simulations indicated that wear affects particle average translational velocity, irrespective of wear compensation procedure. In this sense, power compensation by filling increase did not compensate for particle kinetic energy.

In relation to inter particle collision spectra, it was noted that wear presents a more intensive effect on contacts of greater specific energy. The effect was intensified when

operating at constant filling conditions. As the predominance of high intensity contact is associated with an increase in energy usage, this behaviour might lead to an increase in energy efficiency indicators. The results are in accordance with experimental results obtained in Chapter 3.

# CHAPTER 6 - VIBRATION ANALYSIS

## 6.1. Introduction

The agitator screw is inside a very aggressive environment and consequently it is not possible to install sensors for direct measurement of liner wear. The only way for obtaining an accurate measurement of liner wear is by visual inspection. This can only be performed after fully stopping and unloading the mill.

The present chapter presents a non-intrusive and low-cost method based on power measurement and vibration analysing. Exploratory industrial tests were performed in three VTM-1500 using liners at different lifecycle stages.

## 6.2. Vibration Analysis

According to Chen et al. (2013), in a rotational machine each rotational component introduces different disturbances in the total mechanical behaviour in a complex multi-degree-of-freedom system. Therefore, the total machine behaviour is a composition of all machine parts, such as gears, motors, shafts, bears and load motion. These rotating components can be considered multiple vibration sources and all physical vibrations are coupled to each other, interfering and composing the total system, as presented in the right side of Figure 6.1 . By measuring vibration with an accelerometer, it is possible to analyse the machine total behaviour and extract all parts features by vibration analysis, as can be seen the left side of Figure 6.1.

Vibration analysis is a widely used and high potential method for an automatic detection of mechanical faults in several rotational machines, such as lathe machines, wind turbines, centrifugal pumps, combustion engine driven generators, machine tools and (Baccarini, 2005; Stopa, 2011; Biswal, et al., 2016). Recently vibration analysis is being proposed for monitoring operational variables in horizontal ball (Zeng & Forssberg, 1994; Kang, 2006; Behera, et al., 2007; Gugel & Moon, 2007; Peng, et al., 2009; Tang, et al., 2010; Das, et al., 2011; Esteves, et al., 2014; Esteves, 2016). It is also widely known that

vibration analysis is currently used for predictive maintenance of electrical motors and gears (Baccarini 2005). Because of this reason, most mineral processing plants have the necessary equipment and abilities for performing this technique.

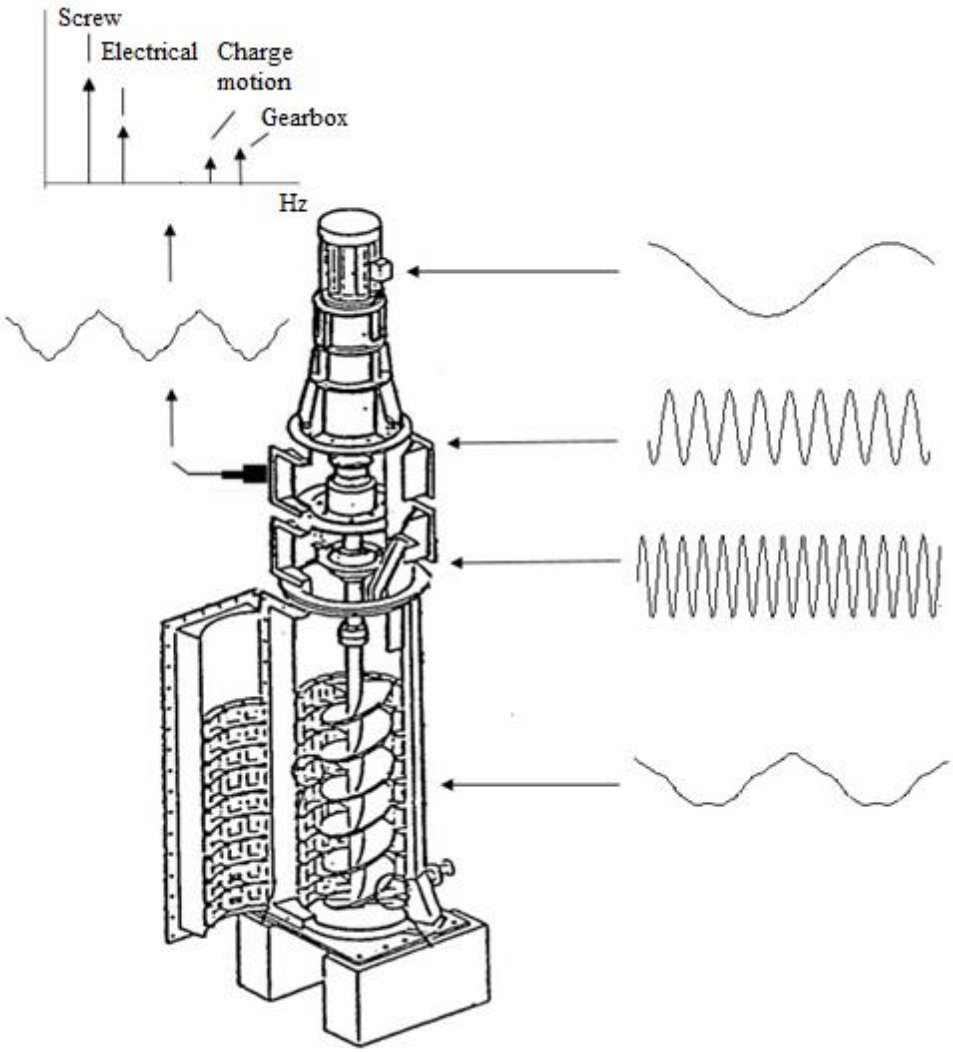


Figure 6.1 – Vibration sources and vibration measurement in the vertical stirred mill. Adapted from Duffy (1994).

Once the liner is responsible for grinding media motion and is directly mounted with drive engine, its movements introduce periodic events in the mechanical system. These events can be detected by vibration analysis and the characteristic vibration spectrum is called vibration signature. As the liner wears, charge motion pattern is modified, affecting grinding, and introducing disturbance in the mechanical system. These disturb affects vibration signature. So, the method is based on the presupposition that vibration signature

of a healthy liner changes as it wears. Based on this, the process consists of searching and identification of frequency components related to faults. By comparing vibration spectrum between a new and a worn liner, changes can be detected and used for developing an indicator.

## 6.3. Experimental

Experimental tests were performed at the Minas-Rio Project, in Conceicão do Mato Dentro city, Minas Gerais State, Brazil. The regrinding installation consists of sixteen VTM-1500 that adequate particle size distribution for transport in a slurry pipeline. It is currently the biggest regrinding installation with VTM's in the world (Mazzinghy, et al. 2017).

Three mills at different liner lifetime stages were chosen for tests as described in Table 6.1. Tests included measurements of three variables affected by liner wear: filling, power and vibration. An additional test was done in Mill C after charging the mill with more 5t of balls.

Table 6.1 – Operational lifetime

| Mill | Liner time (h) |
|---|---|
| Mill A | 110 |
| Mill B | 2653 |
| Mill C | 3397 |

Tests were realized in the most established condition as possible, to minimize disturbs and noise. In this way, it can be considered that liner condition is the main reason for differences between measured signals. Descriptions of the procedures for measuring filling, power and vibration are next.

## 6.4. Filling

Measuring mill filling demands maintenance, process, and operational staffs. First, it is necessary to stop fresh feed to the mill and flush water inside it. After all slurry is

discharged and the water valves are closed, and the motor drive can be turned off. At this moment, a standard rope with a weight at the tip is putted inside the media bin loading platform, as showed in Figure 6.2.

Figure 6.2 – Procedure and equipment for mil filling measurement.

The total ball height is obtained by comparing the total height of rope inside the mill with equipment total height. Using mill dimensions it is possible to obtain mill filling. After that, the motor can be turned on and then fresh feed is restarted. Therefore, measuring VTM fill is not of easy handling and this is the main reason why filling is not continuously monitored.

## 6.5.Power

Measuring power demands electrical maintenance staff to install an energy analyser in the electrical room. The energy analyser is MARH-21 and it can be easily installed at current transforms (CT's) and Potential Transformers (PT's). For installing the equipment, it is not necessary to stop the mill and all procedure is done inside the electrical room. After measurement, data can be exported to a sheet or into a specific

program. The equipment was programmed to measure voltages and currents; true, reactive, and apparent power and, finally, power factors, during all test's intervals.

Electrical signals were processed using statistical analysis. It is a commonly technique employed for analysing time domain series (Salehi-Nik, et al. 2009). Employed techniques are described below.

## 6.6. Standard deviation

Standard deviation (σ) is a popular quantity of dispersion that measures how data is scattered around an average value. Calculation is shown in Equations 6.1 and 6.2

$$\sigma = \sqrt{\frac{1}{n-1}\sum_{i=1}^{n}(x_i - \bar{x})^2} \tag{6.1}$$

$$\bar{x} = \frac{1}{n}\sum_{i=1}^{n} x_i \tag{6.2}$$

Where n is the number of samples and $\bar{x}$ is the average value.

## 6.7. Kurtosis

Kurtosis is a measure of shape that quantifies flatness distribution. Data with normal distribution presents null values of kurtosis. Positive and high kurtosis values indicate that peak values are much bigger than mean. Negative values indicate that data peaks are flatter than for normal distribution.

$$Kurt = \frac{\frac{1}{n}\sum_{i=1}^{n}(x_i - \bar{x})^4}{\frac{1}{n}(\sum_{i=1}^{n}(x_i - \bar{x})^2)^2} - 3 \tag{6.3}$$

## 6.8.Skewness

Skewness is a measure of shape that indicates symmetry of the data. Symmetrical distributions present skewness closes to zero. Asymmetrical distributions can present both positive and negative skewness values. Negative values indicate that data presents a left tail. That means that data distribution has a longer tail to the left of the mean. In contrast, positive skewness values indicate that the right tail is longer.

$$S = \frac{\frac{1}{n}\sum_{i=1}^{n}(x_i - \bar{x})^3}{\frac{1}{n}(\sum_{i=1}^{n}(x_i - \bar{x})^2)^{3/2}} \tag{6.4}$$

## 6.9.Vibration

Seven machine points were tested for vibration measurement as shown in Figure 6.3. The process of measuring all points takes approximately ten minutes and is completely low intrusiveness.

Vibration measurement is monthly performed by predictive maintenance. Tests used same team, procedures, and equipment. Equipment consists of a single axis accelerometer coupled to a CSI 2130 Vibration Analyser. After collecting data is uploaded to a specialized software that performs spectral analysis. Then, the spectrum of data is exported and analysed using Matlab software.

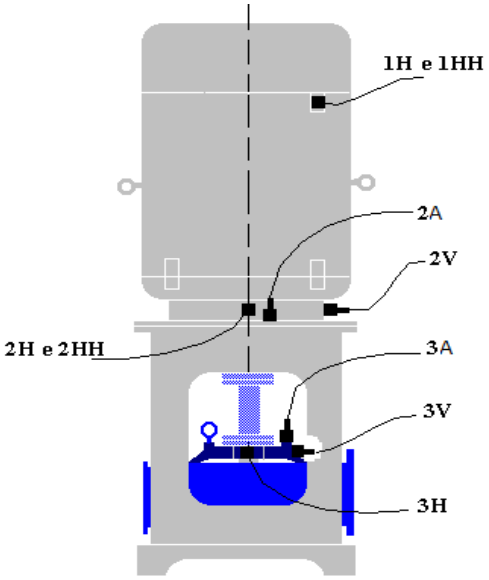


Figure 6.3 –Vibration points in motor and gear.

After an analytical task and mathematical manipulation of spectral data, liner indicators candidates were obtained. Next, they were tested for new data, originated from predictive maintenance database. Those data were measured under uncontrolled conditions, what means that it contains a bigger amount of noise. A linear correlation test was used to evaluate the relation between indicators candidates and liner conditions. Calculating linear correlation indices is a useful tool to identify the simple relation between two variables without the need to assume specific fits or models to data.

## 6.10. Results and Discussion

Figure 6.4 presents results for electrical current, power, power factor and charge filling. As expected, charge filling increases for worn liners, reaching values over 100%.

In contrast, electrical current and total power tend to decrease as the liner wears. On the other hand, power factor did not present direct correlation to liner condition. Charge load also affects all those variables. It is possible to note that current and power do not increase at same rate. A rise of 2.6% in filling increased current around 2.8% and power in 3.7%. It happened because power factor also increased and consequently power and current changed differently.

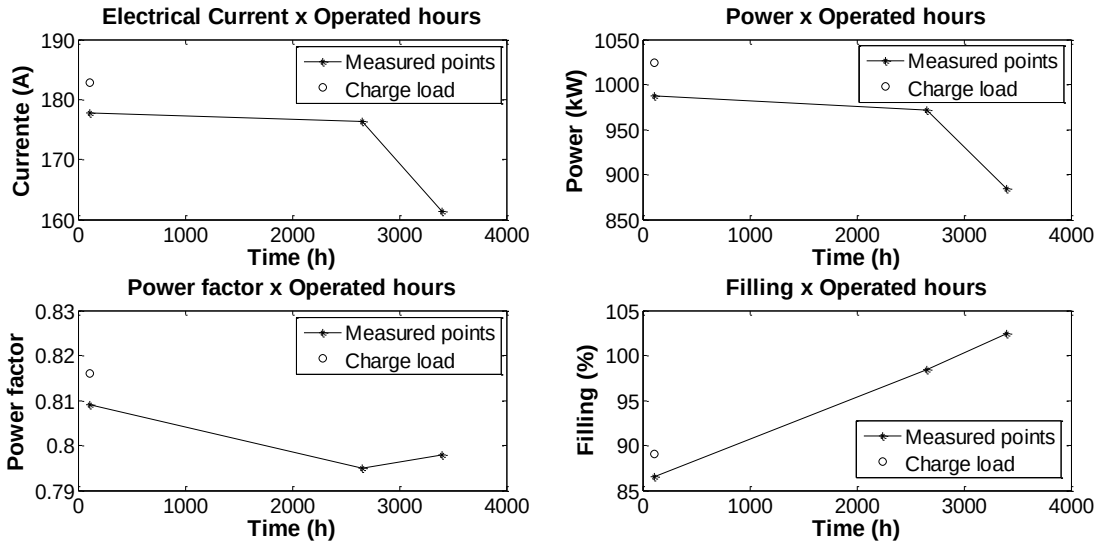


Figure 6.4 - Electrical power, current, power factor and mill filling for different liners lifetime stages

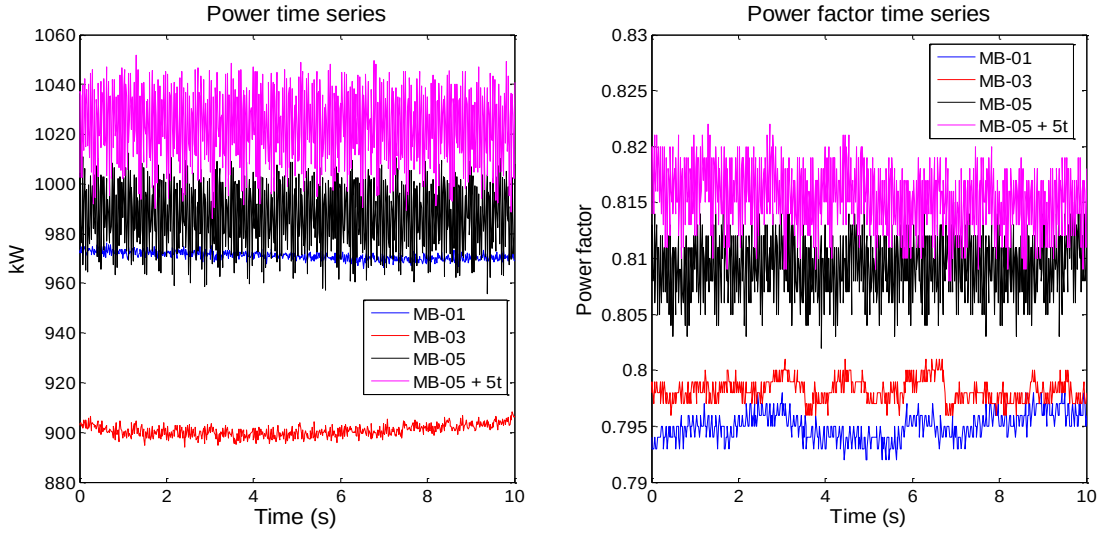


Figure 6.5 - Times series for electrical power and power factor.

Figure 6.5 presents time series for active power and power factor. It is possible to note that curves shape and distribution present a large variation between the two monitored mills. Statistical analysis was applied to those time series in order to test the correlation between liner conditions and electrical variables, as presented in Figure 6.6.

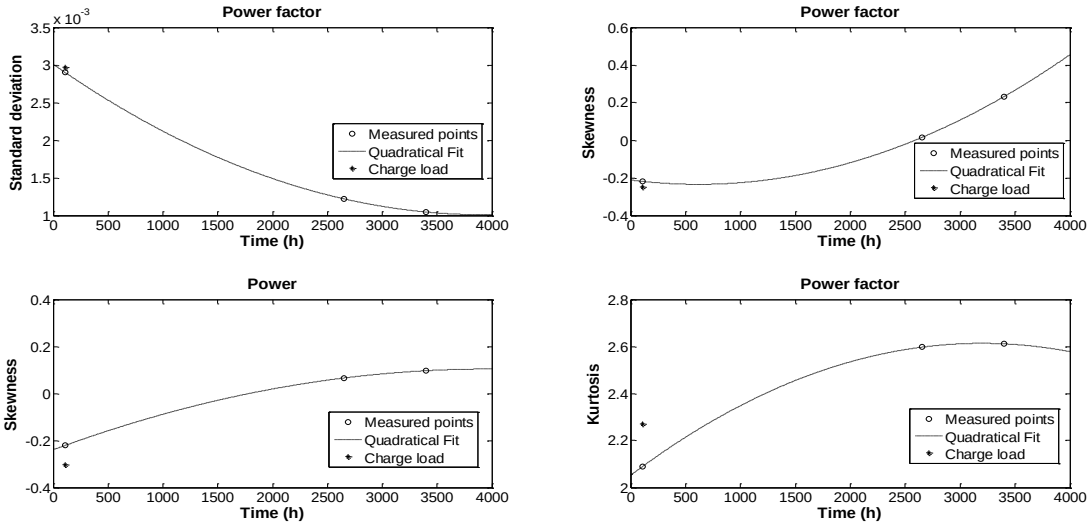


Figure 6.6 - Statistical analysis of electrical measurements.

The standard deviation of power factor is clearly affected by wear but not by charge load. It shows that power factor data scatter decreases for worn liners. Or, in other words, power factors tend to be more stable as the liner wears. On the other hand, wear seems to worsen energy quality once average values of power factor are bigger only for measurements of new liners.

Skewness of power factor shows that data symmetry is very affected by wear but not by charge load. For the new liner skewness is negative, for liners with average time skewness it is close to zero and for the worn liner it was positive.

On the other hand, skewness of power seems to be affected by both charge load and liner wear. As the liner wears, power data tends to be more symmetry and skewness closes to zero. Although charge load interfered in power skewness it seems to affect it in the opposite direction, by decreasing it.

Power factor kurtosis tends to increase as the liner wears and with charge load. It means that both filling and wear tends to increase peak values of power factor data.

Figure 6.7 shows on the top side a typical vibration time series. The downside presents its frequency spectrum. In the frequency domain, it is possible to note that the signal is divided into several frequency bands. The greatest amount of energy is in low-frequency rates, below 100Hz. However, there is a representative amount of energy between 500 e 600Hz, due to gears that couple drive engine.

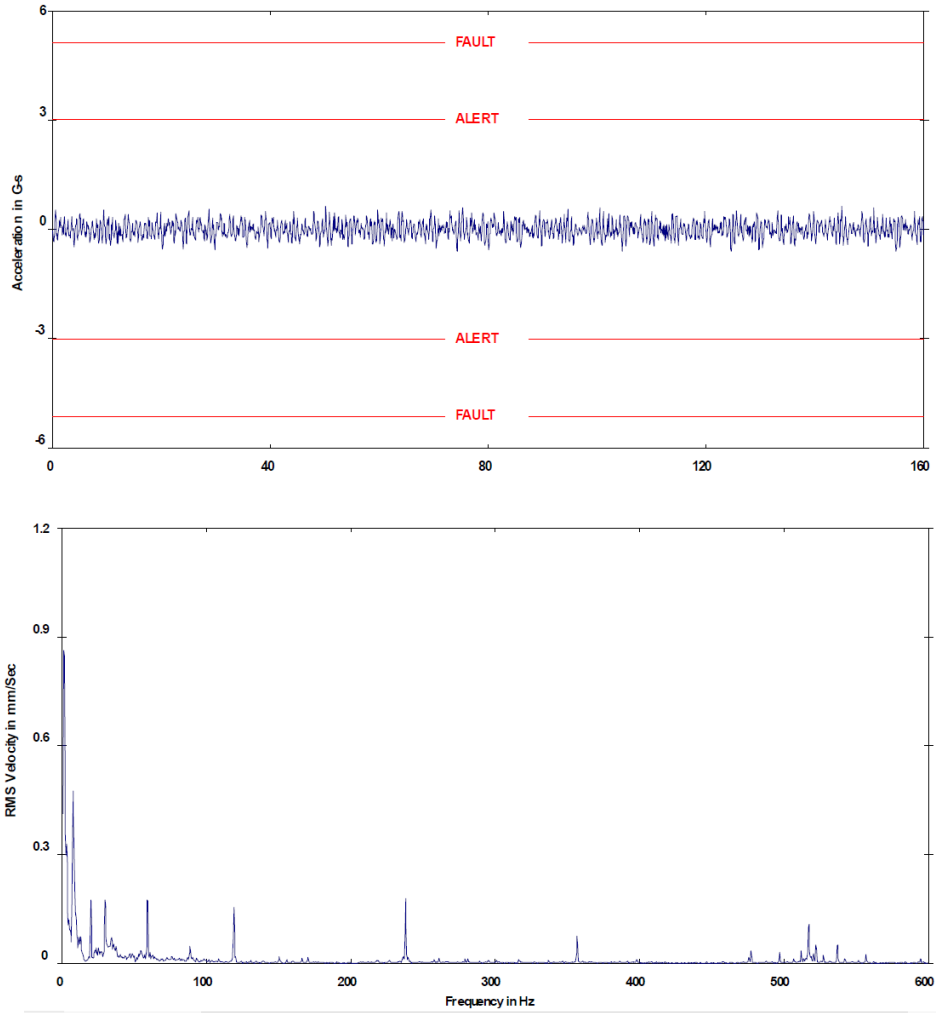


Figure 6.7 – Time series and spectrum of vibration signal.

The next step is to compare vibration spectrums between different mills in the waterfall plot, such as presented in Figure 6.8. It is possible to note several differences between vibration spectrums in mills at different liner lifetime stages. Mill A presents a distributed spectrum, with average peaks all over the frequency band. Mill B, with average lifetime, presents a smaller number of peaks under 60Hz but with higher amplitudes. Above 60Hz,

it presents very few amounts of energy. Mill C, ending liner lifetime, presents only two peak components over 200Hz. For fewer frequencies, energy is very distributed with the biggest peaks between 60Hz and 200Hz and average peaks under 60Hz.

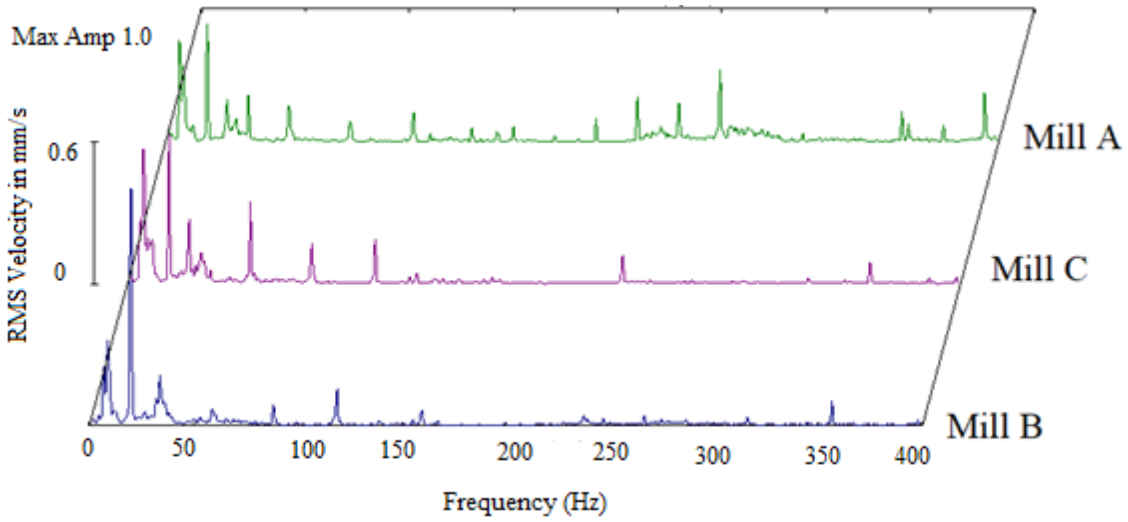


Figure 6.8 - Waterfall plot for vibration of different mills.

From this kind of picture, it is possible to detect how vibration spectrum in a point behaves during liner lifetime. After establishing this analysis for all vibration points one indicator was obtained, as showed in Figure 6.9. It is the amount of energy around harmonics from order 1 to 2.

Indicators indices for controlled and uncontrolled conditions are shown together with correlation coefficients and the linear fit. It is possible to note that indicator decreases as the liner wears. It means that energy around first and second harmonics decreases. This is possible due to the reduction of charge motion inside the mill. In contrast, charge load in the new liner increased the indicator, suggesting that media motion increased.

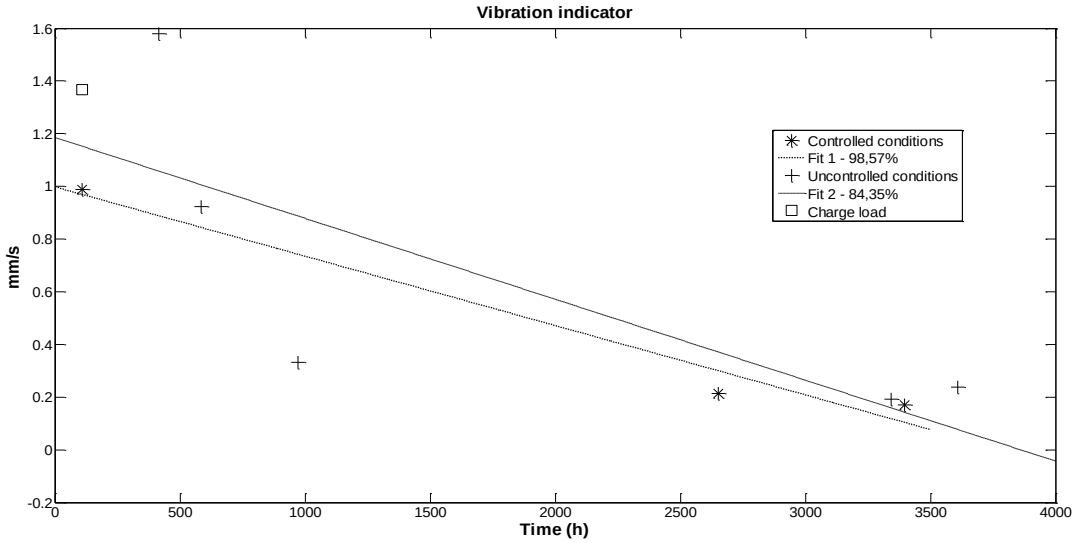


Figure 6.9 – Vibration indicator.

As expected, correlation coefficients decreased when applied for uncontrolled conditions, due to the addition of noise. However, as the liner wears, the indicator errors decrease.

## 6.11. Conclusions

It is a reality that improvement in grinding energy efficiency and operational optimization are key needs for both industry and academic communities. In this context, researchers about grinding innovation are very necessary to provide a change in the current reality.

Due to the growing regrinding need, the VTM points as a key equipment such it presents good energy efficiency in comparison with other equipment. Although they are already widely used in the mining industry, some aspects of its operation are still unknown or decentralized, such as the case of screw liner wear. Once the liner is responsible for media movement and consequently for grinding it is very important to perform an accurate monitoring of wear progress.

To fill this gap the present research proposed a non-intrusive and low-cost method based on power measurement and vibration analysing. Exploratory industrial tests were done in three VTM-1500 with different conditions of wear. While average power and power

factor measurements were susceptible to process variations, statistical analysis presented good relation to lifer lifetime. Vibration signature also presented reasonable correlation to liner lifetime, including tests for uncontrolled data.

Despite the good results already obtained, an evaluation of plant history and additional tests are necessary for consolidating the method. In addition, computational simulations based on DEM can be used to better validate the method and results.

## 6.12. Acknowledgements

Thanks to Anglo American for all the support and for providing data available for this research, PPGEM-UFMG and the Brazilian agencies PROEX-CAPES, CNPq, and FAPEMIG.

## 6.13. References

Baccarini, L. (2005). Fault detection and diagnosis of induction machines. Doctoral thesis submitted at Universidade Federal de Minas Gerais *(in Portuguese).*

Behera, B., Mishra, B. K. & Murty, C. V., 2007. Experimental analysis of charge dynamics in tumbling mills by vibration signature technique. *Minerals Engineering*, Volume 20, pp. 84-91.

Biswal, S., George, J. & Sabareesh, G., 2016. *Fault Size Estimation Using Vibration Signatyres in a Wind Turbine Test-Rig.* s.l., pp. 305-311.

Chen, B. et al., 2013. Detecting of transient vibration signatures using an improved fast spatial-spectral ensemble kurtosis kurtogram an its applications to mechanical signature analysis of short duration data from rotating machinery. *Mechanical Systems and Signal Processing*, Volume 40, pp. 1-37.

Chikuruwo, M., Maregedze, L. & Garikayi, T., 2016. *Design of an Automated Vibration Monitoring System for Condition Based Maintenance of a Lathe Machine (Case Study).* s.l., s.n., pp. 60-63.

Das, S. P., Das, D. P., Behera, S. K. & MIshra, B. K., 2011. Interpretation of mill vibration signal via wireless sensing. *Minerals Engineering*, Volume 24, p. 245–251.

Duffy, S. M., 1994. *Investigation into the performance characteristics of tower mill,* Brisbane: Thesis submitted in fulfilment of the degree of Master of Engineering Science of the University of Queensland.

Esteves, P. (2016). The induction motor as a load torque estimator for motion analysis in ball mills. Belo Horizonte: Master Thesis in the Federal Centre for Technological Education of Minas Gerais (*in Portuguese*).

Esteves, P., Stopa, M., Cardoso Filho, B., & Galery, R. (2014). Development of an aid tool for fault detection in ball mills. Proceedings of International Mineral Processing Congress, Chapter 8. Santiago, Chile.

Gugel, K. & Moon, R., 2007. *Automated Mill Control using Vibration Signal Processing.* Charleston, SC, s.n., pp. 17 - 25.

Kang, E. S., 2006. *Acoustic vibration signal processing and analysis in ball mill.* Dalian, China, s.n., pp. 6690-6693.

Mazzinghy, D. et al., 2017. Vertical stirred mill scale-up and simulation: Model validation by industrial samplings results. *Minerals Engineering*, Volume 103-104, pp. 127-133.

Peng, H., Min-ping, J. & Bing-lin , Z., 2009. Investigation on measuring the fill level of an industrial ball mill based on the vibration characteristics of the mill shell. *Minerals Engineering*, Volume 22, p. 1200–1208.

Salehi-Nik, N. et al., 2009. Determination of hydrodinamic behavior of gas-solid fluidized beds using statistical analysis of acoustic emissions. *International Journal of Multiphase Flow*, Volume 35, pp. 1011-1016.

Stopa, M. M. (2011). Fault detection in rotational machines by using the induction motor as load torque estimator. Belo Horizonte: Doctoral thesis submitted at Universidade Federal de Minas Gerais (*in Portuguese).*

Tang, J. et al., 2010. *Experimental analysis of wet ball mill load based on vibration signals of laboratory_scale ball mill shell.* s.l.:Minerals Engineering.

Zeng, Y. & Forssberg, E., 1994. Application of Vibration Signal Measurement for Monitoring Grinding Parameters. *Mechanical System and Signal Processing*, Volume 8, pp. 703-713.

# CHAPTER 7 - CONCLUSION

It is a reality that improvements in grinding energy efficiency and operational optimization are key needs for both industry and academic communities. Due to the growing need for fine grinding and regrinding applications, the gravity induced stirred mill points as a key equipment, such it presents improved energy performance in comparison with others equipment. Although it has been widely used in the mining industry, some aspects of its operation are still unknown or decentralized, such as the case of screw liner wear.

Once the liner is responsible for media movement and consequently grinding, it is very important to perform an accurate monitoring of wear progress. The wear also affects performance behaviour and thus a better understanding about wear compensation strategies is necessary. In addition, the screw liner wear is directly or indirectly related to all operational costs, which are energy consumption, grinding media consumption and liner replacement. Based on that, the wear monitoring and optimized energy performance of the gravity induced stirred mills, during the complete liner lifecycle, is an important matter.

The present study addressed this issue by different approaches: laboratory scale test work, DEM simulations and industrial measurements.

Laboratory test work of gravity induce stirred mills is itself a recent topic in the literature. Most of previous modelling is based in standard manufactures test work, using conventional tumbling mills. Consequently, the laboratory scale setup of gravity induced stirred mills, such as it and scale up is not well discussed. The present work applies a different methodology for the speed setup, based on equipment dataset and not only in a direct speed scale up factor. Additionally, the test work considered the agitator screw liner wear as a variable, to observe its effects on grinding performance. A comparison between two different operational procedures was performed: operating with fixed power and with fixed filling. The results indicate that signature plot considering P80 and Specific Energy is not representatively affected by tests with increased filling and not suitable for this kind

of evaluation. The 38μm marker size was confirmed to be a reasonable size for evaluation of Size Specific Energy in fine grinding and, finally, the results indicate a tendency for the SSE to decrease when operating under fixed filling conditions.

DEM simulations of gravity induced stirred mills are used for modelling and better understanding of equipment performance. However, the application of DEM for wear modelling in gravity induced stirred mills consists in a more recent approach (Mazzinghy, 2018). The chapter also presents industrial wear measurements, as firstly presented by Silva (2019). The main contribution consists in a deeper evaluation and coupling between those two new approaches. The worn geometries obtained by DEM simulation presents similar wear patterns, in comparison to industrial wear measurements and pictures of the worn screw. Additionally, a correlation between simulation and operational time was established to obtain a time scale up factor. The factor was applied to the simulation results and used to predict wear for the industrial full-scale equipment. The model results present a very similar trend with the wear measurement behaviour, for the 87 rpm mill rotational velocity.

The 87 rpm DEM simulation was used to simulate the experimental conditions presented in Chapter 3. In this sense, the simulations were performed to provide a comparison between operating at constant filling (CF) and constant power (CP) during the liner lifecycle. It was noted that particle kinetic energy decreases with wear, irrespective of power compensation. In relation to power, it decreased when operating at constant filling for worn conditions. This agrees to the experimental results. Additionally, the inter particle collision spectra indicates a decrease in high specific energy contacts, that are associated with an increase in energy consumption. This is since high energy contacts usually apply more energy than necessary for breakage, thus resulting in an over energy usage. Based on that, the decrease in high energy contacts can be used to explain the decrease in SSE observed in the experimental results. However, the absence of high energy contact is also related to a decrease in overall breakage mechanism, thus resulting ibn the generation of a coarser product. This is also in accordance to the experimental results presented in Chapter 3.

Finally, Chapter 6 proposes a non-intrusive and low-cost method based on power measurement and vibration analysing. Exploratory industrial tests were performed in three VTM-1500 at different liner wear stages. While average power and power factor measurements were susceptible to process variations, statistical analysis presented a better correlation with liner lifetime. Vibration signature also presented good correlation with liner lifetime, even with the inclusion of operational data obtained in uncontrolled conditions. This vibration data was obtained based on predictive maintenance measurement within the operational routine. This means this data set is continuously generated and available and thus not require additional investment or changings in the operational routine. Despite the demonstrated potential, a deeper evaluation of historical data and additional test work under controlled conditions are necessary, to consolidate the method and develop trustful indicators.

## 7.1. Main contributions

- The research raises the discussion about the current procedure to compensate wear by increasing operational filling;
- Speed setup for laboratory test work;
- Performance evaluation of fine grinding by using the SSE approach and discussing different marker sizes;
- Application of wear model in the DEM simulations.

## 7.2. Recommendations

- Repeat the laboratory test work with fixed specific energy. Then a direct comparison of product size can be performed;
- Continuous test work in laboratory scale: the effect of the dead zone can be excluded from the sampling;
- Apply the same test work procedure for the evaluation of wear compensation by variation of mill speed;
- Industrial test campaign with continuous sampling and energy measurement, during a complete liner lifecycle;

- Application of DEM wear simulations for the evaluation of different wear compensation strategies, based on mill speeds and grinding media fillings;
- Application of DEM wear simulations to study the effect of non-sphericity grinding media. The results can be compared and validated by industrial data presented by Silva (2019);
- Application of CFD (Computational Fluid Dynamics) or SPH (Smoothed Particle Hydrodynamics) to describe the mill charge with more details;
- Deeper evaluation of vibration historical data and further correlation with liner conditions;
- Additional test work under controlled conditions, measuring power and vibration data.

# CAPÍTULO 7 - CONSIDERAÇÕES FINAIS

Os temas relacionados às melhorias na eficiência energética da moagem e à otimização operacional apresentam-se como necessidades essenciais para a indústria mineral e também para a comunidade acadêmica. Devido à crescente necessidade por aplicações envolvendo moagem fina e remoagem, o moinho vertical aponta como um equipamento importante, uma vez que apresenta melhor desempenho energético, em comparação com outros equipamentos. Embora tenha sido amplamente utilizado na indústria de mineração, alguns aspectos de sua operação ainda são desconhecidos ou descentralizados, como é o caso do desgaste do revestimento do agitador.

Uma vez que os revestimentos são responsáveis pela movimentação da carga moedora e, consequentemente, pela quebra de partículas, o monitoramento e uma melhor compreensão do desgaste apresentam-se como temas relevantes. Soma-se a esses fatores o fato de que o desgaste do revestimento está associado direta ou indiretamente com todos os componentes do custo operacional, que são o consumo energético, consumo de corpos moedores e a substituição do revestimento. Nesse sentido faz-se necessário o monitoramento do desgaste e a promoção de um desempenho energético otimizado, durante todo o ciclo de vida completo do revestimento. O presente estudo abordou esta questão por meio de diferentes abordagens: testes em escala laboratorial, simulações DEM e medições industriais.

Os testes de moinhos verticais de carga agitada em escala de laboratório apresentam-se como um tópico recente na literatura. Dessa forma, a maior parte da modelagem e dimensionamento são realizados com base nos testes padrões determinados pelos fabricantes, utilizando moinhos tubulares convencionais. Consequentemente, ocorre uma carência de informações relativas à definição dos parâmetros de testes em moinhos verticais de carga agitada em escalas reduzidas. O presente trabalho aplica uma nova metodologia para a configuração da velocidade do agitador, baseada numa base de dados de equipamento, ao invés de aplicar um fator direto de escala. Além disso, o trabalho de teste considera o desgaste do agitador como uma variável operacional, buscando observar os seus efeitos no desempenho do equipamento. Dessa forma foi realizada uma

comparação entre dois procedimentos operacionais distintos: operação com potência fixa e com enchimento fixo. Os resultados indicam que a relação entro o P80 e a energia específica de moagem (kWh/t) não é afetada representativamente por testes com enchimentos elevados e, portanto, essa metodologia de avaliação não pode ser utilizada para a análise. Nesse sentido, a escolha do marcador de tamanho de 38μm foi confirmada como um parâmetro razoável para avaliação da Energia Específica do Tamanho (SSE) na moagem fina e, por fim, os resultados indicam uma tendência de diminuição da SSE ao operar em condições de enchimento fixas.

Simulações DEM são amplamente utilizadas para modelamento e entendimento da operação de moinhos verticais. No entanto, a aplicação de simulações DEM para modelagem de desgaste em moinhos verticais consiste em uma abordagem mais recente (Mazzinghy, 2018). Nesse sentido, foi realizada uma simulação de desgaste em escala reduzida, cujos resultados de desgaste foram correlacionados à medições industriais, conforme aprsentadas por Silva (2019). Nesse sentido, a principal contribuição consiste em uma avaliação mais aprofundada e no acoplamento entre essas duas novas abordagens. Verificou-se que as geometrias desgastadas obtidas na simulação apresentam padrões de desgaste semelhantes ao perfil de desgaste do equipamento industrial. Além disso, uma correlação entre o tempo operacional (h) e o tempo de simulação (s) foi estabelecida, resultando na obtenção de um fator de escala de tempo. O fator foi aplicado aos resultados da simulação e utilizado na previsão do desgaste do equipamento em escala industrial. Os resultados do modelo apontam para uma previão de desgaste que se aproxima às medições industriais, no caso da simulação que utiliza a velocidade do agitador como 87 rpm.

Adicionalmente, a simulação DEM com velocidade rotacional de 87 rpm foi usada para simular as condições experimentais apresentadas no Capítulo 3. Nesse sentido, as simulações foram realizadas com o intuito de permitir uma comparação entre distintas estratégias operacionais durante o ciclo de vida do revestimento: enchimento constante e potência constante. Verifica-se a redução da energia cinética das partículas, independentemente da compensação da potência. Em relação à potência, verifica-se uma redução com o desgaste, da mesma forma que foi observado nos testes de laboratório. A

redução de potência ocorre principalmente devido à diminuição da frequência de colisões de elevada energia específica que, por sua vez, estão associados à redução da eficiência energética. Nesse sentido, contatos de elevada energia específica elevam a probabilidade de que seja aplicada energia maior do que necessária para a quebra, resultando em um uso excessivo de energia. Com base nisso, a redução nos contatos de alta energia específica pode ser usada para explicar a diminuição do SSE observada nos resultados experimentais. No entanto, essa redução também está relacionada à uma diminuição na frequência total de mecanismos de quebra, resultando na geração de um produto mais grosseiro. Esse efeito também está em aderência com os resultados experimentais apresentados no Capítulo 3.

Finalmente, o Capítulo 6 propõe um método não intrusivo e de baixo custo para o monitoramento do desgaste, baseado na medição de potência e análise vibracional. Testes industriais exploratórios foram realizados em três VTM-1500, em distintos estágios de desgaste do revestimento. Enquanto as medições de potência média e fator de potência foram suscetíveis às variações do processo, a análise estatística dessas medições resultou numa melhor correlação com a vida útil do revestimento. A assinatura de vibração também apresentou boa correlação com a vida útil do revestimento, mesmo após a inclusão de dados operacionais obtidos em condições não controladas. Esses dados de vibração foram obtidos com base no monitoramento de manutenção preditiva, dentro da rotina operacional da planta. Isso significa que esse conjunto de dados é gerado e disponibilizado continuamente e, portanto, não requer investimentos adicionais ou alterações na rotina operacional. Apesar do potencial demonstrado, faz-se necessário uma avaliação mais profunda dos dados históricos, assim como a execução de testes adicionais.

## 7.1. Principais Contribuições

- A pesquisa realizada propõe uma discussão a respeito do procedimento atual para compensação do desgaste, através da elevação contínua do enchimento de carga moedora;

- Proposição e aplicação de uma nova metodologia para definição da velocidade rotacional em moinhos verticais de carga agitada em escala reduzida;
- Avaliação do desempenho de moagem fina utilizando a abordagem de energia específica de tamanho (SSE);
- Aplicação do modelo de desgaste nas simulações DEM.

## 7.2. Recomendações futuras

- Repetir os experimentos de laboratório na condição de energia específica fixa. Dessa forma, pode-se realizar uma comparação direta da distribuição granulométrica dos produtos;
- Execução de testes de laboratório em condições contínuas, de forma a excluir o efeito da zona morta na amostragem;
- Aplicação da metodologia de testes propostas para a avalação da compensação do desgaste pela variação da velocidade do moinho;
- Realização de uma campanha de testes em escala industrial, para amostragem contínua do produto e medição energética, durante todo o ciclo de vida do revestimento;
- Aplicação de simulações de desgaste utilizando DEM para comparação de diferentes estratégias de compensação de desgaste, como a variação da velocidade rotacional e o enchimento de carga moedora;
- Aplicação de simulações de desgaste de DEM para estudo do efeito de corpos moedores não esféricos. Os resultados podem ser comparados e validados pelos dados industriais apresentados por Silva (2019);
- Aplicação de CFD (Computational Fluid Dynamics) ou SPH (Smoothed Particle Hydrodynamics) para descrição da carga do moinho com mais detalhes;
- Avaliação mais aprofundada dos dados históricos de vibração e potência, para correlação com as condições do revestimento;
- Realização de testes adicionais sob condições controladas, medindo dados de potência e vibração.

# APPENDIX

This section provides the data related to the experimental test work and DEM simulation results. The aim of this section is to provide a step-by-step procedure, such as to make data available for future projects.

The Appendices is divided in three sections. The first section consists in a summary of the data obtained from the laboratory test work presented at CHAPTER 3 -AN ALTERNATIVE STRATEGY TO COMPENSATE FOR SCREW WEAR IN GRAVITY INDUCED STIRRED MILLS.

Second section comprises the numerical data related to the DEM wear simulations used to model the screw liner wear at CHAPTER 4 -USING DEM FOR THE UNDERSTANDING OF GRAVITY INDUCED STIRRED MILLS SCREW LINER WEAR.

Third section includes the numerical data obtained from the DEM simulations of the experimental conditions, as presented at CHAPTER 5 - DEM SIMULATIONS APPLIED TO THE EXPERIMENTAL CONDITIONS.

# SECTION 1

## 1.1 Speed setup for laboratory test work based on equipment dataset.

| Screw diameter (m) | Database from Mazzinghy et al. (2017) | | Modelling | |
|---|---|---|---|---|
| | Rotational speed | Tip Speed | Tip speed (model) | Rotational Speed (Model) |
| 0.14 | 100 | 0.73 | 0.93 | 95.82 |
| 0.22 | 87 | 1.00 | 1.16 | 92.86 |
| 0.35 | 87 | 1.59 | 1.52 | 88.05 |
| 0.45 | 89 | 2.08 | 1.80 | 84.35 |
| 0.69 | 74 | 2.67 | 2.47 | 75.47 |
| 1.00 | - | - | 3.46 | 64.00 |
| 1.07 | 63 | 3.49 | 3.46 | 61.86 |
| 1.07 | 63 | 3.49 | 3.46 | 61.86 |
| 1.07 | 60 | 3.35 | 3.46 | 61.86 |
| 1.20 | 57 | 3.58 | 3.46 | 55.00 |
| 1.52 | 41 | 3.26 | 3.46 | 43.42 |
| 1.85 | 39 | 3.78 | 3.46 | 35.68 |
| 1.96 | 31 | 3.15 | 3.46 | 33.74 |
| 2.42 | 28 | 3.56 | 3.46 | 27.27 |
| 2.70 | 27 | 3.82 | 3.46 | 24.44 |
| 3.30 | 19 | 3.34 | 3.46 | 19.99 |
| 4.83 | 13 | 3.23 | 3.46 | 13.68 |

## 1.2 Relation between mill filling and net torque measurement at different wear conditions

| New Screw | | Half worn screw | | Fully worn screw | |
|---|---|---|---|---|---|
| **Filling (%)** | **Net torque (Nm)** | **Filling (%)** | **Net torque (Nm)** | **Filling (%)** | **Net torque (Nm)** |
| 0.00 | 0.00 | 0.00 | 0.00 | 0.00 | 0.00 |
| 4.60 | 0.00 | 4.59 | 0.01 | 6.00 | -0.01 |
| 10.93 | 0.49 | 9.20 | 0.36 | 12.47 | 0.36 |
| 17.30 | 1.51 | 18.39 | 1.53 | 18.58 | 1.00 |
| 22.24 | 2.49 | 22.98 | 2.28 | 24.07 | 1.70 |
| 27.55 | 3.73 | 27.55 | 2.95 | 29.37 | 2.42 |
| 33.44 | 5.09 | 32.15 | 3.71 | 36.38 | 3.38 |
| 39.49 | 6.53 | 41.32 | 5.23 | 41.91 | 4.13 |
| 48.37 | 8.66 | 50.51 | 7.05 | 48.08 | 5.32 |
| 53.96 | 10.19 | 55.09 | 8.00 | 54.04 | 6.49 |
| 61.16 | 12.03 | 59.69 | 9.39 | 60.48 | 7.72 |
| 72.87 | 15.10 | 68.86 | 11.30 | 73.21 | 10.72 |
| 79.00 | 16.90 | 78.04 | 13.84 | 80.24 | 12.42 |
| 85.53 | 18.80 | 87.22 | 16.17 | 89.53 | 15.12 |
| 92.32 | 21.00 | 96.41 | 19.00 | 96.67 | 17.32 |
| 100.90 | 23.50 | 105.60 | 21.61 | 104.39 | 19.32 |
| 111.66 | 26.80 | 110.19 | 23.12 | 111.95 | 21.52 |

## 1.3 Experimental Test Results

| **Test ID** | | **New Screw** | **Constant Power** | | **Constant Filling** | |
|---|---|---|---|---|---|---|
| | | **0%** | **CP-50%** | **CP-100%** | **CF-50%** | **CF-100%** |
| **Wear stage** | | 0% | 50% | 100% | 50% | 100% |
| **Filling** | | 80% | 92% | 95% | 80% | 80% |
| **Power** | | 0.15 | 0.15 | 0.15 | 0.13 | 0.11 |
| **SE (kWh/t)** | | 17.8 | 15.2 | 14.8 | 14.1 | 13.4 |
| **Size (µm)** | **Feed** | **% Pas** | **% Pas** | **% Pas** | **% Pas** | **% Pas** |
| 212 | 99.9 | 99.9 | 99.9 | 99.9 | 99.9 | 99.9 |
| 150 | 95.3 | 99.5 | 99.3 | 99.0 | 99.3 | 99.1 |
| 106 | 81.6 | 98.3 | 97.7 | 96.3 | 97.3 | 96.1 |
| 75 | 62.3 | 96.7 | 95.1 | 92.4 | 93.8 | 91.5 |
| 53 | 39.0 | 92.8 | 88.2 | 82.7 | 85.8 | 86.9 |
| 45 | 33.4 | 89.7 | 82.4 | 76.3 | 80.8 | 76.3 |
| 38 | 29.1 | 84.6 | 76.6 | 70.5 | 75.4 | 72.2 |
| **New -38µm (%)** | | 55.4 | 47.5 | 41.4 | 46.3 | 43.1 |
| **SSE 38 (kWh/t)** | | 32.1 | 32.1 | 35.9 | 30.4 | 31.2 |

# SECTION 2

## 2.1 Simulation power at different rotational velocities.

| | DEM Wear Simulations | | | | | | | | |
|---|---|---|---|---|---|---|---|---|---|
| | 87 rpm | | | 130 rpm | | | 190 rpm | | |
| **Base Liner (%)** | **100%** | **80%** | **70%** | **100%** | **81%** | **69%** | **100%** | **81%** | **69%** |
| **Power (W)** | 300.72 | 348.93 | 413.56 | 726.76 | 631.12 | 492.24 | 1269.85 | 1043.16 | 772.11 |
| **Power (%** | 73% | 84% | 100% | 100% | 87% | 68% | 100% | 82% | 61% |

## 2.2 Wear modelling at different rotational velocities.

| Wear Modelling | | | | | | | | | | | | |
|---|---|---|---|---|---|---|---|---|---|---|---|---|
| **Liner Part** | **Industrial measurement (Silva, 2019)** | | | **Simulation Model** | | | | | | | | |
| | | | | **87rpm** | | | **130rpm** | | | **190rpm** | | |
| | **Time (h)** | **Mass (kg)** | **Volume %** | **Time (s)** | **Calculated Time (h)** | **Volume (%)** | **Time (s)** | **Calculated Time (h)** | **Volume (%)** | **Time (s)** | **Calculated Time (h)** | **Volume (%)** |
| **Intermediate Liner volume** | 0 | 2450 | 100% | 0.00 | 0.00 | 1.00 | 0.00 | 0.00 | 1.00 | 0.00 | 0.00 | 1.00 |
| | 1200 | 2300 | 94% | 5.60 | 533.33 | 0.98 | 5.00 | 980.39 | 0.93 | 5.00 | 1639.34 | 0.86 |
| | 2400 | 1850 | 76% | 11.15 | 1061.90 | 0.95 | 10.00 | 1960.78 | 0.88 | 11.55 | 3786.89 | 0.77 |
| | 3000 | 1650 | 67% | 16.65 | 1585.71 | 0.93 | 15.00 | 2941.18 | 0.84 | 12.50 | 4098.36 | 0.76 |
| | | | | 47.05 | 4480.95 | 0.85 | 23.50 | 4607.84 | 0.79 | | | |
| | | | | 52.60 | 5009.52 | 0.84 | | | | | | |
| **Base Liner Volume** | 0 | 3200 | 100% | 0.00 | 0.00 | 1.00 | 0.00 | 0.00 | 1.00 | 0.00 | 0.00 | 1.00 |
| | 1200 | 2600 | 81% | 5.60 | 533.33 | 0.87 | 5.00 | 980.39 | 0.93 | 5.00 | 1639.34 | 0.80 |
| | 2400 | 2200 | 69% | 11.15 | 1061.90 | 0.80 | 10.00 | 1960.78 | 0.88 | 11.55 | 3786.89 | 0.69 |
| | 3000 | 1100 | 34% | 16.65 | 1585.71 | 0.75 | 15.00 | 2941.18 | 0.84 | 12.50 | 4098.36 | 0.68 |
| | | | | 47.05 | 4480.95 | 0.59 | 23.50 | 4607.84 | 0.79 | | | |
| | | | | 52.60 | 5009.52 | 0.57 | | | | | | |

## 2.3 DEM collision energy spectral data

| Collision Energy Spectra | | | | | |
|---|---|---|---|---|---|
| 87 rpm | | | | | |
| 80% Base wear | | | 70% Base wear | | |
| Specific Energy [J/kg] | Normal frequency [1/s] | Shear frequency ]1/s] | Specific Energy [J/kg] | Normal frequency [1/s] | Shear frequency ]1/s] |
| 1.00E-05 | 2.79E+05 | 1.20E+05 | 1.00E-05 | 2.49E+05 | 1.09E+05 |
| 2.58E-05 | 1.04E+05 | 4.36E+04 | 2.58E-05 | 9.24E+04 | 3.96E+04 |
| 6.66E-05 | 3.91E+04 | 1.61E+04 | 6.66E-05 | 3.46E+04 | 1.46E+04 |
| 1.72E-04 | 1.44E+04 | 5.71E+03 | 1.72E-04 | 1.28E+04 | 5.17E+03 |
| 4.44E-04 | 5.16E+03 | 1.92E+03 | 4.44E-04 | 4.57E+03 | 1.74E+03 |
| 1.15E-03 | 1.78E+03 | 5.96E+02 | 1.15E-03 | 1.57E+03 | 5.39E+02 |
| 2.96E-03 | 5.77E+02 | 1.61E+02 | 2.96E-03 | 5.05E+02 | 1.45E+02 |
| 7.63E-03 | 1.69E+02 | 3.53E+01 | 7.63E-03 | 1.46E+02 | 3.15E+01 |
| 1.97E-02 | 4.28E+01 | 5.59E+00 | 1.97E-02 | 3.54E+01 | 4.90E+00 |
| 5.08E-02 | 9.01E+00 | 5.50E-01 | 5.08E-02 | 6.68E+00 | 4.52E-01 |
| 1.31E-01 | 1.54E+00 | 2.66E-02 | 1.31E-01 | 8.58E-01 | 1.66E-02 |
| 3.38E-01 | 1.72E-01 | 7.54E-04 | 3.38E-01 | 5.97E-02 | 8.10E-05 |
| 8.73E-01 | 2.04E-03 | 0.00E+00 | 8.73E-01 | 3.55E-03 | 0.00E+00 |
| 2.25E+00 | 0.00E+00 | 0.00E+00 | 2.25E+00 | 0.00E+00 | 0.00E+00 |
| 5.82E+00 | 0.00E+00 | 0.00E+00 | 5.82E+00 | 0.00E+00 | 0.00E+00 |
| 1.50E+01 | 0.00E+00 | 0.00E+00 | 1.50E+01 | 0.00E+00 | 0.00E+00 |
| 3.87E+01 | 0.00E+00 | 0.00E+00 | 3.87E+01 | 0.00E+00 | 0.00E+00 |
| 1.00E+02 | 0.00E+00 | 0.00E+00 | 1.00E+02 | 0.00E+00 | 0.00E+00 |

| Collision Energy Spectra | | | | | |
|---|---|---|---|---|---|
| 130 rpm | | | | | |
| 81% Base wear | | | 69% Base wear | | |
| Specific Energy [J/kg] | Normal frequency [1/s] | Shear frequency ]1/s] | Specific Energy [J/kg] | Normal frequency [1/s] | Shear frequency ]1/s] |
| 1.00E-06 | 5.32E+06 | 2.09E+06 | 1.00E-06 | 4.35E+06 | 1.72E+06 |
| 2.34E-06 | 2.27E+06 | 8.91E+05 | 2.34E-06 | 1.86E+06 | 7.30E+05 |
| 5.46E-06 | 9.72E+05 | 3.80E+05 | 5.46E-06 | 7.91E+05 | 3.11E+05 |
| 1.27E-05 | 4.14E+05 | 1.61E+05 | 1.27E-05 | 3.36E+05 | 1.32E+05 |
| 2.98E-05 | 1.76E+05 | 6.82E+04 | 2.98E-05 | 1.43E+05 | 5.54E+04 |
| 6.95E-05 | 7.44E+04 | 2.85E+04 | 6.95E-05 | 6.00E+04 | 2.31E+04 |
| 1.62E-04 | 3.12E+04 | 1.18E+04 | 1.62E-04 | 2.51E+04 | 9.47E+03 |
| 3.79E-04 | 1.30E+04 | 4.73E+03 | 3.79E-04 | 1.04E+04 | 3.79E+03 |
| 8.86E-04 | 5.28E+03 | 1.83E+03 | 8.86E-04 | 4.20E+03 | 1.45E+03 |
| 2.07E-03 | 2.09E+03 | 6.65E+02 | 2.07E-03 | 1.65E+03 | 5.23E+02 |

| | | | | | |
|---|---|---|---|---|---|
| 4.83E-03 | 7.92E+02 | 2.18E+02 | 4.83E-03 | 6.19E+02 | 1.69E+02 |
| 1.13E-02 | 2.79E+02 | 6.05E+01 | 1.13E-02 | 2.14E+02 | 4.61E+01 |
| 2.64E-02 | 8.83E+01 | 1.32E+01 | 2.64E-02 | 6.52E+01 | 9.84E+00 |
| 6.16E-02 | 2.46E+01 | 1.98E+00 | 6.16E-02 | 1.69E+01 | 1.47E+00 |
| 1.44E-01 | 5.97E+00 | 1.73E-01 | 1.44E-01 | 3.65E+00 | 1.11E-01 |
| 3.36E-01 | 1.19E+00 | 7.59E-03 | 3.36E-01 | 6.23E-01 | 3.86E-03 |
| 7.85E-01 | 2.20E-01 | 0.00E+00 | 7.85E-01 | 9.06E-02 | 0.00E+00 |
| 1.83E+00 | 2.76E-02 | 0.00E+00 | 1.83E+00 | 2.33E-03 | 0.00E+00 |
| 4.28E+00 | 2.24E-03 | 0.00E+00 | 4.28E+00 | 0.00E+00 | 0.00E+00 |
| 1.00E+01 | 0.00E+00 | 0.00E+00 | 1.00E+01 | 0.00E+00 | 0.00E+00 |

| **Collision Energy Spectra** | | | | | |
|---|---|---|---|---|---|
| **190 rpm** | | | | | |
| **81% Base wear** | | | **69% Base wear** | | |
| **Specific Energy [J/kg]** | **Normal frequency [1/s]** | **Shear frequency ]1/s]** | **Specific Energy [J/kg]** | **Normal frequency [1/s]** | **Shear frequency ]1/s]** |
| 1.00E-06 | 9.25E+06 | 3.22E+06 | 1.00E-06 | 7.20E+06 | 2.76E+06 |
| 2.64E-06 | 3.50E+06 | 1.22E+06 | 2.34E-06 | 3.08E+06 | 1.18E+06 |
| 6.95E-06 | 1.33E+06 | 4.60E+05 | 5.46E-06 | 1.31E+06 | 5.03E+05 |
| 1.83E-05 | 5.01E+05 | 1.73E+05 | 1.27E-05 | 5.61E+05 | 2.14E+05 |
| 4.83E-05 | 1.89E+05 | 6.48E+04 | 2.98E-05 | 2.39E+05 | 9.09E+04 |
| 1.27E-04 | 7.08E+04 | 2.40E+04 | 6.95E-05 | 1.01E+05 | 3.83E+04 |
| 3.36E-04 | 2.64E+04 | 8.77E+03 | 1.62E-04 | 4.28E+04 | 1.60E+04 |
| 8.86E-04 | 9.71E+03 | 3.11E+03 | 3.79E-04 | 1.79E+04 | 6.58E+03 |
| 2.34E-03 | 3.49E+03 | 1.05E+03 | 8.86E-04 | 7.45E+03 | 2.64E+03 |
| 6.16E-03 | 1.21E+03 | 3.19E+02 | 2.07E-03 | 3.04E+03 | 1.02E+03 |
| 1.62E-02 | 3.90E+02 | 8.27E+01 | 4.83E-03 | 1.20E+03 | 3.69E+02 |
| 4.28E-02 | 1.13E+02 | 1.63E+01 | 1.13E-02 | 4.49E+02 | 1.20E+02 |
| 1.13E-01 | 2.85E+01 | 2.16E+00 | 2.64E-02 | 1.55E+02 | 3.38E+01 |
| 2.98E-01 | 6.18E+00 | 1.23E-01 | 6.16E-02 | 4.72E+01 | 7.45E+00 |
| 7.85E-01 | 1.17E+00 | 1.87E-03 | 1.44E-01 | 1.21E+01 | 1.05E+00 |
| 2.07E+00 | 2.27E-01 | 0.00E+00 | 3.36E-01 | 2.45E+00 | 6.77E-02 |
| 5.46E+00 | 4.61E-02 | 0.00E+00 | 7.85E-01 | 4.01E-01 | 2.62E-03 |
| 1.44E+01 | 1.71E-03 | 0.00E+00 | 1.83E+00 | 4.97E-02 | 4.91E-04 |
| 3.79E+01 | 0.00E+00 | 0.00E+00 | 4.28E+00 | 9.91E-03 | 0.00E+00 |
| 1.00E+02 | 0.00E+00 | 0.00E+00 | 1.00E+01 | 9.95E-04 | 0.00E+00 |

# SECTION 3

## 3.1 Simulation results for the experimental conditions

| Operational Condition | New Screw | Constant filling | | Constant Power | |
|---|---|---|---|---|---|
| **Case Scenario** | **0%** | **CF - 50%** | **CF - 100%** | **CP - 50%** | **CP - 100%** |
| **Base Liner Volume** | 0% | 81% | 69% | 81% | 69% |
| **Power** | 413.56 | 348.93 | 300.72 | 422.90 | 396.64 |
| **Velocity** | 0.463 | 0.376 | 0.321 | 0.407 | 0.371 |

## 3.2 DEM collision energy spectral data for the experimental conditions

| Normal Contact (Inter-Particle) | | | | | | | | | |
|---|---|---|---|---|---|---|---|---|---|
| **New Screw** | | **Constant filling** | | | | **Constant Power** | | | |
| **0%** | | **CF - 50%** | | **CF - 100%** | | **CP - 50%** | | **CP - 100%** | |
| **Specific Energy (J/kg)** | **Collision Frequency (1/s)** | **Specific Energy (J/kg)** | **Collision Frequency (1/s)** | **Specific Energy (J/kg)** | **Collision Frequency (1/s)** | **Specific Energy (J/kg)** | **Collision Frequency (1/s)** | **Specific Energy (J/kg)** | **Collision Frequency (1/s)** |
| 1.00E-05 | 4.02E+05 | 1.00E-05 | 2.79E+05 | 1.00E-05 | 2.49E+05 | 1.00E-05 | 3.45E+05 | 1.00E-05 | 2.86E+05 |
| 2.58E-05 | 1.52E+05 | 2.58E-05 | 1.04E+05 | 2.58E-05 | 9.24E+04 | 2.58E-05 | 1.31E+05 | 2.58E-05 | 1.07E+05 |
| 6.66E-05 | 5.78E+04 | 6.66E-05 | 3.91E+04 | 6.66E-05 | 3.46E+04 | 6.66E-05 | 4.94E+04 | 6.66E-05 | 4.01E+04 |
| 1.72E-04 | 2.15E+04 | 1.72E-04 | 1.44E+04 | 1.72E-04 | 1.28E+04 | 1.72E-04 | 1.83E+04 | 1.72E-04 | 1.48E+04 |
| 4.44E-04 | 7.79E+03 | 4.44E-04 | 5.16E+03 | 4.44E-04 | 4.57E+03 | 4.44E-04 | 6.59E+03 | 4.44E-04 | 5.29E+03 |
| 1.15E-03 | 2.72E+03 | 1.15E-03 | 1.78E+03 | 1.15E-03 | 1.57E+03 | 1.15E-03 | 2.27E+03 | 1.15E-03 | 1.81E+03 |
| 2.96E-03 | 8.91E+02 | 2.96E-03 | 5.77E+02 | 2.96E-03 | 5.05E+02 | 2.96E-03 | 7.30E+02 | 2.96E-03 | 5.75E+02 |
| 7.63E-03 | 2.65E+02 | 7.63E-03 | 1.69E+02 | 7.63E-03 | 1.46E+02 | 7.63E-03 | 2.09E+02 | 7.63E-03 | 1.63E+02 |
| 1.97E-02 | 6.87E+01 | 1.97E-02 | 4.28E+01 | 1.97E-02 | 3.54E+01 | 1.97E-02 | 4.99E+01 | 1.97E-02 | 3.84E+01 |
| 5.08E-02 | 1.54E+01 | 5.08E-02 | 9.01E+00 | 5.08E-02 | 6.68E+00 | 5.08E-02 | 9.75E+00 | 5.08E-02 | 7.22E+00 |
| 1.31E-01 | 3.10E+00 | 1.31E-01 | 1.54E+00 | 1.31E-01 | 8.58E-01 | 1.31E-01 | 1.66E+00 | 1.31E-01 | 1.09E+00 |
| 3.38E-01 | 5.32E-01 | 3.38E-01 | 1.72E-01 | 3.38E-01 | 5.97E-02 | 3.38E-01 | 2.77E-01 | 3.38E-01 | 1.74E-01 |
| 8.73E-01 | 7.41E-02 | 8.73E-01 | 2.04E-03 | 8.73E-01 | 3.55E-03 | 8.73E-01 | 5.00E-02 | 8.73E-01 | 1.97E-02 |
| 2.25E+00 | 5.95E-03 | 2.25E+00 | 0.00E+00 | 2.25E+00 | 0.00E+00 | 2.25E+00 | 1.12E-02 | 2.25E+00 | 0.00E+00 |
| 5.82E+00 | 0.00E+00 | 5.82E+00 | 0.00E+00 | 5.82E+00 | 0.00E+00 | 5.82E+00 | 0.00E+00 | 5.82E+00 | 0.00E+00 |
| 1.50E+01 | 0.00E+00 | 1.50E+01 | 0.00E+00 | 1.50E+01 | 0.00E+00 | 1.50E+01 | 0.00E+00 | 1.50E+01 | 0.00E+00 |
| 3.87E+01 | 0.00E+00 | 3.87E+01 | 0.00E+00 | 3.87E+01 | 0.00E+00 | 3.87E+01 | 0.00E+00 | 3.87E+01 | 0.00E+00 |
| 1.00E+02 | 0.00E+00 | 1.00E+02 | 0.00E+00 | 1.00E+02 | 0.00E+00 | 1.00E+02 | 0.00E+00 | 1.00E+02 | 0.00E+00 |

| Shear Contact (Inter-Particle) | | | | | | | | | |
|---|---|---|---|---|---|---|---|---|---|
| New Screw | | Constat filling | | | | Constant Power | | | |
| 0% | | CF - 50% | | CF - 100% | | CP - 50% | | CP - 100% | |
| Specific Energy (J/kg) | Collision Frequency (1/s) | Specific Energy (J/kg) | Collision Frequency (1/s) | Specific Energy (J/kg) | Collision Frequency (1/s) | Specific Energy (J/kg) | Collision Frequency (1/s) | Specific Energy (J/kg) | Collision Frequency (1/s) |
| 1.00E-05 | 1.82E+05 | 1.00E-05 | 1.20E+05 | 1.00E-05 | 1.09E+05 | 1.00E-05 | 1.62E+05 | 1.00E-05 | 1.31E+05 |
| 2.58E-05 | 6.80E+04 | 2.58E-05 | 4.36E+04 | 2.58E-05 | 3.96E+04 | 2.58E-05 | 6.02E+04 | 2.58E-05 | 4.82E+04 |
| 6.66E-05 | 2.53E+04 | 6.66E-05 | 1.61E+04 | 6.66E-05 | 1.46E+04 | 6.66E-05 | 2.24E+04 | 6.66E-05 | 1.78E+04 |
| 1.72E-04 | 9.12E+03 | 1.72E-04 | 5.71E+03 | 1.72E-04 | 5.17E+03 | 1.72E-04 | 8.05E+03 | 1.72E-04 | 6.33E+03 |
| 4.44E-04 | 3.12E+03 | 4.44E-04 | 1.92E+03 | 4.44E-04 | 1.74E+03 | 4.44E-04 | 2.74E+03 | 4.44E-04 | 2.13E+03 |
| 1.15E-03 | 9.79E+02 | 1.15E-03 | 5.96E+02 | 1.15E-03 | 5.39E+02 | 1.15E-03 | 8.48E+02 | 1.15E-03 | 6.52E+02 |
| 2.96E-03 | 2.69E+02 | 2.96E-03 | 1.61E+02 | 2.96E-03 | 1.45E+02 | 2.96E-03 | 2.26E+02 | 2.96E-03 | 1.71E+02 |
| 7.63E-03 | 6.01E+01 | 7.63E-03 | 3.53E+01 | 7.63E-03 | 3.15E+01 | 7.63E-03 | 4.72E+01 | 7.63E-03 | 3.54E+01 |
| 1.97E-02 | 1.00E+01 | 1.97E-02 | 5.59E+00 | 1.97E-02 | 4.90E+00 | 1.97E-02 | 6.86E+00 | 1.97E-02 | 5.11E+00 |
| 5.08E-02 | 1.14E+00 | 5.08E-02 | 5.50E-01 | 5.08E-02 | 4.52E-01 | 5.08E-02 | 6.02E-01 | 5.08E-02 | 4.00E-01 |
| 1.31E-01 | 7.24E-02 | 1.31E-01 | 2.66E-02 | 1.31E-01 | 1.66E-02 | 1.31E-01 | 2.10E-02 | 1.31E-01 | 1.14E-02 |
| 3.38E-01 | 8.77E-04 | 3.38E-01 | 7.54E-04 | 3.38E-01 | 8.10E-05 | 3.38E-01 | 1.55E-04 | 3.38E-01 | 3.31E-05 |
| 8.73E-01 | 0.00E+00 | 8.73E-01 | 0.00E+00 | 8.73E-01 | 0.00E+00 | 8.73E-01 | 0.00E+00 | 8.73E-01 | 0.00E+00 |
| 2.25E+00 | 0.00E+00 | 2.25E+00 | 0.00E+00 | 2.25E+00 | 0.00E+00 | 2.25E+00 | 0.00E+00 | 2.25E+00 | 0.00E+00 |
| 5.82E+00 | 0.00E+00 | 5.82E+00 | 0.00E+00 | 5.82E+00 | 0.00E+00 | 5.82E+00 | 0.00E+00 | 5.82E+00 | 0.00E+00 |
| 1.50E+01 | 0.00E+00 | 1.50E+01 | 0.00E+00 | 1.50E+01 | 0.00E+00 | 1.50E+01 | 0.00E+00 | 1.50E+01 | 0.00E+00 |
| 3.87E+01 | 0.00E+00 | 3.87E+01 | 0.00E+00 | 3.87E+01 | 0.00E+00 | 3.87E+01 | 0.00E+00 | 3.87E+01 | 0.00E+00 |
| 1.00E+02 | 0.00E+00 | 1.00E+02 | 0.00E+00 | 1.00E+02 | 0.00E+00 | 1.00E+02 | 0.00E+00 | 1.00E+02 | 0.00E+00 |